UNIVERSITÀ DEGLI STUDI DI PADOVA

UNIVERSITA' DEGLI STUDI DI PADOVA

DIPARTIMENTO DI INGEGNERIA INDUSTRIALE DII

Corso di Laurea Magistrale in Ingegneria Meccanica

TESI DI LAUREA

Micro-injection moulding for production of polymeric lab-on-a-chip – simulation, production and optimization

Relatore: Ing. Marco Sorgato

Laureando: Ludovico Ricci
Matricola: 2018692

Anno Accademico 2021/2022

Micro-injection moulding for production of polymeric lab-on-a-chip-simulation, production and optimization

Master Thesis
February, 2022

By
Ludovico Ricci

Preface

The presented work is part of the innovative AcouPlast project, that aims to move from a glass chip to a polymer-based platform for the separation of blood cells, moving from conventional centrifuge separation to acoustic separation where a standing wave separates the particles.

This thesis was carried out from September 2021 to February 2022 at the Department of Manufacturing Engineering of the Technical University of Denmark (DTU), under the supervision of Associate Professor Guido Tosello, Senior Researcher Matteo Calaon, Researcher Marco Sorgato and PhD Student Komeil Saeedabadi.

Kongens Lyngby
February 2022
Ludovico Ricci

Acknowledgements

Here I would like to extend my thanks to everyone that supported me during this work.

Firstly, I would like to express my gratitude to my supervisor, Komeil Saeedabadi, for having been always available when I needed help. Furthermore, the fruitful discussions with him during the weekly meeting have significantly improved the outcome of the work.

Moreover, I would like to thank Prof. Guido Tosello and Matteo Calaon, who also supported my permanence in Denmark and all the staff members of the Section of Manufacturing who helped me in the molding experiments and subsequent measurements of the produced parts.

Last but not least I would like to thank my family, which gave me the opportunity to live a semester abroad, where I could improve my knowledge and make friends from all over the world, as well as for their support throughout my whole University career.

Abstract

Currently micro injection moulding is an efficient replication technology that combines mass production with a low cost. Because of its increasing application in many fields nowadays one of the main challenges is the possibility to simulate a process at microscale. This work aims to exploit the potential of process simulation to improve the production of a lab-on-a-chip with two different materials: PMMA and COC. An initial benchmark based on previous production and datasheets allowed identifying suitable process parameters by varying four factors: Mould temperature, Melt temperature, Packing pressure and Injection velocity. The combinations of different values of these factors were used to set up the experimental design. Then, the effects of the process parameters on the Volumetric shrinkage of the chip, caused by the cooling process, were quantified with a proper metrology analysis.

Finally, the results were compared with the simulation.

Based on the metrology analysis of produced chips and the simulations, COC showed better results in term of volumetric shrinkage, with the dimensions of the channel closer to the mold value. Has the least shrinkage values both in practice and simulation.

For each material the full factorial design was also analyzed with a statistical software (Minitab®) making it possible to determine which of the four parameters under analysis contributes more to modifying the volumetric shrinkage. The accuracy of the simulations for COC compared to the injection molded parts showed deviation within 15%, whilst PMMA has larger deviations from the real values (around 25-30 %).

Even though the simulations differ a bit from the experiments a common trend could be identified: in all the simulation the parts shrink less than the real one, hence the results can be used for further production keeping in mind that the simulations underestimate actual behaviour.

Contents

Nomenclature

The next list reports all the abbreviations that will be later used within the body of the document

μIM Micro Injection Moulding

CAE Computer Aided Engineering

CMM Coordinate Measuring Machine

COC Cyclic Olefin Copolymer

DoE Design of Experiment

EDM Electrical Discharge Machining

HTC Heat Transfer Coefficient

L_s Linear shrinkage

$LASER$ Light Amplification by the Stimulated Emission of Radiation

LOC Lab-on-a-chip

$LSCM$ Laser Scanning Confocal Microscope

$PMMA$ Poly(methyl methacrylate)

SI International System of Units

V_s Volumetric shrinkage

List of Figures

List of Tables

1 Introduction

The current chapter introduces the project to the readers. After motivation, defines the project background and sets the goals of the thesis.

1.1 Motivation

In the last decades, the miniaturization of plastic components has become the principal trend in several fields such as medicine, automotive, communication components, and so on [7]. Micro injection molding (μIM) is the most diffused technology in the industry of polymer micro components since it can ensure net-shaped plastic parts with tight tolerances and short cycle times, two aspects that are becoming more and more important. It is considered one of the key technologies of the 21st century. In fact, it accounts for most of today's production of plastic parts. A research from Fior markets [11] reports that the Medical & Healthcare segment dominates the market in μIM parts. This growth is attributed to the increasing number of micro-size components in the medical and healthcare industry. Additionally, the global polymer microinjection molding market is expected to grow from USD 1.925 billion in 2018 and to reach USD 6.667 billion by 2027. North America is expected to hold a significant share in the global polymer microinjection molding market followed by Asia Pacific. Many of the key players are primarily focusing on developed economies of North America. (see the Figure 1.1)

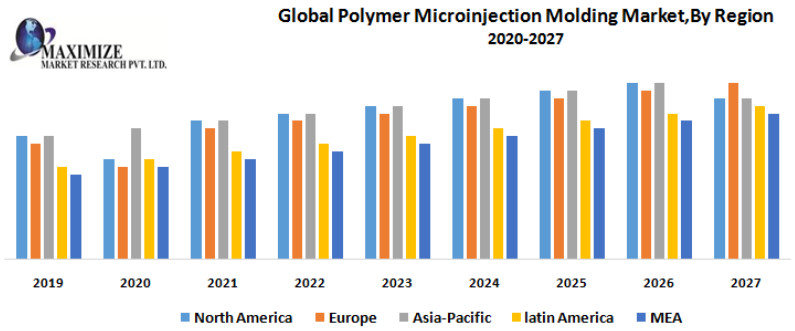

Figure 1.1: Global microinjection molding market by Region [10].

Satisfying product specifications and functional requirements for all injection moulded components is a challenging task [9]. Metrology inspections are an essential step to ensure good quality part but are not enough. Also simulation programs such as Moldex3D and Autodesk Moldflow are developed to achieve this purpose. They are carried out for the same reasons as for conventional injection molding: to ease tasks, to avoid waste of time and hence leading to cost savings, and, last but not least, forecast possible defects on the final part. In order to obtain reliable results that comply with the product specifications, the simulations need to be validate by comparison with experimental results. An accurate simulation set-up including all elements involved in the process can greatly improve the accuracy of the simulated results. [21].

1.2 Project definition

This work is part of the innovative AcouPlast project, that aims to move from a glass chip to a polymer-based platform for the separation of blood cells. The well-known conventional centrifuge is in this way replaced by exploiting the principle of acoustic separation where a standing wave separates the particles. (See Figure 1.2).

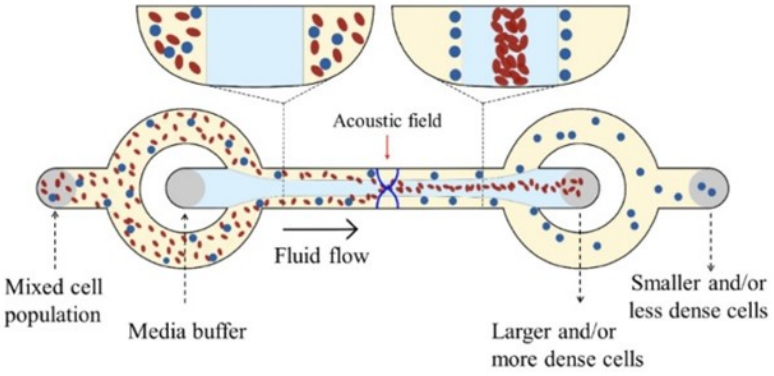

Figure 1.2: Working principle of acoustic separation [1].

Lab-on-a-chip (LOC) is a device that integrates one or several functions on a single integrated circuit. In the recent years this system has become widely widespread because of the lower manufacturing costs, faster analysis and response times, and also for the compactness [17]. For its dimensions a µIM part is considered . When dealing with micro-injection molding, it is worth to clarify how *micro* is defined. According to the literature, there are three definitions for micromolded plastic products [22] as described in Table 1.1:

1. Microfeatured parts with outer dimension in the millimeter range or larger, but locally featuring structures in the micrometer range.
2. Microparts with very small outer dimensions, tipically in the micrometer range, and weights in the order of milligrams.
3. Parts with larger dimensions, but tolerances in the micrometer range.

µIM Product	Average Part Size	Part Mass	Dimensional Tolerance Range	Equipment
Single Microparts	<10 mm	0.0001-0.1 g	10 µm	µIM metering and dosing system
Parts featuring micro-or nanos-tructures	>10 mm	>0.1 g	0.01-1 µIM (on features)	Conventional IM injection system
Micro precision IM Parts	>10 mm	>0.1 g	10-100 µm	µIM and IM systems

Table 1.1: Product classification for micro-injection molding (µIM) [19].

Several companies are involved: AcouSort will design chips based on simulations from DTU which are then manufactured by Ortofon and tested together with Lund University

to iteratively arrive at a well-functioning product. Also involved are DTU physics, whose outputs obtained from FEM numerical simulations are used as input for this work. At the start of the project a prototype of the chip obtained from a previous study was already available [3]. The initial efforts were addressed to the quality part: in particular, how to avoid the sink marks that may put in risk the phisics behind acoustic separation and the functionality of the chip.

1.3 Objectives

Starting from a previous work [3], the purpose of this thesis is to further minimise the deformation of the produced samples by investigating different materials and process parameters. The main focus is the shrinkage of the micro-channel, whose dimensions have to be monitored to avoid to putting at risk the functionality of the chip. Both the volumetric shrinkage and linear one were measured for the two materials tested.

This was achieved through several steps (Figure 1.3). First of all, a virtual Design of Experiment was developed to study the relationship between the input variables (Mold Temperature, Melt Temperature, Packing Pressure, Injection velocity) and the key output of the experiment (Shrinkage). This latter was obtained by running all the recipes on Moldex3D. Once this had been done, two lab sessions were performed to produce the chips with DoE parameters and finally an accurate metrology analysis on the produced samples to measure the deformation in the channel. In the end, the shrinkage of the simulations was compared with the molded part.

Through the comparison between Moldex3D simulations and experiments it is also possible to carry out the other important goal of the thesis: evaluate the accuracy of the simulation predictions.

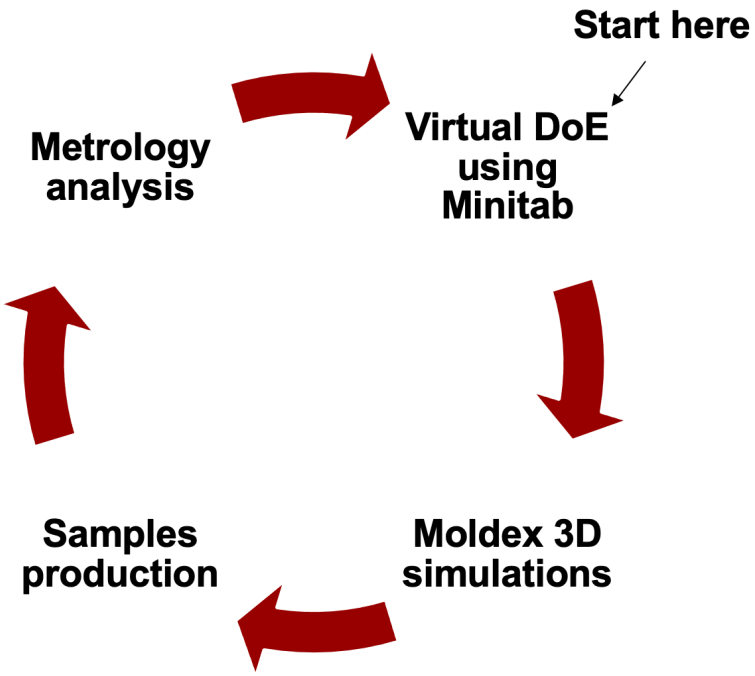

Figure 1.3: Workflow of the project

2 Literature

The second chapter focuses on the manufacture technology of the injection molding, in particular in the development that occurs in the recent years.

Firstly, makes a reminder of the conventional injection molding, the components of the machine and its main phases. Then, it discussed the recent introduction of μIM to meet the fast growing of miniaturized parts. It ends with a brief overview of the process simulations.

2.1 Conventional injection moulding

Conventional injection moulding is the most used manufacturing process for the large scale production of parts made of polymeric materials, basically because ensures to generate form and geometry even complex with a low cost [32]. It is a discontinuous and cyclic replication technology that enables a low cycle time and repeatable manufacturing of net-shaped parts. The process can be fully automatized to achieve the extremely high throughput rates required for setting large-volume productions. In figure 2.1 is depicted a typical injection molding machine. Each machine usually has a specific code which indicates:

$$T/P$$

- T is the Clamping force, hence represents the performance of the clamping unit;
- P is an indicator of performance for the clamping unit;

$$P = \frac{V_{MAX}(cm^3) \cdot P_{MAX}(Bar)}{1000} \tag{2.1}$$

As it is discussed below there are several parts of an injection molding machine, the major components are:

- Plasticating/Injection unit;
- Mold;
- Clamping unit;

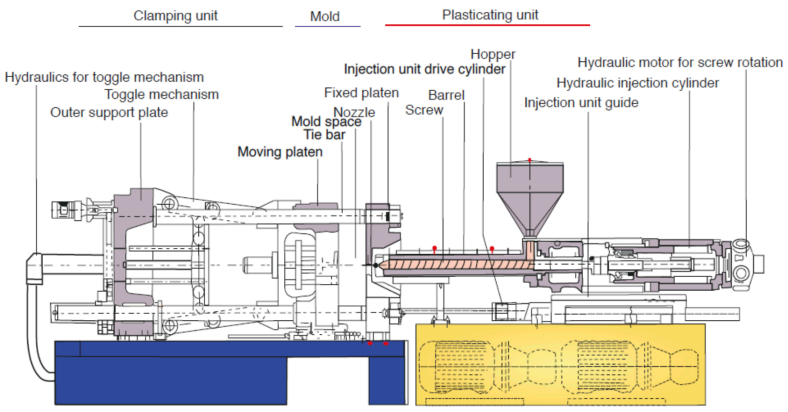

Figure 2.1: Injection Molding Machine [31]

The **plasticating unit** is designed to:

- Melt the polymer pellets;
- Accumulate the melt in the screw chamber;
- Inject the melt into the cavity;
- Maintain the holding pressure during cooling;

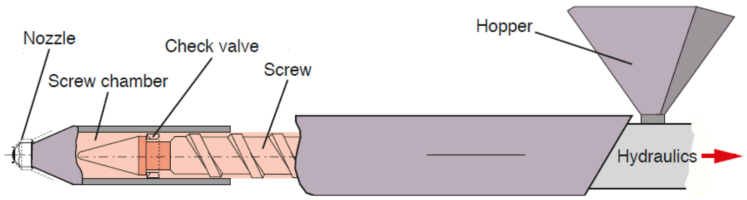

Figure 2.2: Schematic of the plasticating unit [31]

it consists of a hopper and a reciprocating screw, whose function is to melt the polymer and to inject it into the cavity. A hopper is the first part of the injection unit and can be described as a large container in which plastic in the form of small pellets are poured through the hopper throat into the barrel. The more common technique applied to heating and injecting is the use of a reciprocating screw, that moves the material forward by both rotating and sliding axially. The reciprocating screw consists of three zones called the feeding zone, the compression zone and the metering zone. The depth of the flights on the screw decreases from the feeding zone to the beginning of the metering zone, whose role is to compress the material against the inside diameter that melts the material. The heater bands outside the barrel help maintain the material to remain in the molten state. In general, a molding machine can have three or more heater bands or zones with different temperature settings.

During this movement, the material gets melted by pressure, friction, and additional heaters that surround the reciprocating screw. Due to the buildup of pressure and the forward action of the screw, the molten plastic is thereafter injected very quickly into the mold through the nozzle at the end of the barrel.

This increasing pressure allows the material to be packed and forcibly held in the mold. Once the material has been solidified or cooled inside the mold, the screw can retract and fill with more material for the next shot.

The **mold** is the core of the injection molding process and it must be make precise functions:

- Distribute the polymer melt into and throughout the cavities;
- Shape the part;
- Solidify the part by cooling;
- Eject the finished part;

The simplest type of molds is *cold runners*, which can be of two types:

- Two plates, consisting of a movable plate that separates from the fixed plate. This solution is simple, inexpensive, but technologically constrains the power supply system on the partition plane because only in this way can everything be extracted.

- Three plates, in this case an intermediate plate is added, called floating, which allows the extraction of the feed system, separating it from the rest of the component. On one hand it increases the complexity of the mold, but there is more freedom in the positioning of the gate.

As an alternative to cold runners, there are *hot runners*, a system in which the sprue and feed system are located in the machinery and grouped in the manifold, which has the task of redistributing the hot melt to the injectors. The whole manifold is kept warm through an appropriate heating system to always keep the plastic melted, for this reason it is called hot runners. The injector is equipped with a valve, and this allows further adjustment for the opening of each individual gate, and this allows to guarantee:

- High control of the melt injection;
- A reduction in the required cycle time, as you do not have to wait for the sprue to cool down;
- The absence of cooling of the sprue does not generate polymeric waste;
- Freedom in the positioning of the injection point with a lot of reduced unsightly mark;

Clearly this technology compared to the cold runner has higher costs and energy consumption.

The molds are usually made of hardened steel, which lends itself to possible processing and is easy to treat even thermally. As an alternative to this material there is aluminum, which is evident that it will wear out more easily and will be less rigid than hardened steel, but you have some advantages that are not entirely negligible, such as greater ease of processing and with reduced times (times are reduced in classical milling compared to EDM), greater thermal conductivity (reduction of cycle time) and it is also lighter and easier to handle. There are also some variables in the material adopted for the molds, an example are the copper-beryllium inserts, which are used in those slow-cooling regions to accelerate and uniform it with respect to the entire component. In summary, the properties that a material must has in order to be used as a mold are:

- Workability;
- A reduced coefficient of thermal expansion;
- A high thermal capacity;
- High thermal conductivity;
- Weldability, as it may be necessary to apply coatings in case that the mold presents defects;

Moulds are manufactured through two main methods: standard machining and Electrical Discharge Machining (EDM). Standard machining, in its conventional form, has historically been the method of building injection moulds. With technological developments, CNC machining became the predominant means of making more complex moulds with more accurate mould details in less time.

The Electrical Discharge Machining (EDM), also known as spark erosion, has become widely used in mould making. Primarily used for hard metals or those that would be very difficult to machine with traditional techniques.

The **clamping unit** is designed to securely close the two halves of the mold before injecting the molten plastic into the mold, hence to generate enough pressure to prevent

flash during mold filling and holding. There are two types of clamping methods, namely the toggle type and the hydraulic type. In the first one the mold is moved with an electric press, in the hydraulic type the mold is directly opened and closed with a hydraulic cylinder. The main advantages of the mechanical closure are the greater clamping force (up to 600 tons), more accurate, less noised and consume less than hydraulic one. On backward it is correlated with a precise thickness of the mold. Once the part is cooled, the clamping motor opens the mold and pushes the solidified part out of the cavity.

As above mentioned IM is a cyclic process. The different phases of a process cycle are the following:

- Plastification;
- Injection;
- Packing;
- Cooling;
- Mould opening/Ejection;

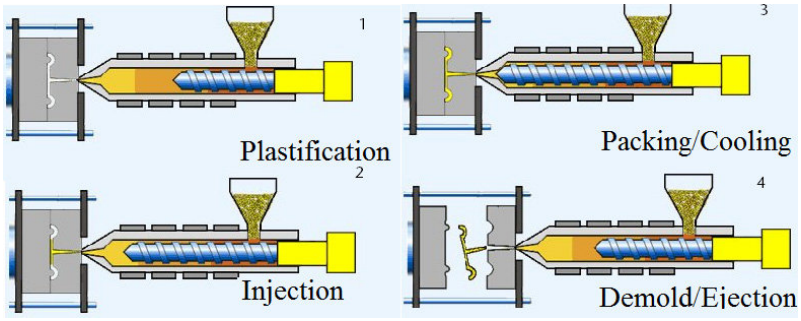

Figure 2.3: Processing cycle of conventional IM [42]

2.2 Micro injection moulding

Micro injection molding is a molding process for the manufacture of micro-scale plastic components widely used for shot weights of 1 to 0.1 grams with tolerances in the range of 10 to 100 micrometers. This molding process permits the manufacture of complicated small geometries with maximum possible accuracy and precision and is comprised from the same process phases as the conventional one [38]:

- Melting of the plastic granules;
- Metering of the molten plastic;
- Injection of the material into the cavity of the mold;
- Packing of the part;
- Cooling;
- Ejection from the mold;

This paragraph intends to review the state of the art of micro injection moulding for micro components, to highlight the differences with the conventional one and research gaps of this process.

This technology was firstly introduced from traditional injection moulding since late eighties but no appropriate machine technology was available and only modified commercial units of traditional injection moulding machine could be used. Only in the middle of nineties, special new micro injection machines were developed specifically addressing micro moulding parts and thus, research efforts have still to be done. In order to meet the fast growing demand of μIM products in several engineering fields, conventional injection molding has been adapted to the micro-scale with some additional factors that must be kept in mind:

- Conventional IM machines have a reciprocating screw, while μIM ones have a screw for plasticising pellets and a separate plunger for metering and injection;
- Dedicated μIM machines have higher injection speeds required to prevent the premature solidification of the parts;
- The no-slip boundary condition at the wall is no longer a valid hypothesis;
- Capillary effects generated by surface tension forces become relevant;
- A local heat transfer coefficient (HTC) is assigned to the model properties;
- Imperfect venting of micro-injection molds and the consequence counter pressure;

A comparison from μIM and conventional is shown in Table 2.1:

Macro/Meso	**Micro (μ)**	**Nano (n)**
Conservation of Mass	Wall-Slip Effect	
Conservation of Momentum	Surface tension	
Conservation of Energy	Local HTC	Molecular Dynamics
Polymer constitutive equation (PvT)	Unvented air	
Viscosity model	Surface Roughness	

Table 2.1: Modeling governing equations depending on scale size [19].

It is also important to underline that in micro injection molding the runner system and the sprue of the moulded parts usually occupy a volume larger than the volume of the parts, this fact contributes to waste a lot of the material as well as affecting the cooling and the whole cycle time.

Determining the most effective processing conditions for micro injection moulding was the subject of many studies [6], which used different experimental conditions and test parts. It has been shown that the main process parameters affecting the part quality include:

- Mould Temperature;
- Melt Temperature;
- Injection speed;
- Injection pressure;
- Holding time;
- Holding pressure;
- Cooling time;

with regard to the material, the flowability makes very proper for microparts, since a very low flow resistance is needed to completely fill the microcavities. In the next raws it will be analyzed more accurately some of the aspects that distinguish this process.

Most of the micro-injection molding parts are characterized by an higher *aspect ratio* and thus has to be investigated. The *aspect ratio* of a shape is defined as the ratio of its longer one to its shorter dimension [33]. The aspect ratio, achievable in replicating micro features is one of the most important characteristic of the micro fabrication processes and it constitutes a constraint in applying injection moulding. Concerning achievable aspect ratios, there is a limitation which is a function of the geometry of the micro-features, their position on the sample, the polymer type and the process parameters.

Apart from aspect ratio, also physical phenomena have to be taken into account in the micro world differently from macro as for example the *hesitation effect*. This effect (Figure 2.4) is a phenomenon that can occur during the filling of polymers, and it is common when an injection moulded part contains different thicknesses. The polymer melt flows more easily into larger cavities with relatively low resistance, on the other hand it tends to hesitate when enters in the small sections because of the higher flow resistance; the result is that the melt freezes in this area because the filling time of the substrate is usually greater than the freezing time of the micro feature.

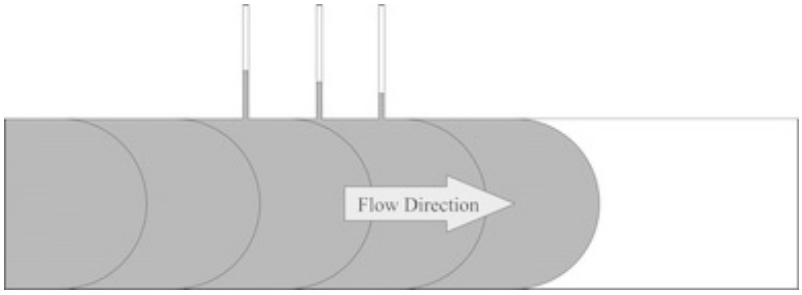

Figure 2.4: Hesitation effect of the melt flow in the proximity of micro channels [35]

One of the main goals related to the design of a micro mouldable component is the reduction of the *shrinkage* affecting shape stability in the form of induced warpage. The warpage is due to the non-uniformity of the shrinkage induced by the complex thermal variation inside the mould. Warpage prediction is important for parts with relatively large area compared to their thickness. Different techniques have been suggested to decrease the effect of shrinkage:

- By increasing the value of holding pressure, which, on the other hand, will also increase stresses inside the part.
- To have a long cooling time so that the part can thermally equilibrate inside the mould cavity and become approximately uniform.
- By increasing the cycle time, as a trade-off of a long cooling time.

Figure 2.5: micropart [41]

2.3 Process simulation

Simulations are helpful tools widely applied in the plastic industry but not only, in general also when the objective is to simplify and assist the product development. More in general we can indicate with Computer-Aided Engineering (CAE) all the tools that assist the engineer by creating virtual prototypes. It is taken for granted that this approach avoid to save a lot of time and money, since is not required to produced the real part. In the case of Process simulation it is possible to create a *digital twin*, which simulates as close as possible the boundary conditions of the real process or even better can give an overview of the behaviour before the part is manufactured, enabling us to investigate systems details that in reality would be not possible.

The simulations are carried out in micro injection molding with the same purpose as in conventional one. Nowadays, one of the main challenges is the possibility to simulate the process at microscale. Nonetheless, it must be kept in mind that the implemented model in simulation software included assumptions, idealization that are not in the actual part. Moreover it is worth pointing out that the available simulation software right now are not well suited for µIM because they are developed for conventional part.

The main goals, that researchers all over the world try to achieve, can be summed up in the following steps:

- Visualization of the flow and prediction of the last-filled sections of the mould. A method to evaluate all these aspects is the short-shots method, in which the mould is filled with different amounts of material in order to evaluate the distribution of the flow during the injection phase. This method is useful to identify some defects that are usually in the last filled parts like incomplete filling, weld lines and voids.
- Optimization of the design of the moulds before manufacturing in order to prevent high cost of reconstruction or remaking. The simulation approach would be very useful to try different geometrical designs, sprue and gating systems, flow-paths to determine the optimum mould design.
- Simulation of the thermal conditions of the flow during filling and cooling which would be useful in estimating the cycle time and determine the critical processing areas.
- To identify post-processing properties, such as residual stresses, shrinkages and warpage. In fact during micro injection moulding process, the material is subject to

the increasing of pressure and temperature due to significant shear deformation, followed by a rapid decay of temperature and pressure in the mould cavity. This leads to solidification, high residual stress, complex molecular orientation, that determine the moulded part quality.

- Supporting the experimentation and in particular the design of experiments in determining the most influential processing parameters on the part quality.

In a more general approach virtual prototyping is carried out to perform these goals [38]:

- Reduce development time and time-to-market for the new product.
- Support the part design, since the early stages.
- Avoid design errors and consequently costly re-engineering
- Eliminate the need to realize prototypes
- Give an approximated idea of the final product

2.3.1 State-Of-The-Art and Challenges of Micro Injection Molding Simulations

Numerical simulation for injection molding has been developed and accepted by the processing industry to improve productivity, part quality and to shorten start-up times [39][2]. In the particular case of micro injection molding, numerical simulation is all the more crucial since processors deal with much more basic problems than in the case of classical injection molding. Due to the small part dimensions prevailing in micro molding, it is not uncommon to be faced with the total incapacity to achieve complete filling of the micro cavity or to eject the solid part. This entails solutions such as changing the processing parameters, trying another material, modifying the mold inserts, or even making a new mold insert, when the trial-molding has resulted in irreversible insert damage, needless to say how expensive and time-consuming this trial and error process can be. There is, therefore, considerable need for reliable numerical simulation tools dedicated to micro injection molding. Commercial simulation packages are based on a usually legitimate approximation, when dealing with traditional injection molding, which consists in disregarding a dimension in front of the other two. Indeed, they fail to capture important aspects of injection mold filling, such as edge effects through narrow channels, transverse flow in corners, transverse flow at changes in mold thickness unless there are appropriate boundary conditions in these zones. Of course, these effects are more significant for small parts than for conventional ones. As a matter of fact even if have some similarity, micro injection molding show significant differences compared to the conventional injection molding process. These differences thus influence the simulation accuracy of software primarily developed for macroscopic thermoplastic parts:

- Relevant microscopic effects such as wall slip, surface tension, or microscale viscosity are not or insufficiently implemented in today's commercially available simulation packages.
- There are dedicated micro injection molding machines. The screw of the IM machine has a greater diameter and a different shape, the metering section is longer in the micro-IM. The diameter of the IM being smaller, leads to a more accurate tolerance than the screw of the IM machine. These are only some of the differences that distinguish from conventional machines.

  The IM machine also presents an additional key component for guaranteeing a high quality metering: a pressure sensor in the bored hole that accurately measures the

liquid material characteristic in front of the injection plunger [8]. However, conventional machines are the only available for software tools and micro machines are not provided.

- Due to the larger surface-to-volume ratio and the smaller thickness, the surface roughness and the altering heat transfer coefficient are no longer negligible. Current simulation software, nonetheless, provides only very limited possibilities to account for changing the heat transfer coefficient, not to mention the implementation of surface roughness.
- The smaller cavity size in micro cavities causes considerably increased shear rates and shear heating. The material data offered might only be available or valid over a limited range of temperatures or shear rates and are perhaps also outdated, leading to a demand for the extrapolation of material data or the acquisition of such data by non-standard methods.

The programs have especially difficulties with micro cavities exhibiting high aspect ratios. In order to improve the simulations results, a multitude of studies on the process and on simulation validations have been performed in science and research in recent years [13][39][19][37].

3 Design of Experiment

3.1 Design of Experiment (DoE)

In the DoE approach, a set of conditions for a stable injection molding process that produces acceptable molded parts is first supposed. The four factors chosen are:

- Melt Temperature [°C]
- Mould Temperature [°C]
- Injection speed [mm/s]
- Packing pressure [MPa]

According to well-established research [5][40], these are among the most relevant parameters affecting the quality of injection molding components. Other information regarding the mold and injection molding machine were given at the start of the project. Then, for each material, the parameter values along with the number of levels have been established from the data sheet provided by the supplier [18][36] and from previous production on this project [3]. In this case, the 4 factors are the independent variables in the process model. The dependent variable is the volumetric shrinkage of the micro-channel (i.e. the output of the DoE).

A full factorial statistically designed experiment was utilized in order to investigate the experimental process window. The total number of runs for each material required for the full factorial is $2^4 = 16$. Some studies [14], as a matter of fact, report that the most efficient and effective strategy is to implement the full factorial; obviously time permitting. The combination of the values of these different factors are used to set up the experimental designs. The goal was to figure out how to reduce volumetric shrinkage by understanding the effects of these variables. The measurements on the molded parts were carried out to determine the values of volumetric shrinkage.

Then, the effects of the four parameters and their interaction, were investigated using the statistical software Minitab.

Fixed variables	**Free variables**	**Response**
Material	Mold Temperature	Volumetric shrinkage
Mould design	Melt Temperature	
Arburg Machine	Packing Pressure	
Injection pressure	Injection velocity	

Table 3.1: Main parameters involved in the experimental set-up

It will be explained that this initial set up had to be changed due to inconveniences during experiments. As a matter of fact, it was not possible to run all 16 combinations.

3.1.1 COC DoE parameters

Two parameter levels (Table 3.2) were selected respect to equipment capabilities and the limit of the process window provided by the material datasheet [36]. Note that the pressure is reported in [MPa] according to the international system of units (SI) but the pressure on the Arburg machine was set-up in [Bar].

Factors	Level 1	Level 2
Mould temperature [°C]	100	120
Melt temperature [°C]	250	280
Packing pressure [MPa]	55	80
Injection velocity [mm/s]	50	100

Table 3.2: Initial DoE values for COC. Two levels for each factor

3.1.2 PMMA LG 840 DoE parameters

The DoE values were derived from LG technical datasheet [18] and based on previous productions.

Factors	Level 1	Level 2
Mould temperature [°C]	65	85
Melt temperature [°C]	220	240
Packing pressure [MPa]	90	120
Injection velocity [mm/s]	90	120

Table 3.3: Initial Parameters for PMMA

4 Experimental Part

In this chapter, after a description of the product specification and the materials used, the set-up will be explained, as well as the equipment used in the experimental part of the project. Finally metrology results and the uncertainty evaluation will be reported.

4.1 Product specification

The micro part object of study is a thermoplastic component for medical applications (see Figure 4.2) whose CAD model was given at project start (Figure 4.1). As it has been said before, according to the literature [22] the chip is considered a micro part. The most important dimensions that ensure the functionality of the part, are focused on the micro-channel:

- Channel depth with nominal value of 0.150 mm;
- Channel width with nominal value of 0.375 mm;
- Channel length with nominal value of 36.093 mm;

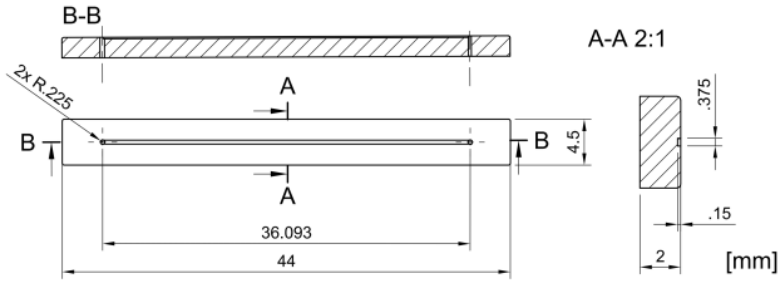

Figure 4.1: Design specification of the polymer chip with the micro channel

All the efforts were concentrated on these three dimensions.

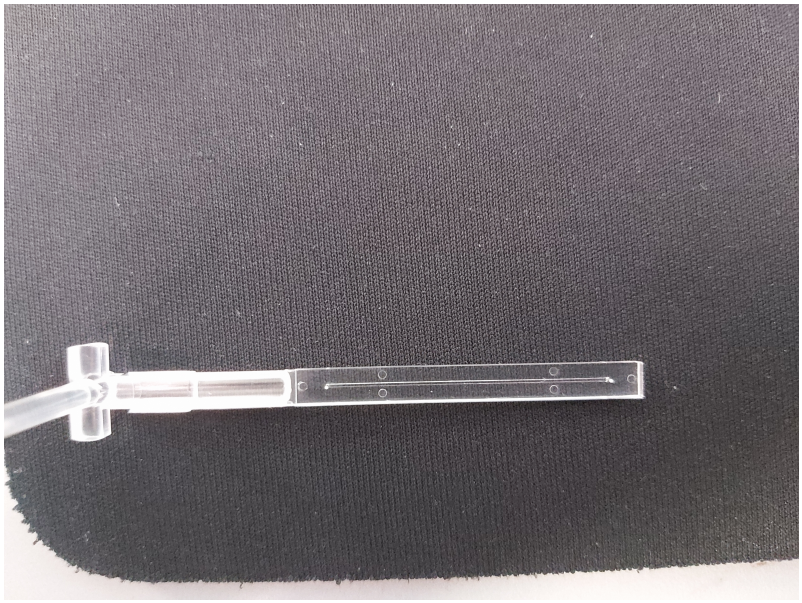

Figure 4.2: Picture of a molded part. The micro-channel can be seen as well as 6 ejector pins marks and the two holes.

4.2 Materials

The polymer materials used for the production of the chips were COC (5013L-10) manufactured by TOPAS® and PMMA LG 840.

PMMA LG 840 is a particular type of Polymethyl methacrylate, a transparent and rigid thermoplastic material, completely amorphous with excellent optical properties and resistance to atmospheric agents. Transparency in white light reaches 92%, even more than glass. It is very resistant to UV rays and does not turn yellow. Thanks to its very high transparency and its low cost, it has succeeded in many applications to replace glass [18].

However, PMMA has also many limitations over other transparent polymer (PC, polystyrene etc.), few of them include:

- Poor impact resistance;
- Limited heat resistance (80°C);
- Limited chemical resistance, prone to attack by organic solvents;
- Poor wear and abrasion resistance;
- Cracking under load is possible;

With regards to life-cycle, PMMA is 100% recyclable and non-biodegradable material.

There are several ways to recycle PMMA. Often, these recycling processes involve pyrolysis, in which the PMMA is extremely heated in the absence of oxygen. Another procedure involves depolymerization of PMMA. However, this recycling process is not environmentally viable due to the use of lead and the generation of harmful gases.

COC, which stands for cyclo olephi copolymer or cyclic olefin copolymer, is an amorphous thermoplastic material with several interesting characteristic. Some of these are reported:

- High flowability and excellent optical properties;

- Excellent clarity with a transmission above 90%;
- Low density;
- Good mechanical properties and barrier properties (especially against moisture);
- Good electrical insulation;
- High transition temperature (up to 250°C);
- Good recyclability and no generation of harmful gases when melted;
- Dissolves easily in the hydrocarbons;

These materials are recommended for applications such as optical parts, e.g. lenses, and optical storage media, where low birefringence and high molding accuracy are essential, as well as for medical and diagnostic applications. Table 4.2 and 4.1 show the main properties of PMMA and COC, respectively. For more information about thermal properties see the appendix [12].

Property	Values
Density [g/cm^3]	1.19
Heat deflection Temperature [°C]	102
Glass transition temperature [°C]	80

Table 4.1: Phisycal properties for PMMA

Property	Values
Density [g/cm^3]	1.02
Heat deflection temperature[°C]	130
Glass transition temperature [°C]	138

Table 4.2: Phisycal properties for COC

4.3 Machine and mold

4.3.1 Machine

The experiments were performed using a hybrid Arburg Injection-moulding machine Allrounder 370 A 600-70-18 (Arburg GmbH & Co KG, Lossburg, Germany), with a clamping unit of maximum 600 kN clamping force and a screw whose diameter is 18 mm. Figure 4.3 shows the injection molding machine used, and Table A.1 contains all the specifications.

(a) Arburg machine (b) Mold Temperature controller

Figure 4.3: Injection molding equipment used in plastic lab to produce the parts

4.3.2 Mold

The mould was given at the project start and the nominal dimensions are reported in Figure 4.4. The mould is made of aluminum, has a single cavity and a cold runner system. It consists on two parts with an ejection system based on pins installed in the mobile half that automatically separates the cold runner system from the moulded components. The mould was connected to a temperature controller (see Figure 4.3) in order to monitoring its temperature during the experiments.

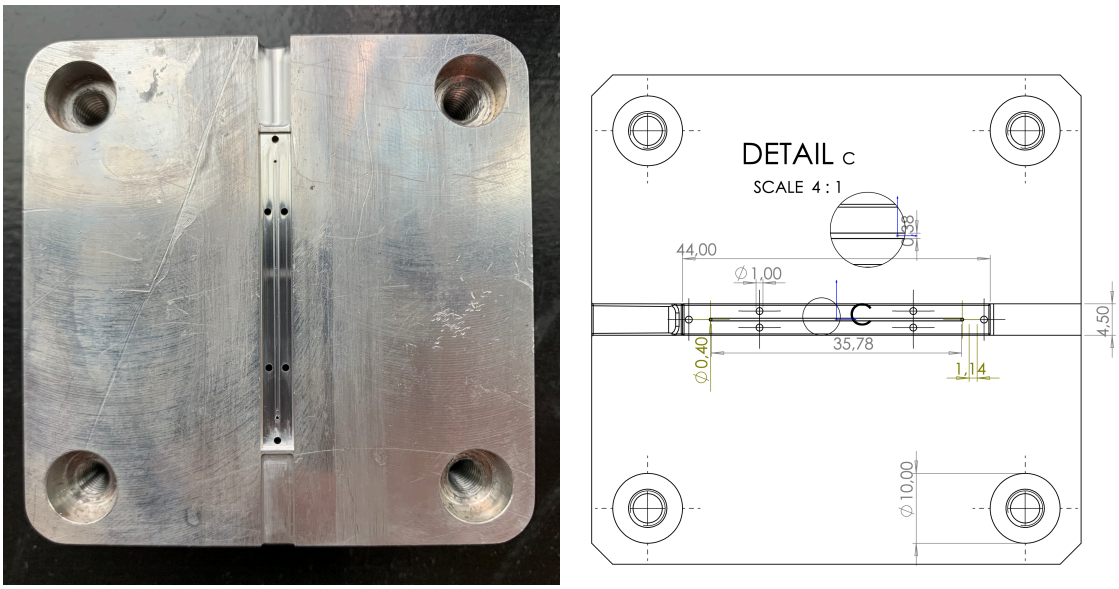

(a) The mold. 1 cavity, 6 ejector pins (b) Mold drawing

Figure 4.4: Mold details.

4.4 Injection molding sessions

The aim of the injection molding sessions was to carry out the DoE for COC and PMMA in order to determine the volumetric shrinkage. Then, these values were plugged into

Minitab® statistical analysis software to understand the individual and combined effects of the four parameters on the volumetric shrinkage. Due to some issues that occured during the molding session, it was not possible to carry out all the 16 simulations. In this section the reader will be guided through the two experimental sessions. Tables A.2 and A.3 in the appendix report in detail all the process parameters. These can be useful for further studies.

4.4.1 COC production

The first step, for each experimental session, is the drying of the plastic. The resins can be used without pre-drying but they absorb moisture if they are stored for a long time or under unfavorable conditions. When moisture absorption rate exceeds 0.1 %, there is a chance that silver streaks will form on the molded product's surface. For this reason, it is desirable to perform preliminary drying.

According to the processing datasheet [36] COC needs to be dried for 6 hours at 100°C. Hence, the day before the experiments, the material was put in a dryer. The machine was pre-heated for at least 1 hour before the experiment and the barrel was purged completely before and after the session. This was done to prevent contamination of materials.

Since there were 4 different parameters (see Table 3.2) and the process takes some time to became stable, an attempt was made to first print all the parts with low mould temperature and then shift to higher temperatures. After switching packing pressure and injection velocity, only 10 parts were discarded before collecting the ones of the next recipe. However, the change of melt temperature and mould temperature took longer than expected because the mold temperature controller takes a lot of time to change the temperature and consequently the process takes longer to acquire stability. So, it was decided to discard much more parts (approximately 50). Once the process was stable, 10 parts were collected in a bag for each combination of parameters and 3 of these were taken for the measurements of the micro-channel.

Other considerations were observed.

For the session the melt temperature profile was set by using 5 °C intervals per each heating zone of the reciprocating screw to facilitate a gradual heating of the material throughout the barrel (Figure 4.5). This differs compared to the simulation in which the temperature is constant.

Moreover the cooling time differs a bit in the experiments. To be precise, 15 s was set-up to make sure that parts had enough time to cool down before being ejected from the mold.

Figure 4.5: Boundary conditions. The melt temperature profile through the barrel. Note the temperature near the hopper is lower to avoid the pellets stick in the barrel.

The initial values of injection velocity chosen for the DoE (Table 3.2), although in the range recommended of the processing datasheet, were changed because not compatible with this case-study. As a matter of fact, the first values result in an excessively short filling time. Respectively 50 mm/s and 100 mm/s have been replaced with 14 mm/s and 22 mm/s.(see Table 4.3).

Factors	Level 1	Level 2
Mould temperature [°C]	100	120
Melt temperature [°C]	250	280
Packing pressure [MPa]	55	80
Injection velocity [mm/s]	14	22

Table 4.3: New data table

Even with this adjustment of the injection velocity, during the COC session some issues were experienced . It was not possible to carry out all 16 recipes. To be precise, in the last two recipes, a broken part was obtained (see Figure 4.6) with high values of Mold temperature (120°C) and Packing pressure (80 MPa).

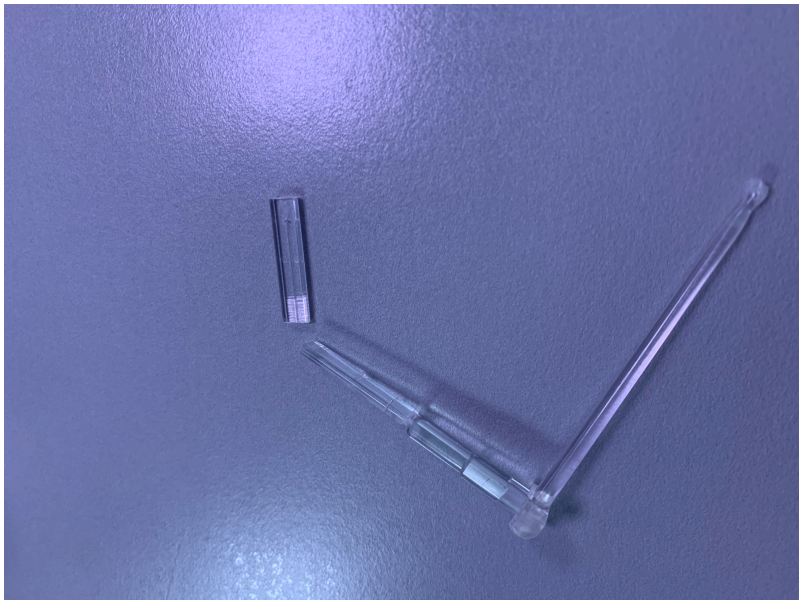

Figure 4.6: Effect of an high Packing pressure. Note that the part is broken in the middle, hence discarded for the metrology analysis.

4.4.2 PMMA production

Basically all the procedures followed for COC and described above are the same of the PMMA. Before proceeding with the molding of the part PMMA was stored at 80 °C for 6 hours as required by the protocol [18]. Then, the strategy is the same as for COC. The same amount of samples collected and even in this case the session took a lot of time because of the need to wait between one recipe and the other to have a stable process.

The initial values of the DoE are reported in Table 3.3, but during the session it was noticed that with 90 and 120 mm/s of injection speed the filling times were too short.

For this reason, these values were replaced respectively with 22 and 36 mm/s. (see Table 4.4)

Factors	Level 1	Level 2
Mould temperature [°C]	65	85
Melt temperature [°C]	220	240
Packing pressure [MPa]	90	120
Injection velocity [mm/s]	22	36

Table 4.4: New data for PMMA

In addition, another issue was experienced. after the tenth recipe, as it can be seen from the picture 4.7, the mold was damaged, which caused an unacceptable part.

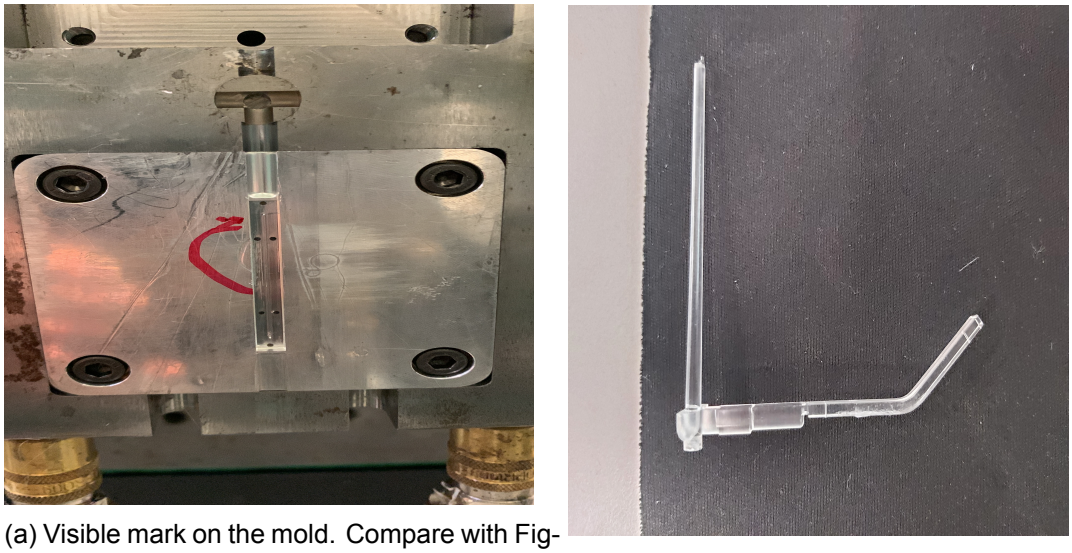

(a) Visible mark on the mold. Compare with Figure 4.4 to see the difference.

(b) Crooked part

Figure 4.7: Experimental issues. The damaged cavity prevents an automatic detachment of the part

If, in future, someone want to repeat the experiments, Tables A.2 and A.3 in the appendix provide details on the process parameters of the two sessions.

4.5 Metrology

After producing the specimens, they were examined in the metrology lab at least 2 days after moulding in order to allow them to shrink and reach their final dimensions. This section will describe the machines used, the strategy for the measurements, and, finally, the results obtained.

In order to determine how the produced chip warps, a Laser Scanning Confocal Microscope (LSCM), model LEXT™ OLS 4100 [30] manufactured by Olympus company, was used in combination with The *DeMeet 220* coordinate measuring machine. In particular, the first one was used to determine the depth and width of the channel, since these dimensions are in the order of micrometres. *DeMeet 220* was used for measuring length. If the DeMeet220 had been used for depth and width, there would have been a large uncertainty in the measurement of the chip.

The measurements of the depth and the width of the micro-channel were based by taking three acquisitions in three different positions (TOP,MID,BOTTOM) for each sample, to see if there is a variation of them along the length of the channel.

The microscope was focused manually using a 10X magnification lens (image size of 2564 µm x 2568 µm). Image acquisition was performed using the LEXT™ software (Olympus® OLS 4100. Product version: 3.1.9) which allows the user to preview the image and give a rough estimate of the dimensions.

All the acquisitions were performed by using a manual setup with *FINE* option. Once identifying the bottom and the top of the channel by regulating the focus, an acquisition was taken. All images were captured from the same perspective to allow an easier post-processing.

Finally, all the LEXT files were stored in a pen drive and subsequently treated using the

SPIP® software [15][24]. Here, after applying the suitable filter, a profile was created by selecting the Line Drawing toolbar button and a line was drawn on the image.

The software would then create the corresponding profile (Figure 4.10). In each acquisition three cross sections were evaluated in order to obtain a more accurate average value for each position along the length of the micro-channel. Hence, in total, $3 \cdot 3 = 9$ measurements were taken for each sample.

For the length three measurements were taken for each sample.

An uncertainty evaluation was also conducted, in order to verify the quality of the measurements. This has been estimated based on the ISO 15530-3 [16]. The uncertainty was calculated with a coverage factor $k = 2$ to achieve a confidence level of 95 %.

4.5.1 Mold measurements

Not only measurements of the molded parts have been done, but also the cavity was measured to compare the CAD values (Figure 4.8a) with the ones obtained with the microscope; the values measured were used then for estimate the shrinkage. The same strategy mentioned for the chip was adopted to evaluate the depth and the width of the micro-channel in the mold, but in this case 7 measurements were taken for bottom, middle and top (see Figure 4.9). The length was measured with DeMeet.

In Figure 4.8b, a picture of the equipment is shown.

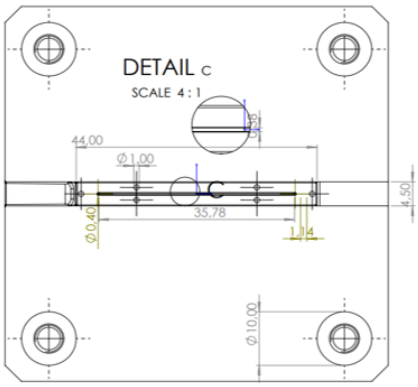

(a) Mold design specification.

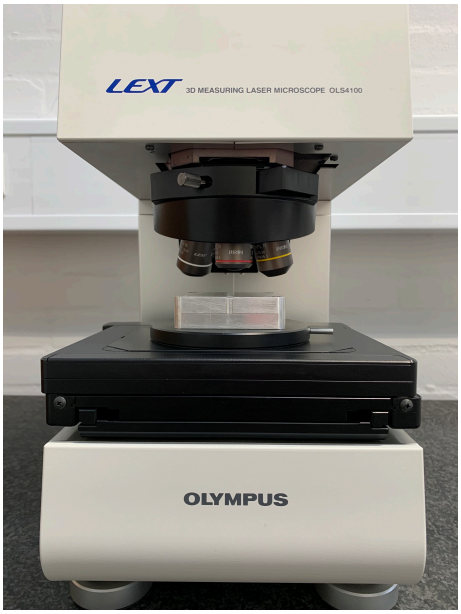

(b) LEXT™ Light Optical Microscope used for measurements of the mold.

Figure 4.8

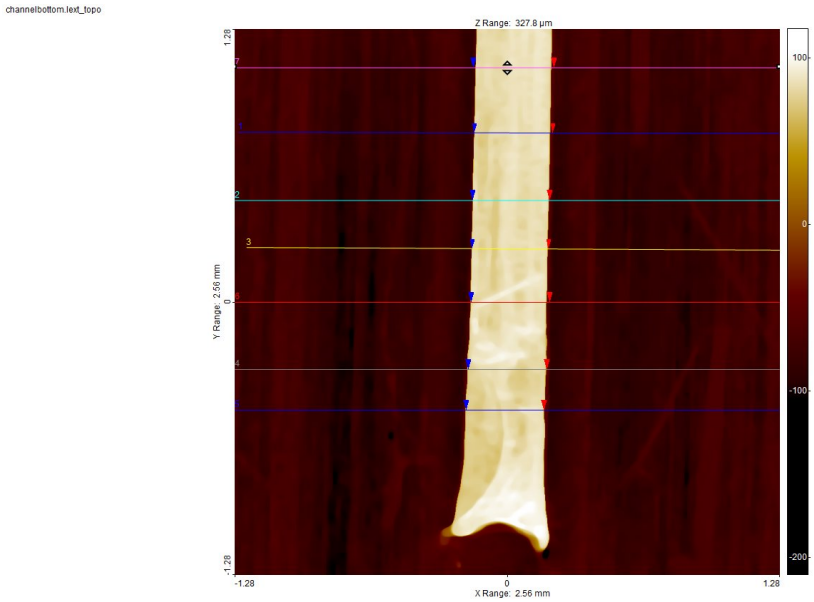

Figure 4.9: The picture shows the 7 cross sections evaluated on the bottom

Channel depth

Once taken the acquisition with LEXT™, the file was open on SPIP™ to analyze the cross section. To reduce noise, the filter *Mean 15x15 full* was used. Picture 4.10 shows the 3D profile of the section on one side, and on the other the cross section profile.

Note the blue and red cursor located on the top and bottom of the channel. In this mode, it is possible to interactively move the blue and red cursor to cause the associated distance and height values to be displayed in the box to the right. The height difference is given by M2-M1.

It is clear that the depth measure might changes a little bit because there are some peaks in the profile.

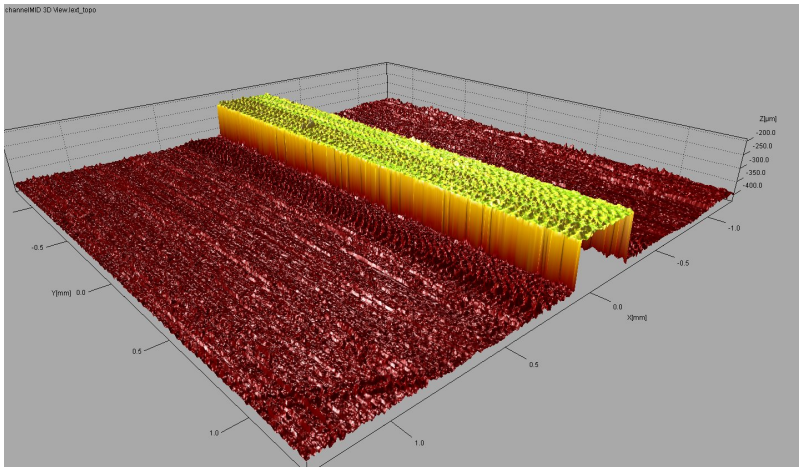

(a)

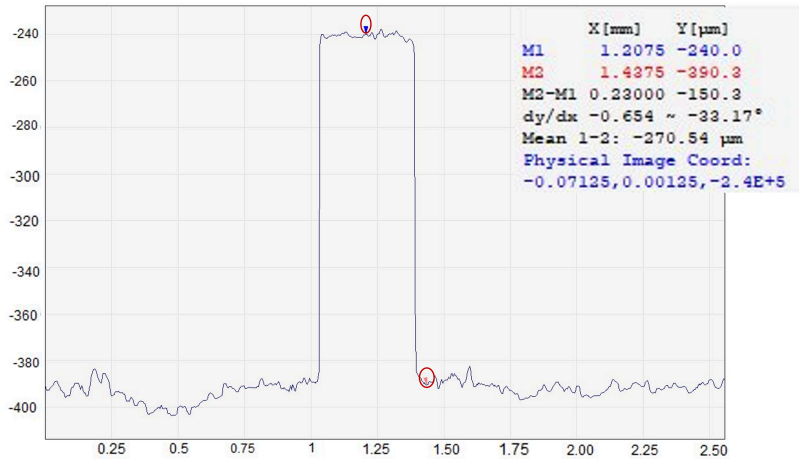

(b)

Figure 4.10: Measurement Settings. (a) 3D view of the section; (b) Note the two arrows on top and bottom of the section. This is the profile after the application of the filter.

Channel width

The width was measured using a procedure similar to the one just described. This time, the two arrows are located on the opposite side of the channel to take the width. The built-in function *mean 15x15* was used to reduce noise.

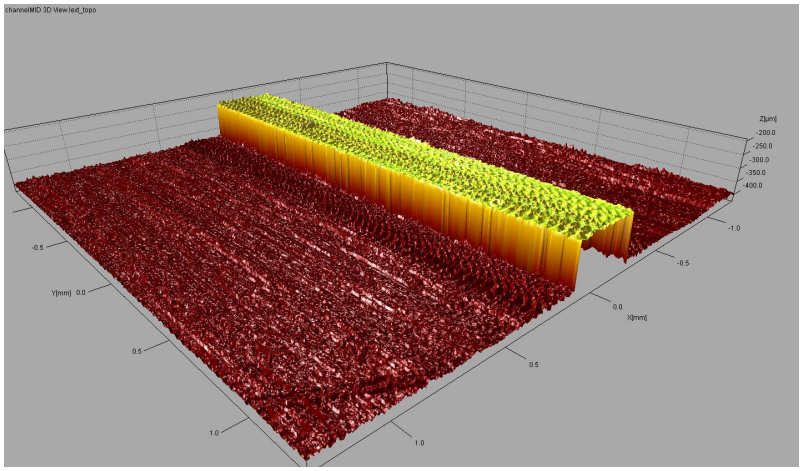

(a)

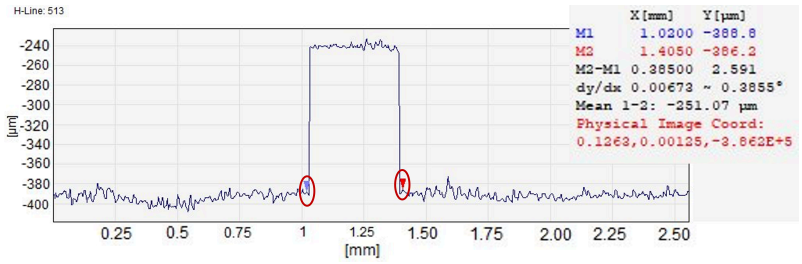

(b)

Figure 4.11: Measurements Settings. (a) 3D view; (b) Image after noise reduction. Note the two arrows in the opposite side of the channel.

The measurements settings are reported in the Appendix (Table A.4 and A.5). For the channel length the same procedure as for the chip was adopted. See Section 4.5.2.

Results

The Table 4.5 presents the average length, width and depth for the micro-channel of the mold. Are reported also the values derived from the CAD (Figure 4.8a). It is important to underline that the channel width and depth were measured with LEXT™, unlike the length, which was performed using DeMeet.

For the measured values also the uncertainty was reported.

	Length [mm]	Width [µm]	Depth [µm]
Channel (CAD values)	35.78	380	147
Channel (measured values)	36.054 ± 0.105	375.8 ± 1.5	149.4 ± 0.7

Table 4.5: Mold measurements results.

The plots showed in Figure 4.12 must be kept in mind for the measurements of the chip. We will see a similar distribution of the depth and width on the produced chips, in particular all the samples have a minimum of width in the mid section.

We can observe that the depth of the mold increases from the top to the bottom, with

a very small deviation of the measurements. All the values are within a range of $\pm 5 \mu m$ except for the outliers. With regards to width, the minimum is in the middle with a deviation slightly larger than the depth (within $\pm 10 \mu m$).

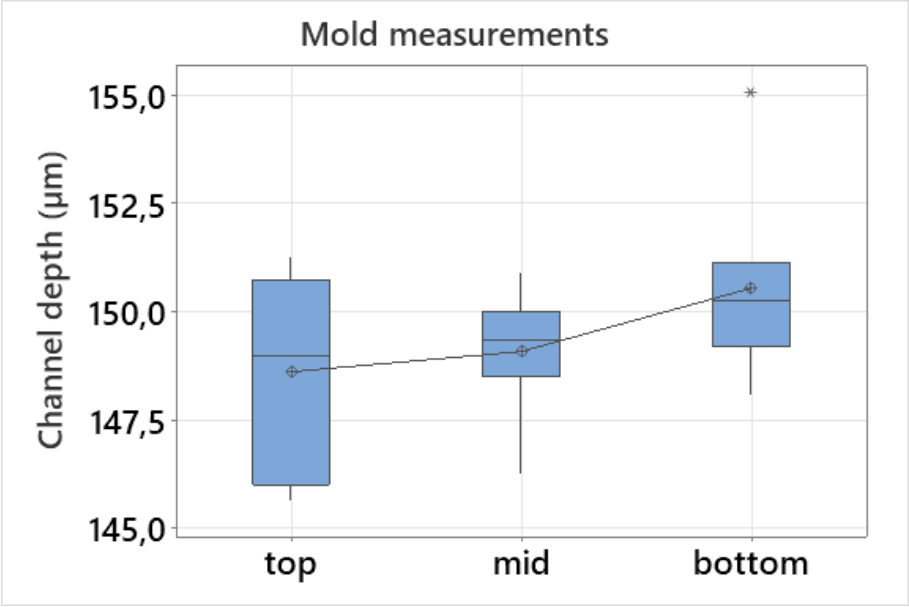

(a) Depth plot along the channel

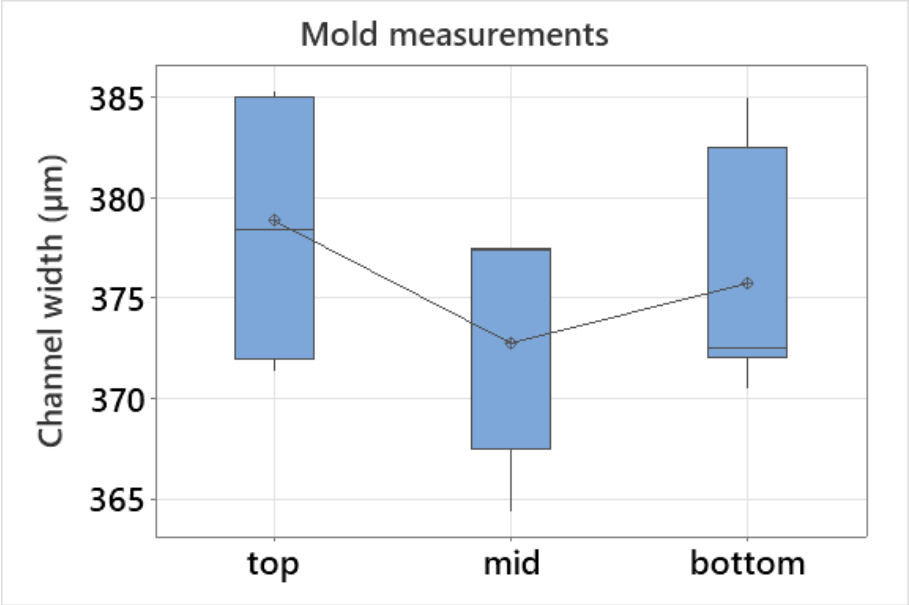

(b) Width plot along the channel

Figure 4.12: Mold measurements results. In each boxplot there are 7 measurements.

Some scratches have been detected in the surface of the mold, perhaps caused by the manufacturing process.

4.5.2 Chip measurements

As anticipated in the previous paragraph for each combinations of parameters (i.e., recipe) were measured three parts to have more data to analyze. In Table A.6 it can be seen the details of the acquisitions made with the microscope.

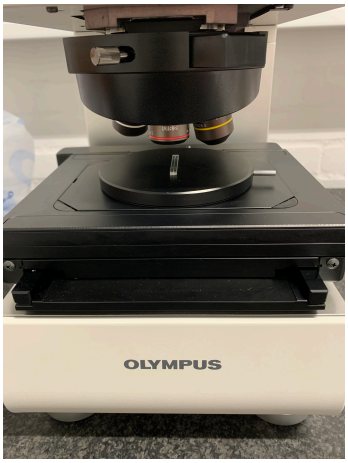

(a) Set-up

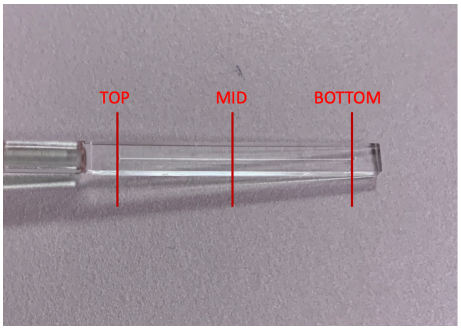

(b) This picture shows where have been taken the acquisition

Figure 4.13: Picture from the metrology session

Channel width and height

Once imported the LEXT files, three cross-section profiles have been created as seen in Figure 4.14 for each acquisition. The profiles obtained with SPIP™ (version 6.7.7) was filtered in order to reduce the noise. After clicked on *noise reduction*; *Median 15x15 full* was chosen.

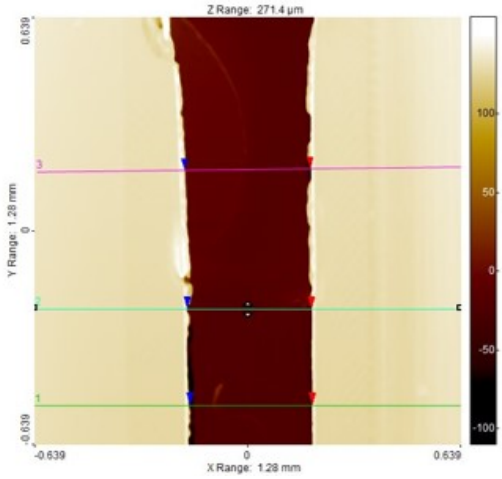

(a) Bottom

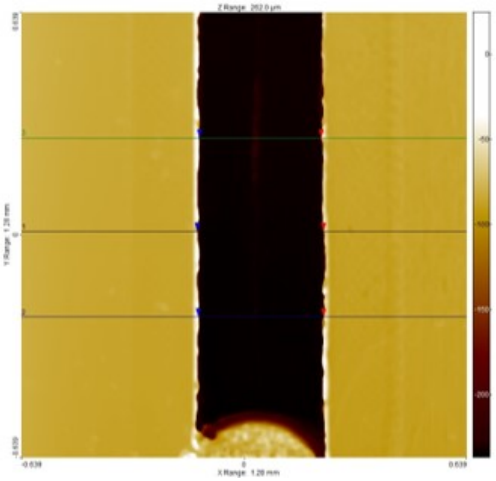

(b) Top

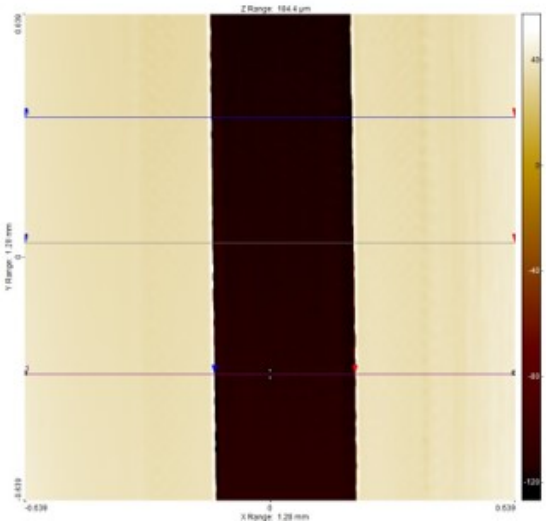

(c) Middle

Figure 4.14: SPIP™ Set-up for width. 3 cross sections for each acquisition. The colored bar indicates the height measured by the microscope. The images were taken with a 10X magnification lens.

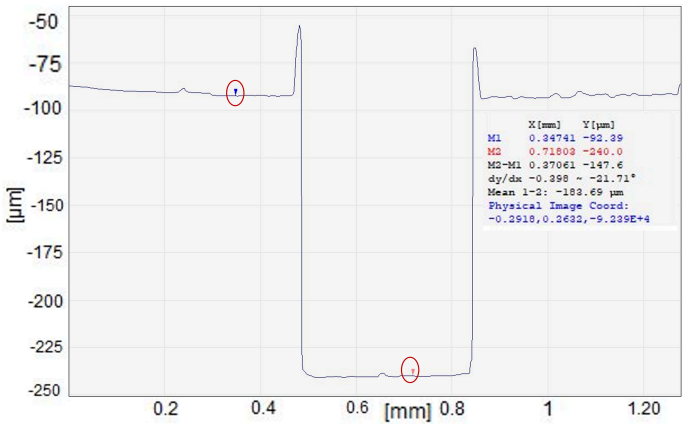

(a) depth

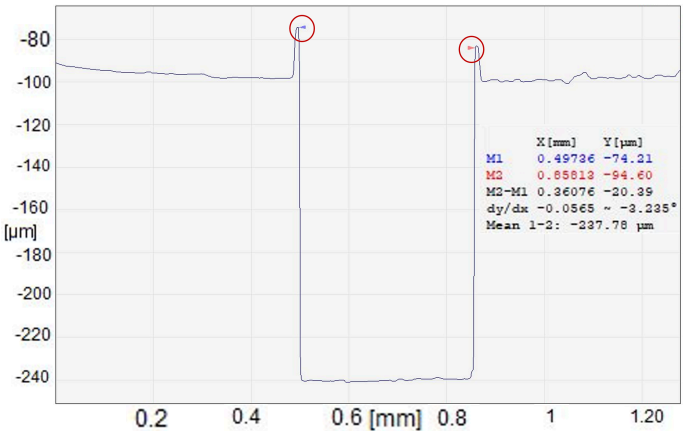

(b) width

Figure 4.15: Note that the width is calculated locating the two arrows in the limit part for each side of the channel, while the depth by locating the blue arrow at the highest point and the red one at the center bottom of the channel.

Channel length

The DeMeet 220 optical CMM machine [23] was used only for the measurements of the length since it has a resolution of 0.1 µm. To be more precise in the measurements, the used references should be constant from one part to another; hence, using the DeMeet® software (Approve for DeMeet®, 1.3.3) after selecting the built-in *circle* function, as it can be seen in Picture 4.16, a red circle was inscribed in the inlet/outlet hole. The length of the channel is measured as the distance between the center of the inlet/outlet hole. This choice ensure an optimal approximation of the measurements. Each measurements was repeated 3 times.

In Table A.7 are reported the settings for the DeMeet.

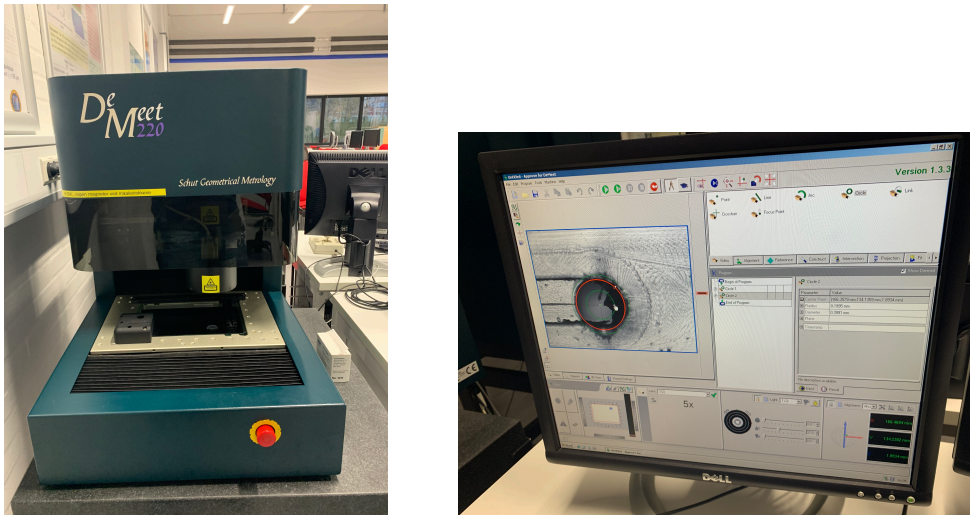

(a) DeMeet machine (b) Reference point:inlet/outlet holes

Figure 4.16: Set-up measurements for the channel length

Results

In Table 4.6 are seen the average length, width and depth of the produced parts, the values obtained from the CAD file and the values measured from the mold.

	Length [mm]	Width [µm]	Depth [µm]
CAD files	36.093	375	150
Mold (measured)	36.054$\pm$0.105	375.8$\pm$1.5	149.4$\pm$0.7
COC - Produced part	35.819$\pm$0.007	369.5$\pm$1.1	148.6$\pm$0.7
PMMA - Produced part	35.883$\pm$0.008	366.0$\pm$1.1	149.0$\pm$0.6

Table 4.6: Chip measurements results

The box plots in Figure 4.17 [26] show the results of the depth along the channel. The differences observed in the dimensions along the channel can be explain looking at the same distribution of the mould insert.

Keeping in mind the mold values, for PMMA it can be concluded that:

- Observing the distribution in the plot, the depth of the micro-channel increases from the top to the mid and remains almost constant from the mid to the top.
- In the boxplot of the top section, both the mean and the first quartile are higher than the mid one.
- In the boxplot of the bottom section, compared to that of the mid section, the variance is higher.
- The asterisk, in the boxplot of bottom section, identifies some outliers, which could be caused by noise in the acquisition, which negatively affects the measurements. In this case, the reason could be explained by looking at the bottom section (see Figure A.10), which has a step, that might bring different values. In fact, if the slider is located above the step, the height would be lower compared to the other sections.

- Cumulative means that include all the samples collected.
- It is important to note that the difference in average height between top and mid is in the order of $1\mu m$, so the values are relatively close to each other.

For COC it is worth pointing out:

- At first glance, observing the plot the average depth shows a very little variation along the length of the micro-channel.
- Even though the mean is almost at the same level for the sections, the first and the third quartile in the top boxplot are lower compared to the mid.
- The boxplot in the bottom section shows the highest variance of the measurements and the lowest first quartile.
- The outliers, in this case, are present in both mid and bottom sections, as it can be seen by the presence of asterisks (*). For the bottom section the reason could be again the step. Regarding the mid section, it might be due to errors in the acquisition or in placing the arrows in SPIP™.
- The data range $\pm 2\mu m$ from the average value.
- This graph is cumulative of all the collected samples.

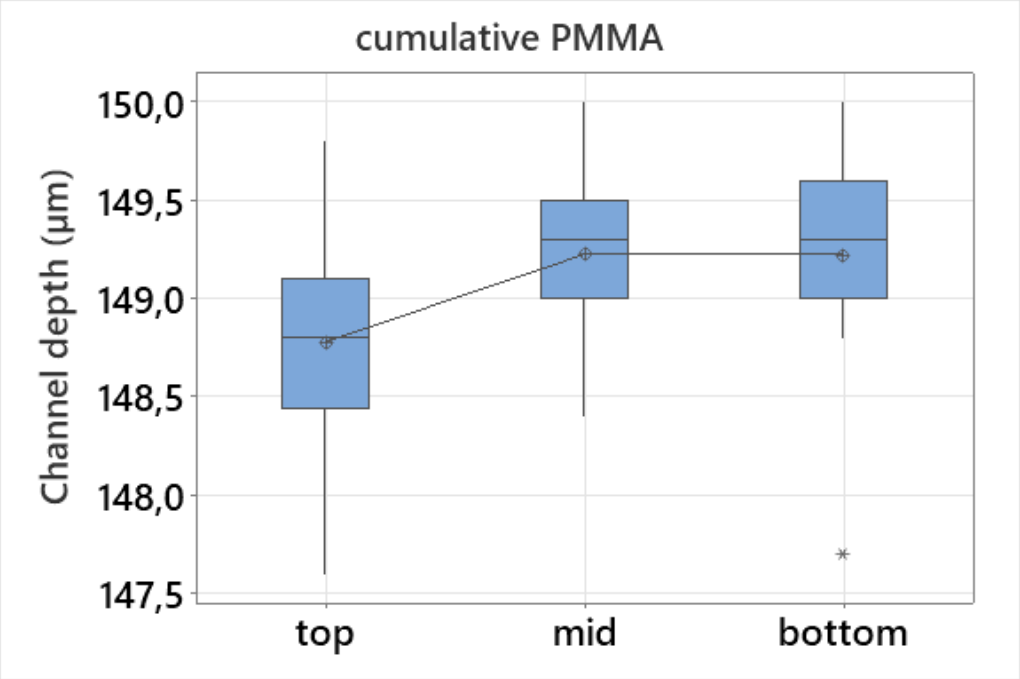

(a) Channel height measurements for PMMA

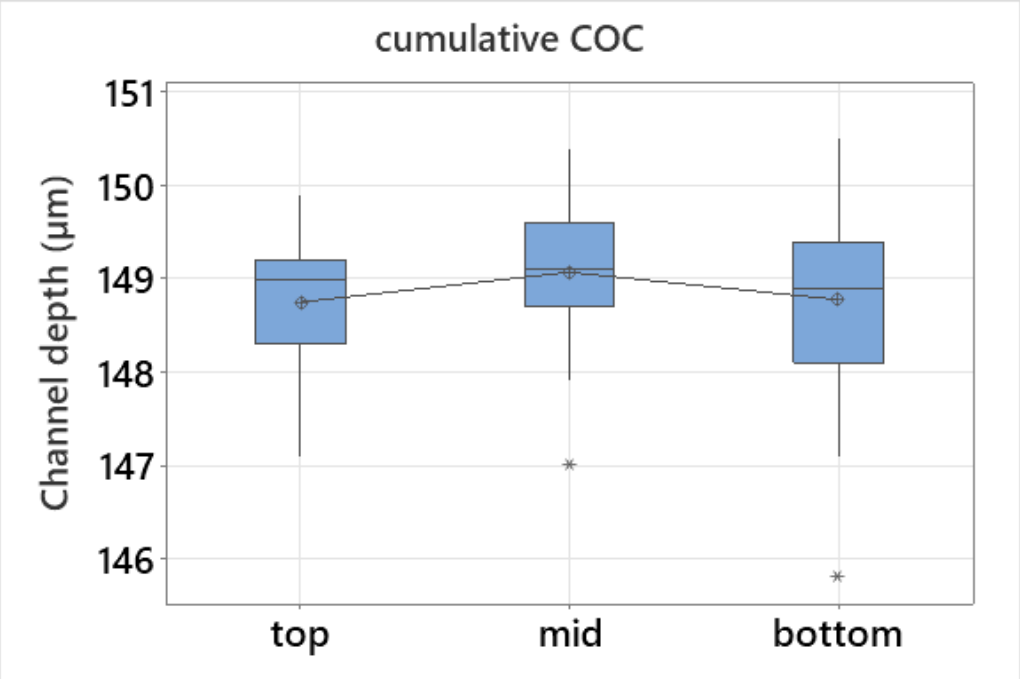

(b) Channel height measurements for COC

Figure 4.17: Channel height measurements. The boxplot includes all the values.

The figure 4.18 offers an interesting comparison between the two materials.

Some outliers can be noted in COC measurements. In particular these refer to the 2nd and 9th recipes of the DoE, where the values of the measurements are far away compared to the simulations. (see Figure A.17). The means in the boxplots correspond to 149 µm for PMMA and 148.6 µm for COC.

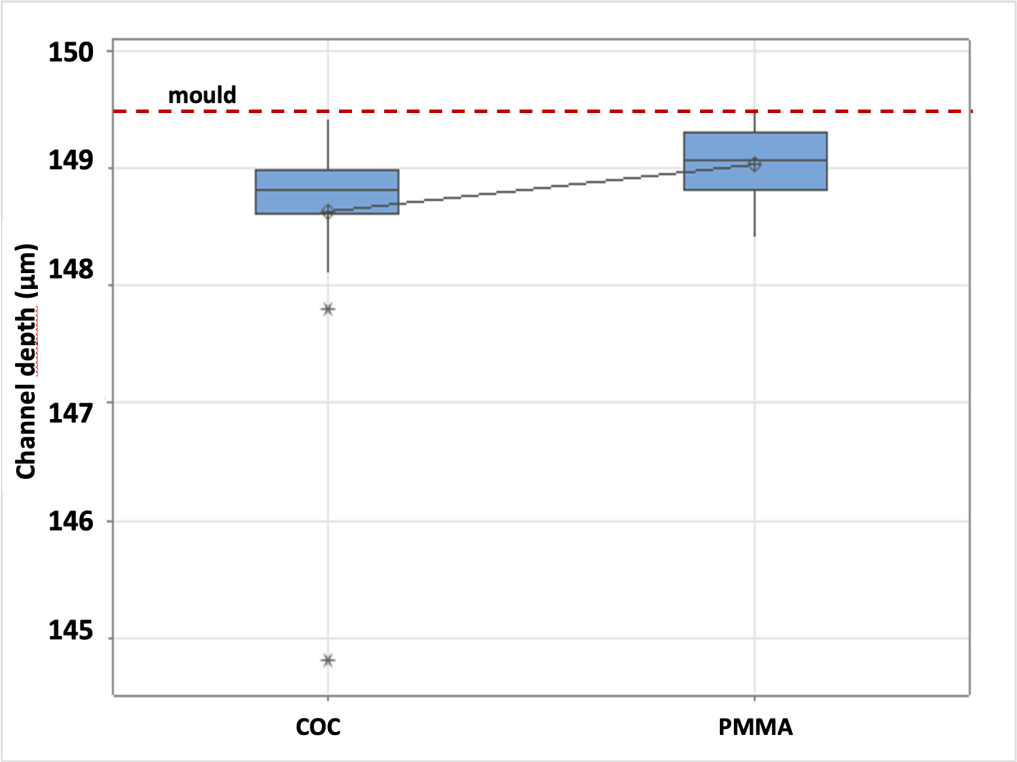

Figure 4.18: Height materials comparison. COC shrinks more than PMMA in this direction.

The results of the width along the channel are reported in Figure 4.19[26]. Some comments can be made:

For PMMA

- The distribution of data in the three different sections looks very similar to the one of the mold, this confirmed that the minimum in the mid section is due to non constant dimensions of the mold.
- The variance of data (i.e. height of boxplot) in the top and bottom section is almost equal. The mean value is higher in the top section.
- Observing the plot, the tendency of the width of the micro-channel is to decrease from the top to the mid, and to increase from the mid to the bottom.
- For the mid section, the one with the highest dispersion of data, the 50 % of values are included in a range of 7 µm. The measure is stable.

For COC the distribution is similar:

- The mid section, even though has the highest dispersion of data, includes the 50 % of the measurements in a range of 8 µm. This indicates a good stability of the measurements.
- The highest mean value is in the bottom section.
- Some values out are observed in the top section, but except of this, the distribution of data are in the range of $\pm 10 \mu m$ around the mean value.

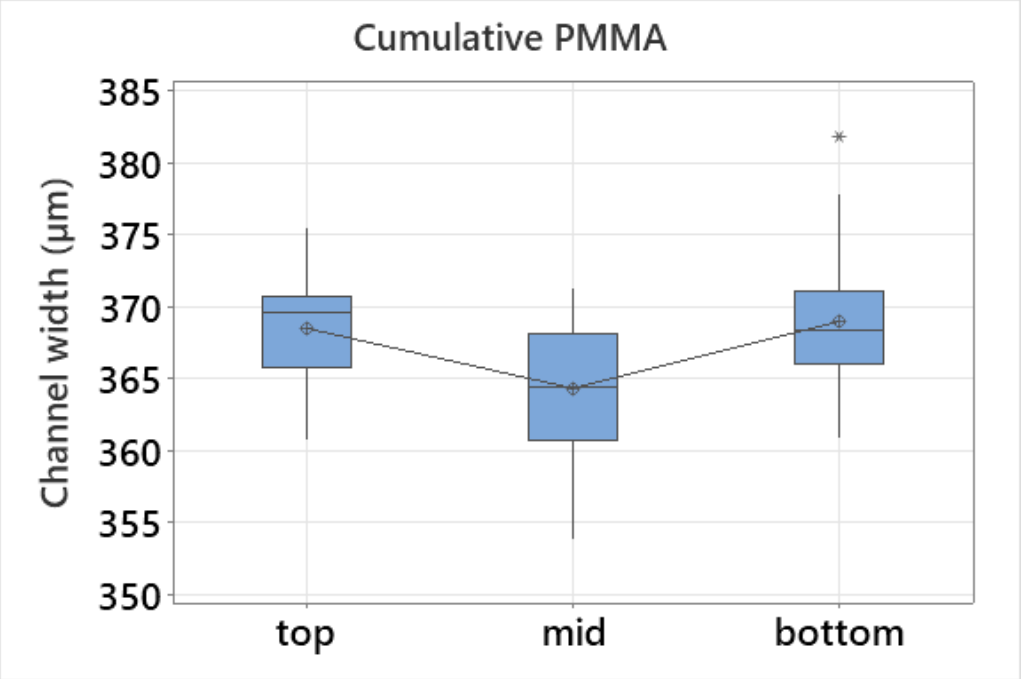

(a) Channel width measurements for PMMA

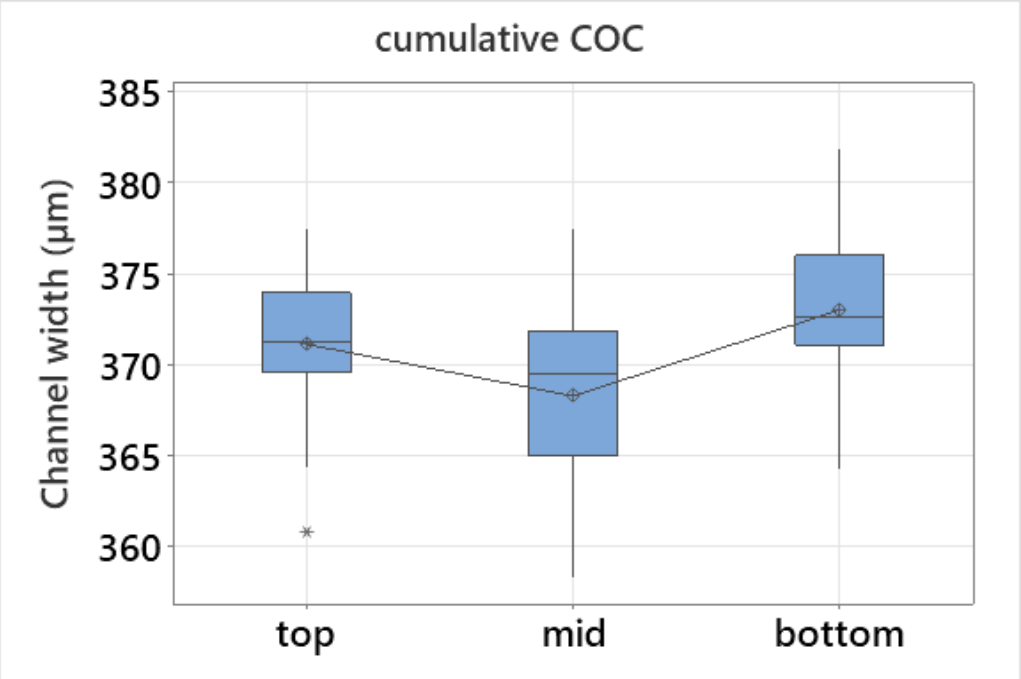

(b) Channel width measurements for COC

Figure 4.19: Channel width measurements derived from the produced parts.

The Figure 4.20 depicts, in one chart, the distribution of width for COC and PMMA.

With regard to PMMA, nothing relevant is observed, because the results are relatively close to each other (Figure A.21). On the other hand for COC we can note the outlier which correspond to the second recipe (see Figure A.18).

The measured value is, as a matter of fact, over the mold, which means expansion.

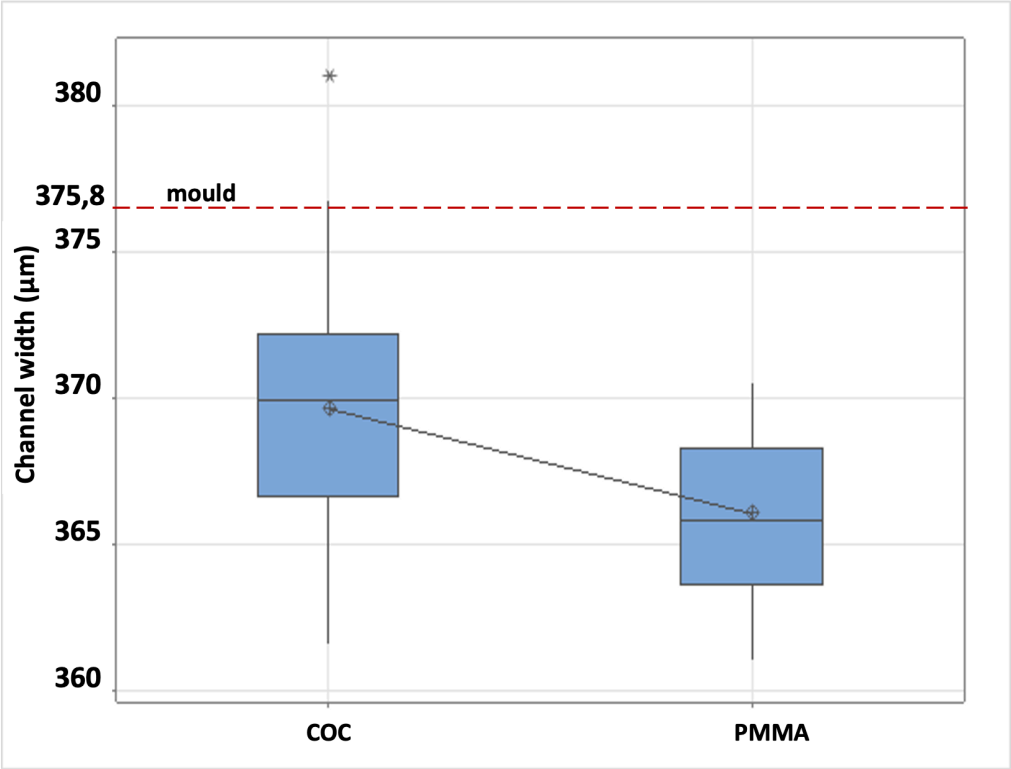

Figure 4.20: Width materials comparison. COC shrinks less than PMMA, unlike the height.

For the length, the target value derived from mould measurements is 36.054 mm. Results are reported in Figure 4.21. All the measurements are below that value, showing again the presence of shrinkage.

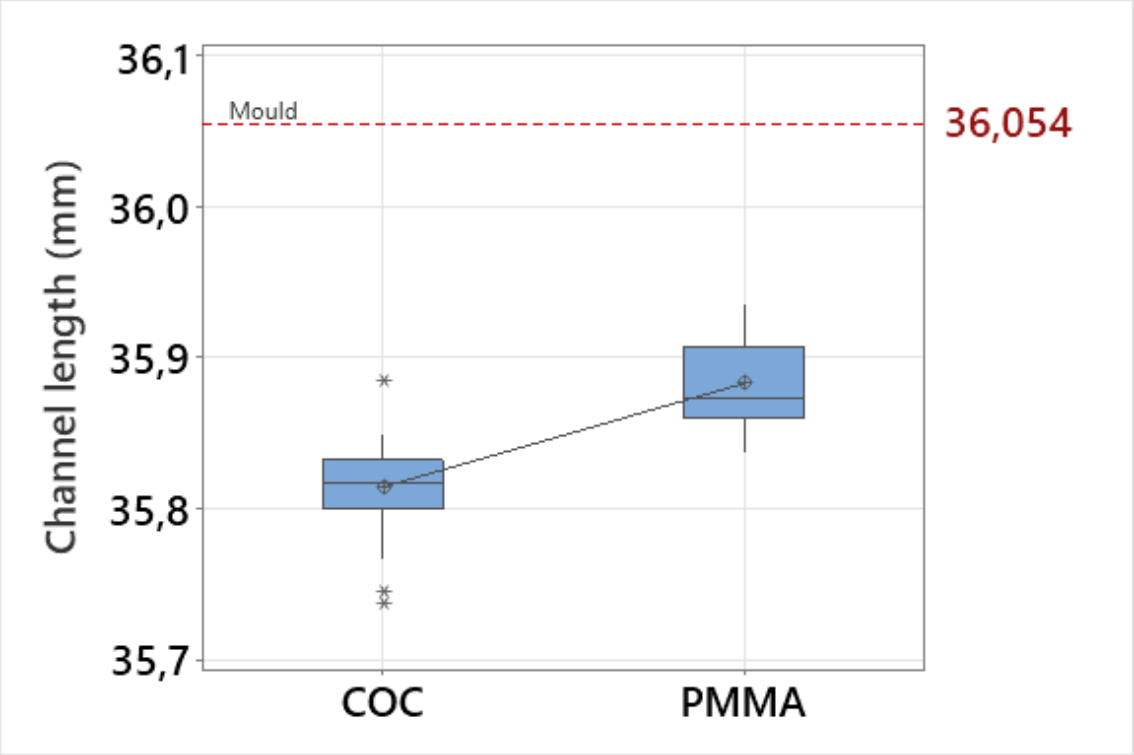

Figure 4.21: Length materials comparison.

4.5.3 Uncertainty Evaluation

The measurement uncertainty was evaluated according to the procedure detailed in the ISO 155330-3 [20]. The uncertainty calculation is defined as follows:

$$U = k \cdot u_c$$

Multiplying the u_c by a coverage factor k gives a result which is called the combined expanded uncertainty, usually shown by the symbol U. u_c is the combined standard uncertainty, which can also be written as:

$$U = k \cdot \sqrt{u_{cal}^2 \cdot u_p^2} \tag{4.1}$$

k is the coverage factor that gives a particular confidence level for U; it was assumed $k = 2$ providing a level of confidence of approximately 95%.

Moreover, assuming that the input quantities in the formula are independent of each other, the combined standard uncertainty was found using the law of propagation of uncertainty by squaring the uncertainties, adding them all together, and then taking the square root of the total. Two uncertainty contributions were taken into account:

- u_{cal} is the standard uncertainty of Calibration (information supplied by DTU Equipment Information System); $u_{cal} = 0,3\mu m$ (LEXT) $u_{cal} = 2\mu m$ (DeMeet)
- u_p is the standard uncertainty of the measurement procedure and corresponds to the standard deviation of the n repeated measurements;

$$u_p = \frac{STD}{\sqrt{n}} \tag{4.2}$$

The number of measurements n used to calculate STD corresponds to the samples investigated. For COC, 3 samples for each of the 14 combinations ($n = 42$). For PMMA the recipes molded are 11, hence 33 different measures.

The extended formula to calculate the combined standard uncertainty u_c would include other error sources (e.g. workpiece expansion, instrument expansion and so on) but in this case were neglected.

Uncertainty Contribution	**length [mm]**	**width [µm]**	**Depth [µm]**
STD	0,011	2,87	0,82
u_p	0,003	0,44	0,13
u_{cal}	0,002	0,3	0,3
U (k=2)	0,007	1,1	0,7

Table 4.7: Uncertainty contributions and expanded uncertainty U for COC.

Uncertainty Contribution	**length [mm]**	**width [µm]**	**Depth [µm]**
STD	0,009	2,78	0,47
u_p	0,003	0,48	0,08
u_{cal}	0,002	0,3	0,3
U (k=2)	0,008	1,1	0,6

Table 4.8: Uncertainty contributions and expanded uncertainty U for PMMA.

The uncertainty was also calculated for the cavity measurements. The uncertainty was calculated using Equation 4.1 and always a coverage factor *k*=2. In the calculation of width and depth $n = 21$, as a matter of fact was taken 7 measures for the three cross sections. For length $n = 7$. The uncertainties are presented in Table 4.9

Uncertainty Contribution	**length [mm]**	**width [µm]**	**Height [µm]**
STD	0,139	3,05	1,01
u_p	0,052	0,67	0,22
u_{cal}	0,002	0,3	0,3
U (k=2)	0,105	1,5	0,7

Table 4.9: Uncertainty contributions and expanded uncertainty U for the cavity.

4.6 Injection molding defects

In the first part of the project, the sinkmarks that were reported during the previous production with PMMA Lucite [3], addressed the efforts into the investigation of the proper

process parameters that can avoid this type of defects. The picture 4.22b shows the relevant sinkmarks between the hole and the ejector pin mark. Changing the material from PMMA Lucite to COC, the entity of the defect is negligible, 14.26 µm depth against 87.84 µm of PMMA Lucite (Figure 4.23b). The latter in particular could be noted without the microscope, simply touching the surface of the workpiece.

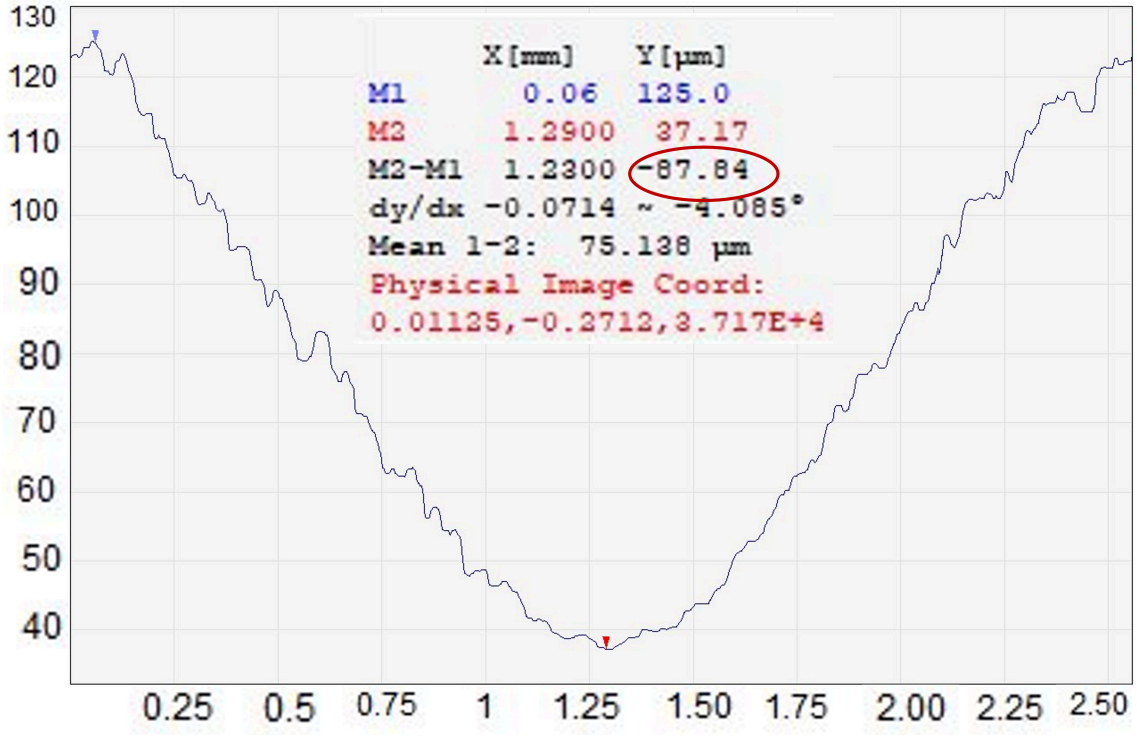

(a) cross section

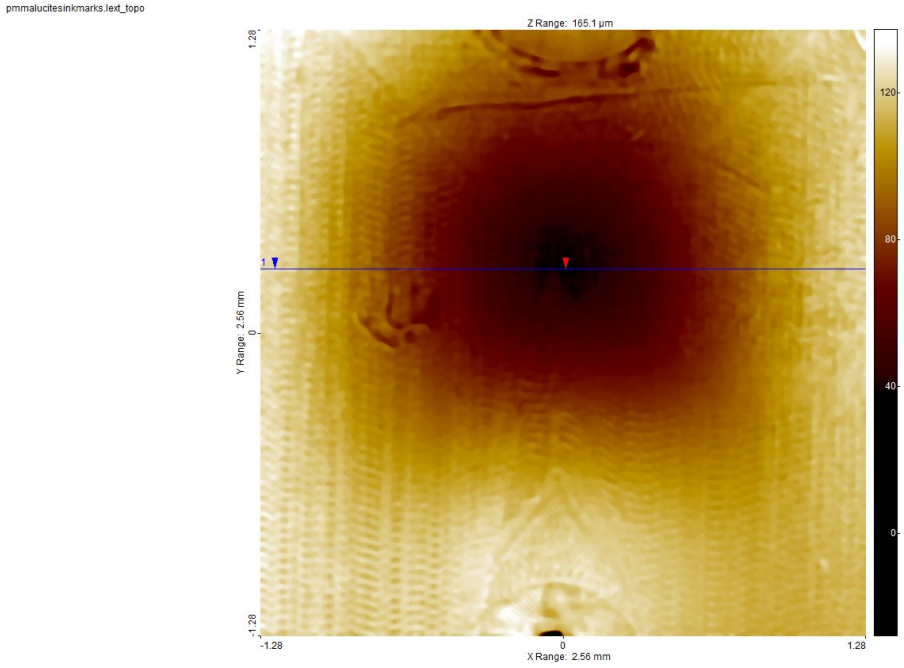

(b) view from above

Figure 4.22: PMMA Lucite

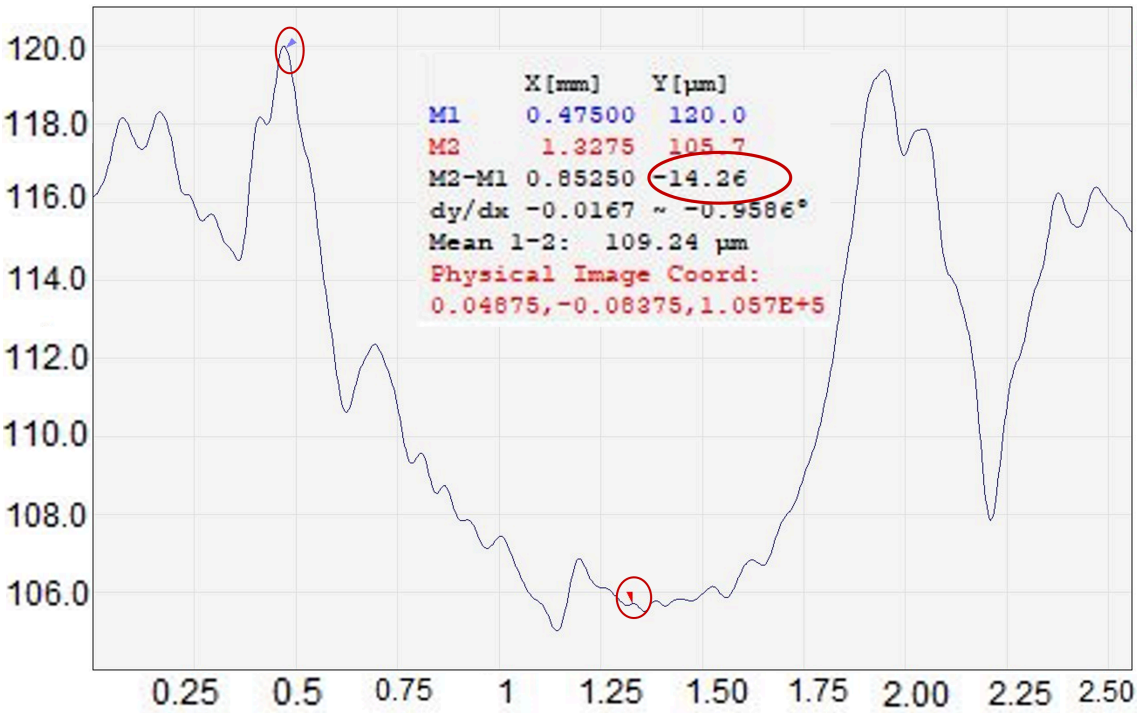

(a) cross section

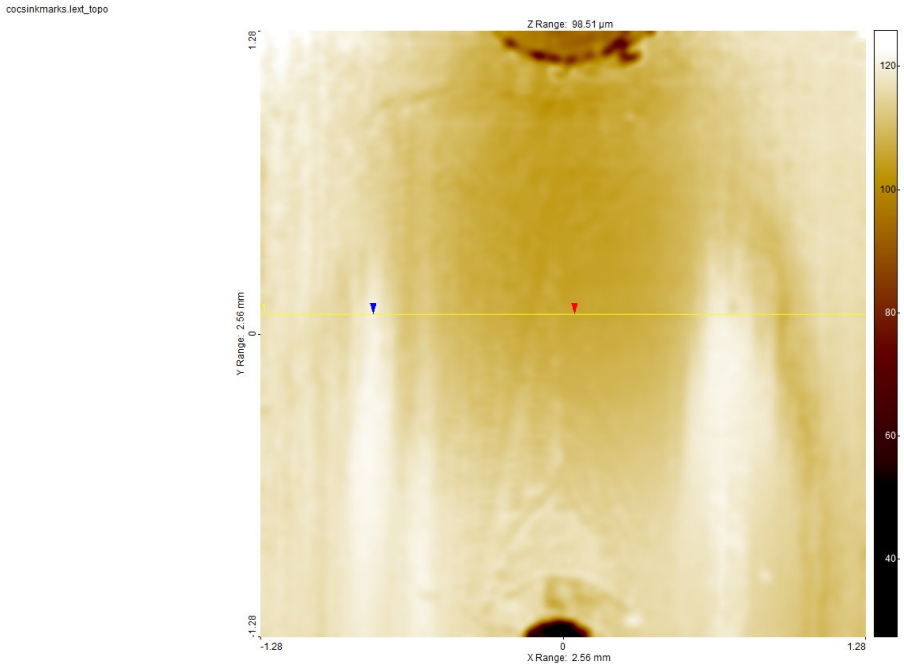

(b) view from above

Figure 4.23: COC

Other microscopic pictures of the samples revealed the presence of several common injection-moulding defects, and, some issues that were experienced in the production. In the figure 4.24a it can be seen the droplets of oil that fell on the parts during the first COC production.

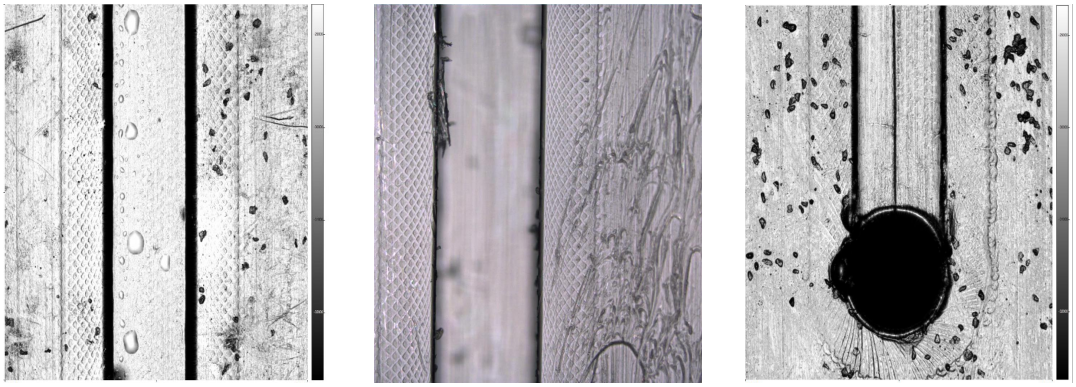

(a) Oil drops (b) Scratches (c) Air bubbles and breach

Figure 4.24: Metrology picture of the produced samples

In Figure 4.24c it was detected a breach along the channel. This can be explained by the fact that mould and part are at different temperatures. They have different thermal expansion coefficients throughout the cooling process, hence the risk is the formation of residual stress and consequently, breaches. Some PMMA workpieces contained air bubbles (Figure 4.24c). This could be a result of an high injection speed or due to the plastic materials that may have absorbed a certain quantity of moisture. This surface defect was observed actually with higher values of injection velocity.

Certain PMMA samples contained scratches in the surface, as illustrated in Figure 4.24b, which could be explained with the damage of the mold occured during the session. As a matter of fact, an improper mold matching design bring the core and the cavity to be misaligned during the mold opening process, making the product to be prone to scratches.

5 Moldex3D simulations

5.1 Simulation set-up

In this section, each step of the simulations in Moldex3D will be explained. The detailed procedure is as following:

- Importing the CAD model
- Selecting the material
- Meshing
- Set-up proper process Parameter
- Run Analysis
- Result analysis

By setting the process parameters it is possible to specify the Mold temperature, Melt temperature, injection velocity and packing pressure. At the start of the project, the plan was to carry out all 16 simulations of the Design of Experiments (DoE) to optimize the shrinkage of the part.

A brief flow chart of the procedure followed in Moldex3D is reported in Figure 5.1

Figure 5.1: Flow chart of IM simulation

5.1.1 Importing CAD and attribute

The first step is importing the given CAD file, giving a name to the project and attributing the function of each components; in this way the program can distinguish between the different parts. In this case there are three different parts in the assembled model: two cold runner and the part on which will be focused the attention. In the next section will be provided the details. A pin gate was positioned on the top of the cold runner.

5.1.2 Selection of the material

Good simulation result relies on many factors, and material is the crucial one. The second step consists of selecting the material, for both of the ones used in the production Moldex3D wizard provide the same exact grade of material. This ensure to have good agreement in the behaviour of the polymer when fill the cavity.

In the chart below it can be seen the PvT curve for COC and PMMA LG 840 taken from software database. For other properties see appendix A.11. The machine ARBURG 370 A 600-70-18 used for the experiments was also present in Moldex3D and hence used in the simulations.

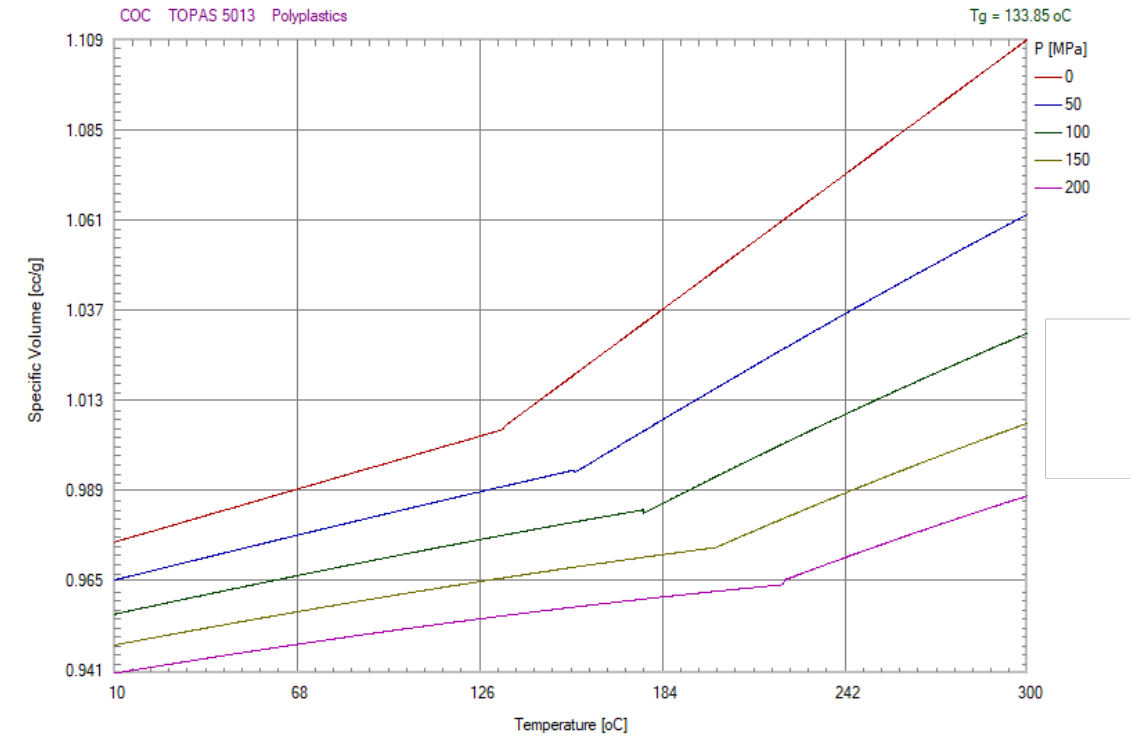

(a)

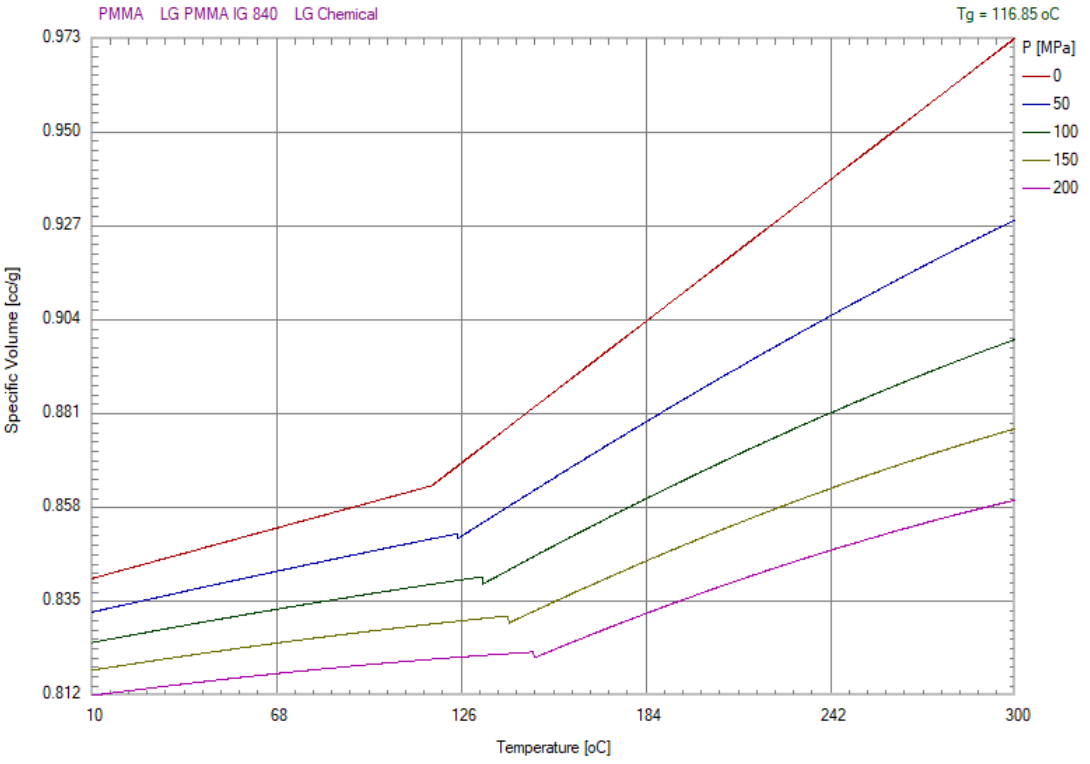

(b)

Figure 5.2: Material properties. (a) PvT chart for COC (b) PvT chart for PMMA LG 840 [29]

5.1.3 Cooling system

Once the moldbase had been created, it was set its dimensions in the workspace. For the cooling layout it was followed the default values, except for the parameter H (cooling channel depth).

Other parameters: diameter of the channel (D), number of channels on the top and bottom (N), distance between one to another (C). All these details are shown in Figure 5.3.

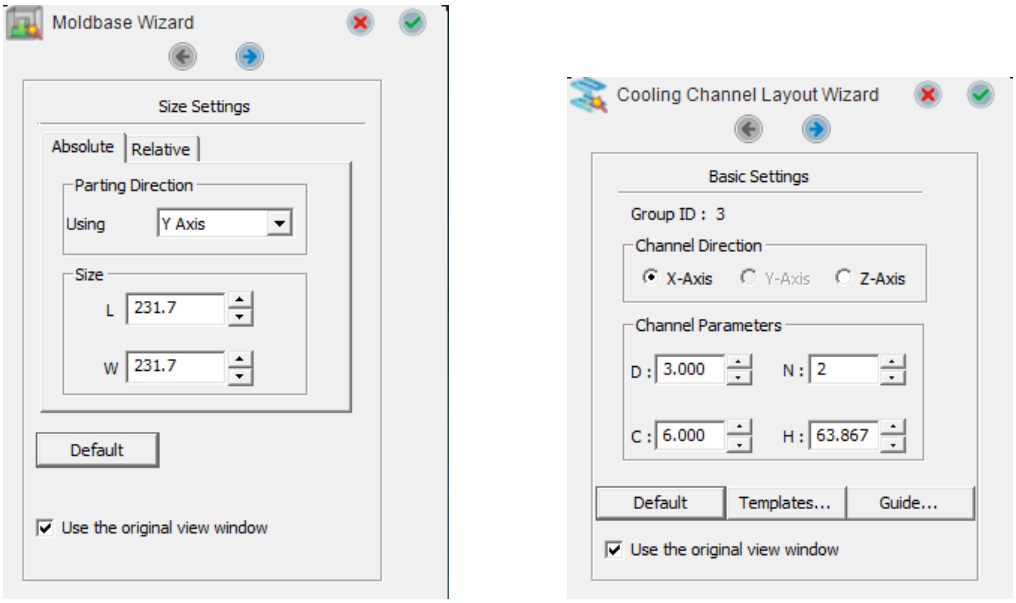

(a) Moldbase wizard (b) Cooling channel Layout Wizard

Figure 5.3: Cooling system layout

H is the most crucial dimension. For the cooling line depth (H) two aspects were evaluated:

- Structural considerations: it is desirable to place the cooling lines far from the surface of the mold cavity, if the cooling channels are too close to the geometry this may lead to warpage.
- The cooling line depth influences the cooling time, the rate of heat transfer is maximized by placing the cooling lines as close to the surface as possible.

After setting cooling channel, Moldex3D has the function *Check Cooling System* which detects possible problems of the current cooling channel. If certain errors occur in the cooling system, a warning message appears. Sometimes it could be caused when the cooling channels are too close to the geometry.

5.1.4 Meshing

When working with micro-components, it is necessary to decrease the meshing size to increase the precision of the results. By default, Moldex3D automatically creates a mesh size. In the picture below (Figure 5.4), it has been reported. According to the software, the nodes are about 2.807 millimeters apart from one another; however in this work it is important to focus on the chip results and for this reason it is essential to find a middle point that gives a reasonable compromise between computation time and resolution. As the reader already knows, to determine a proper mesh size two aspect are needed to be taken into account: by decreasing the mesh size more accurate will be the result but

unfortunately this increases the computation time. On the other hand, a low number of elements leads to shorter computation times but results in a less accurate model compared to the smaller mesh. A good user should be aware to find a middle point that gives a reasonable solution between the two aspect before mentioned. A multi-scale mesh was used for the simulations, the default value for the macro mesh and a smaller for the refined near the channel. Table 5.1 reports all the details.

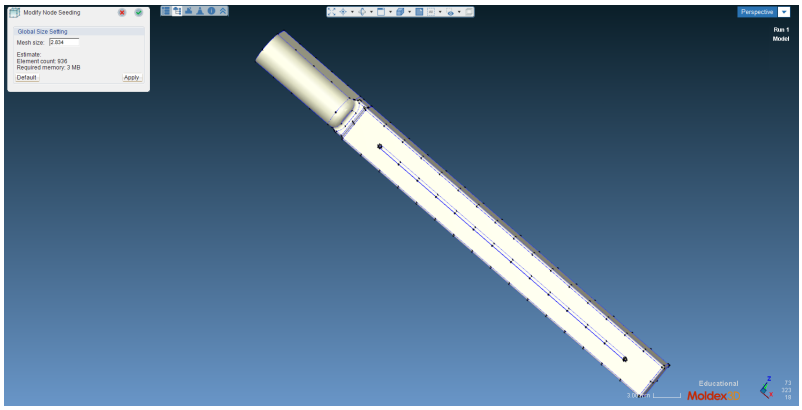

Figure 5.4: Seeding of the chip.

The software give us the possibility to increase the seeding in particular areas that have more complex geometries. After selected the interested geometries their seeds are increased to increase the resolution of the model. As it can be seen in the Figure 5.6, the mesh is denser in the two holes and along the channel, less dense in the rest of the geometry.

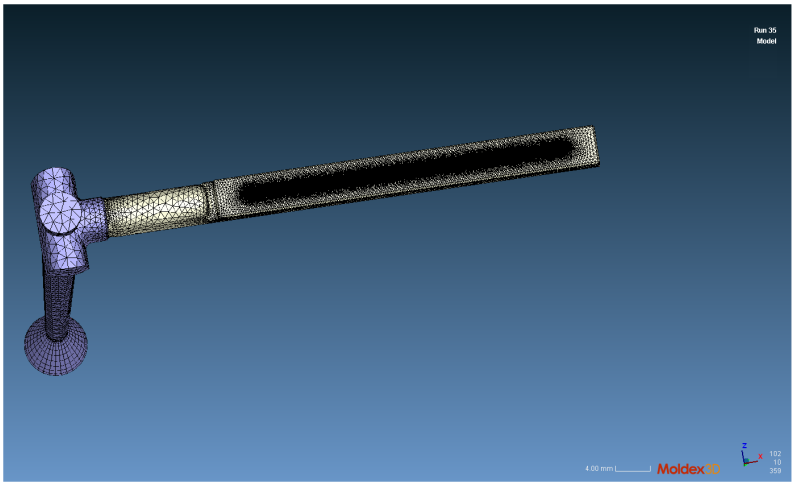

Figure 5.5: Final mesh

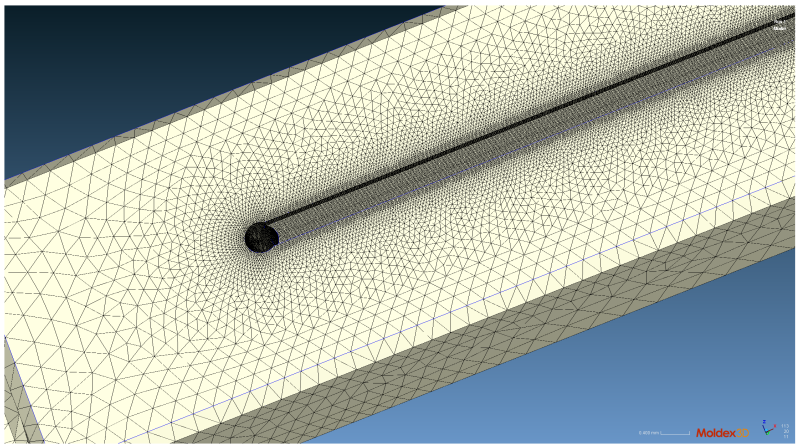

Figure 5.6: Final mesh

Model Details	
Mesh type	Solid
Solid Mesh elements	3,852,421
Part	2,539,700
Cold Runner	23,176
Moldbase	1,234,505
Cooling Channel	55,040
Surface Mesh Elements	253,194
Part	251,088
Runner	2,106

Table 5.1: Mesh details

5.1.5 Process settings

Process parameters are also crucial factors to simulation. Improper process parameters will lead into an unreasonable simulation result, so it is very important that user sets the correct parameters. Once the process wizard has been opened, there is a function *classic mode* in which the user can specify the proper process parameters; compared to simple mode the classic one has more details as it can be seen in the Figure 5.7 below:

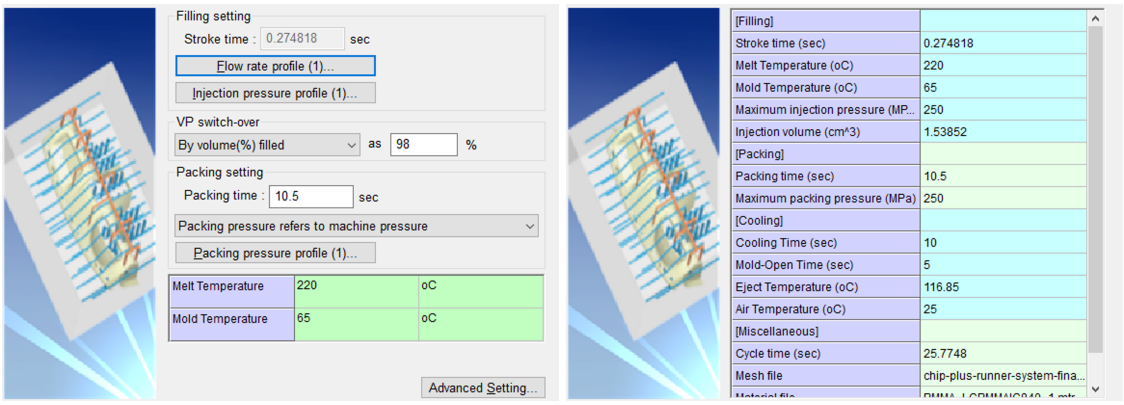

(a) (b)

Figure 5.7: Process settings. (a) Filling/Packing settings (b) Summary of the process wizard

For each combination, in this window were set-up the four parameters of the DoE.

In particular was selected the option *Packing pressure refers to machine pressure* in order to obtain the profile of Packing pressure [MPa] versus time [s]. To adjust the Packing pressure profile making it as close as possible at the one of the machine a setting method was chosen in *Profile type*: Polyline. The packing time used was the same of the production.

The profile of injection velocity was set similar of the injection moulding machine and switch-over at 98 % of filled volume. Regarding the melt temperature it is worth to clarify that the one in the settings is the temperature of the plastic melt at the melt inlet of the mesh model. In practice, it is different from the barrel temperature at the nozzle, as melt temperature may rise due to viscous heating. This might differ from the actual conditions.

5.1.6 Analysis

The software has many analysis types, for this project it has been chosen a Full Analysis-C F P C W, which are the Filling-F, Packing-P, Cooling-C, Warpage-W. The most relevant results will be focus on the warpage of the chip.

5.2 Results

With the complete analysis, the software gives the user a lot of information that can help to predict and optimize the production of the component. Several parameters like Melt temperature and sprue pressure can be visualized but for this project are not relevant. In the subsequent pictures will be report the main results.

5.2.1 Sinkmarks

Sink mark is a depression on the surface of a molded part. Although sink marks do not affect part strength or function, they are perceived to be serious quality defects. Technically, sink mark occurs when inside plastic shrink and the strength of solidified surface layer deforms due to inner pressure of shrinkage at cooling stage. Compared to the previous production with PMMA Lucite (Figure 5.8), with COC (Figure 5.9) there are no more sinkmarks detected. For PMMA LG 840 neither relevant sinkamrks were observed.

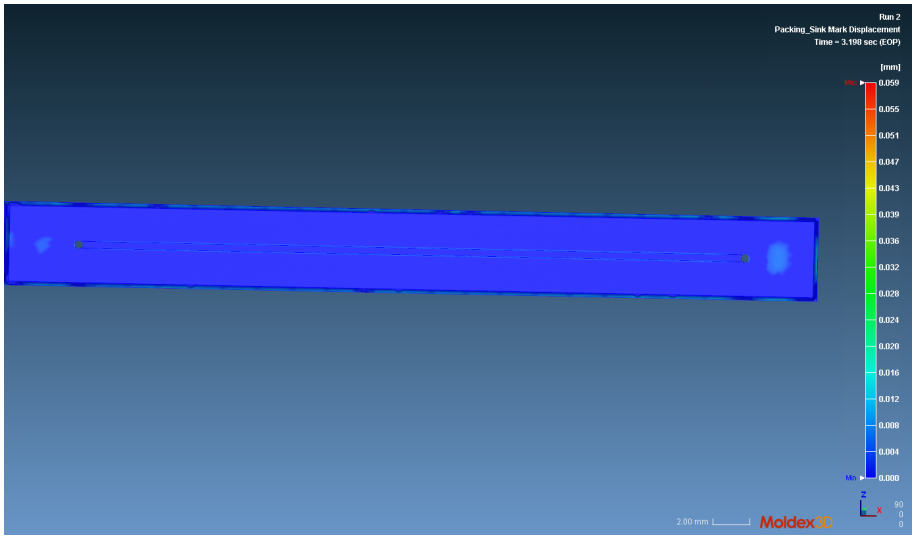

Figure 5.8: SinkMarks detected with PMMA Lucite between the ejector pin and the hole. Note the good agreement with the actual part (Figure 4.22b).

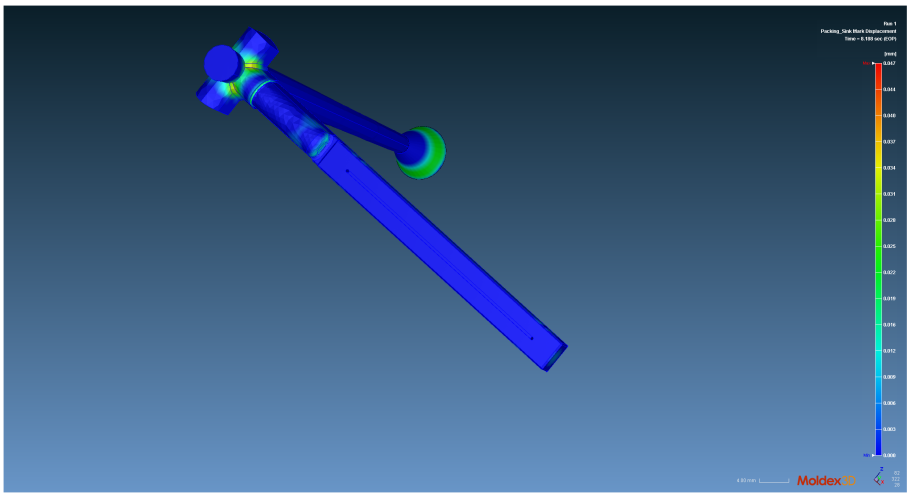

Figure 5.9: COC simulation. Along the chip the blue area means the sinkmarks are negligible.

5.2.2 Filling results

The filling of the cavity is visualized in Figure 5.10. Blue represents the longest time since the material has left the melt entrance. It is clear that the design of the sprue, injection velocity and the gate have an impact on how the cavity fills.

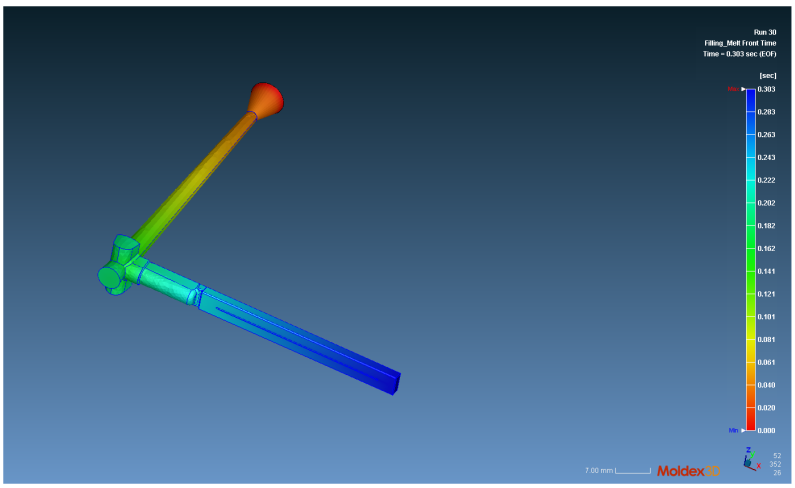

Figure 5.10: Filling results - melt front time for COC

5.2.3 Shrinkage

Volumetric shrinkage result shows the distribution of part volume change percentage as the part is cooled from high temperature and high pressure at the end of packing to ambient temperature. This calculation is based on PvT relationship of the plastic material. Positive value represents volume shrinkage while negative value represents volume expansion [27].

For an optimized result, uniform volumetric shrinkage is desired. Non-uniform volumetric shrinkage is caused by two reasons:

- Non-uniform pressure distribution
- Non-uniform temperature distribution

Non-uniform volumetric shrinkage can lead to Warpage after the part is ejected.

Figure 5.11 and 5.12 present the volumetric shrinkage for both the materials giving a rough idea of the Shrinkage of the part. The color distribution is a representation of how much each node move after the process and is similar for COC and PMMA. The material shrinks more near the sprue (green color), which is not an issue because is a waste part. The light blue on the chip predict a uniform shrinkage.

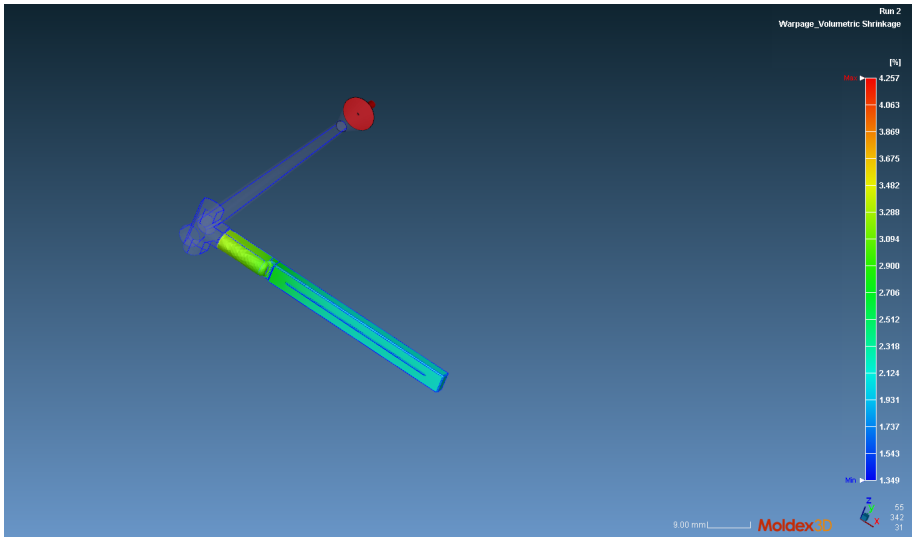

Figure 5.11: Volumetric shrinkage PMMA

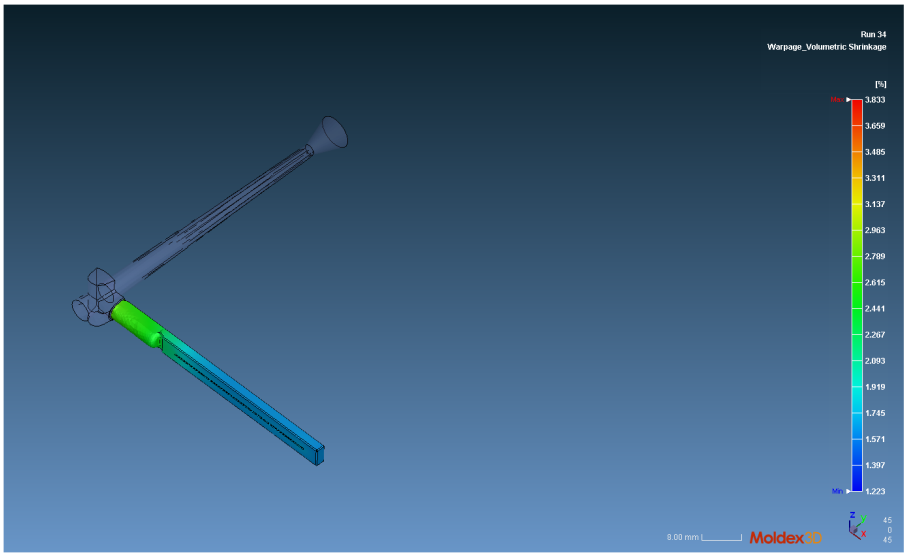

Figure 5.12: Volumetric shrinkage COC

5.2.4 Post processing

After runned the simulations, it has been exported the deformed model as an STL file [28]. In the software there is a built-in *Export Deformed Model* function that allows the user to export the part.

Finally was opened in Solidworks [34] in order to calculate the dimensions of the channel. And then, once calculated for all the three directions, the data were collected in an Excel spreadsheet and used to calculate the Linear and volumetric shrinkage. See the formulas 6.1 and 6.3.

Following the same strategy of the actual part it has been taken three sections of the chip: bottom, mid, top. For each section was taken three measurements for the width and for the depth. $3 \cdot 3 = 9$ measurements in total for each virtual part.

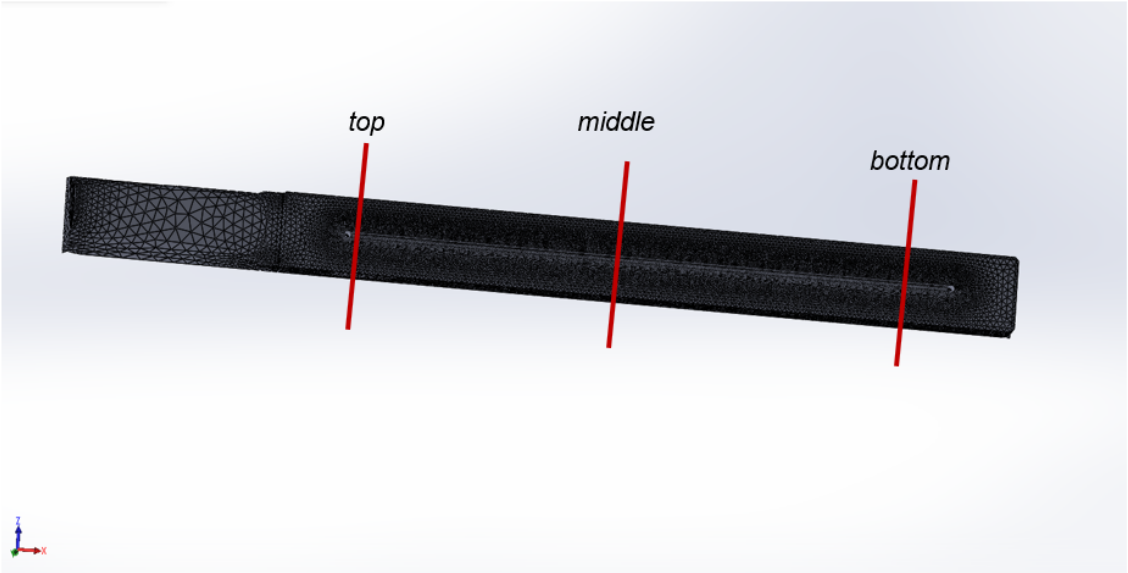

Figure 5.13: The same strategy was adopted for the simulations: the red lines indicate the cross sections investigated

Channel length
For the channel length was chosen the external diameter as a reference point: hence the distance was calculated in this way:

$$Length = Distance_{inlet-outlet} - Diameter_{hole} \tag{5.1}$$

The diameter of the hole is 0.45 mm

To avoid misunderstood see the Figure 5.14

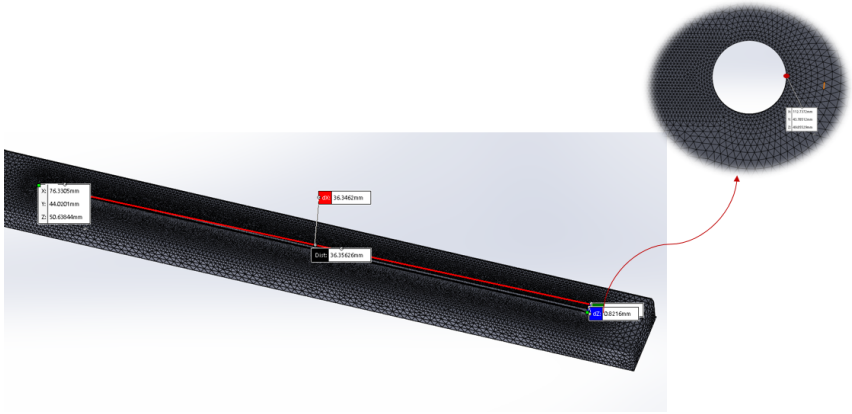

(a)

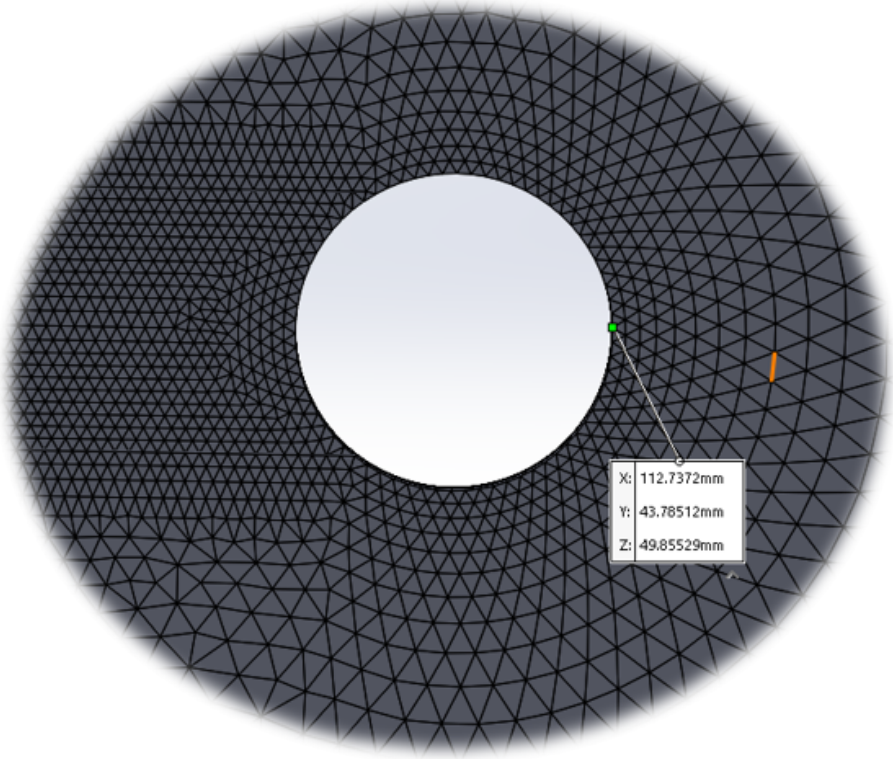

(b)

Figure 5.14: Measurements settings. (a)Chip length ; (b)zoom

Channel width
As mentioned above for the channel width was taken three measurements for each cross sections: bottom, middle, top. See the Figure 5.15

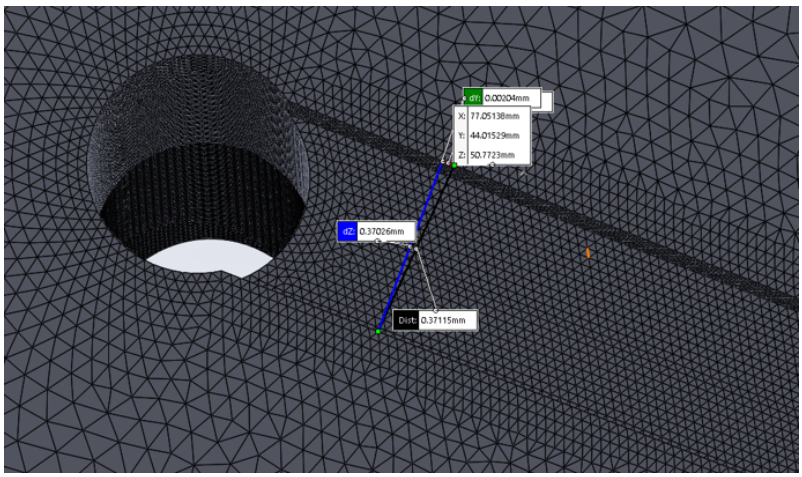

(a)

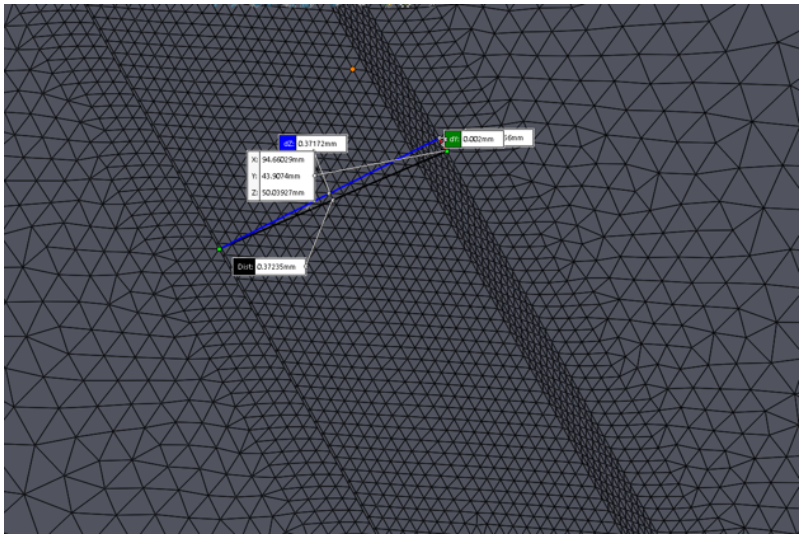

(b)

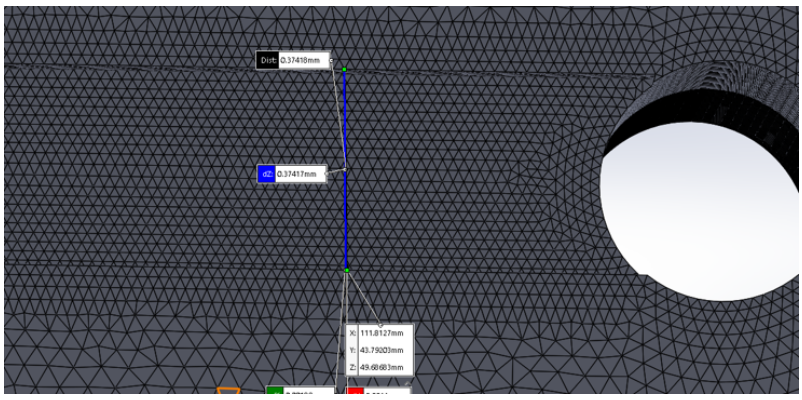

(c)

Figure 5.15: Set-up. (a) top; (b) middle (c)bottom

Channel height

As shown in Figure 5.16 to measure the height was once again used the built-in *Measure* function given from Solidworks®.

The user can, after select two nodes in the part, measure the distance between them. One reference was located in the highest point whilst the other is located at the bottom. The measurements were done on both sides of the channel.

This procedure was repeated for three cross-sections: TOP, MIDDLE, BOTTOM.

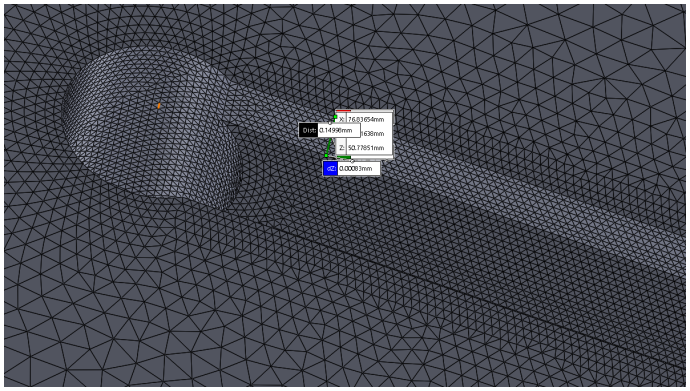

(a)

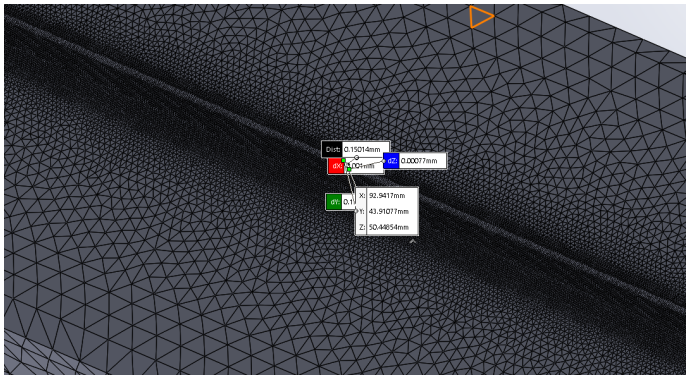

(b)

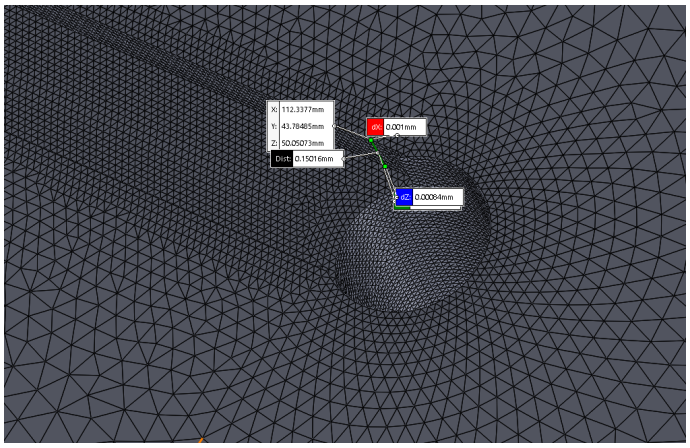

(c)

Figure 5.16: Set-up. (a) top; (b) middle (c)bottom

6 Results and Discussion

In this chapter it will discuss the results obtained from the experiments and the ones from the simulations.The aim is to compare the two different values. Briefly some comments will be give also on the DoE results.

6.1 DoE COC results

First of all, the data derived from the production were reported in Table A.8.

The confidence level used for the analysis is of 95 %.

For COC, all the results of the main effects plot are reported in Figure 6.1.

The most significant factors (i.e. the ones that contribute to modifying the volumetric shrinkage) are the melt temperature, mould temperature and injection velocity. Since the slope of the line which connects the two point determines the magnitude of the main effect, we can say the mould temperature affects the response to a greater extent compared to the other two. If there were no significant interactions between the factors, a main effects plot would adequately describe the relationship between each factor and the response. Here, it is also necessary to examine the interaction plot and Pareto chart.

An interaction plot was created using the process window with the new values of injection velocity. The results are presented in Figure 6.2. The first aspect that can be seen is that shrinkage is consistently lower with high values of packing pressure and injection velocity. This is a logical result explained by the fact that the packing pressure plays an important role in the compensation of shrinkage. Packing pressure must be high enough to overcome the gate resistance for shrinkage compensation. Moreover, increasing the packing pressure and prolonging packing time would delay the solidification time for polymers, which help enhance pressure transmission and reduce the volumetric shrinkage rate of plastic parts.

Regarding the injection speed if it is too low, the filling time would increase. The risk is that melted polymer will be cooled before the cavity is completely filled.

It is also clear that there is no influence of low levels of packing pressure and injection velocity. Low levels of injection velocity show, on the other hand, highest amount of shrinkage. This can be explained by the fact that a low injection velocity implies a longer filling time, thus, the risk is that the plastic freeze before applying packing pressure.

It can also be seen that an high Melt temperature combined with high injection velocity shows good results in term of shrinkage. As a matter of fact, the polymer ad high temperature, in addition replicating better the surface, has low viscosity that make easier to fill the cavity. Hence there is no risk of solidification of the polymer before the cavity is completely filled.

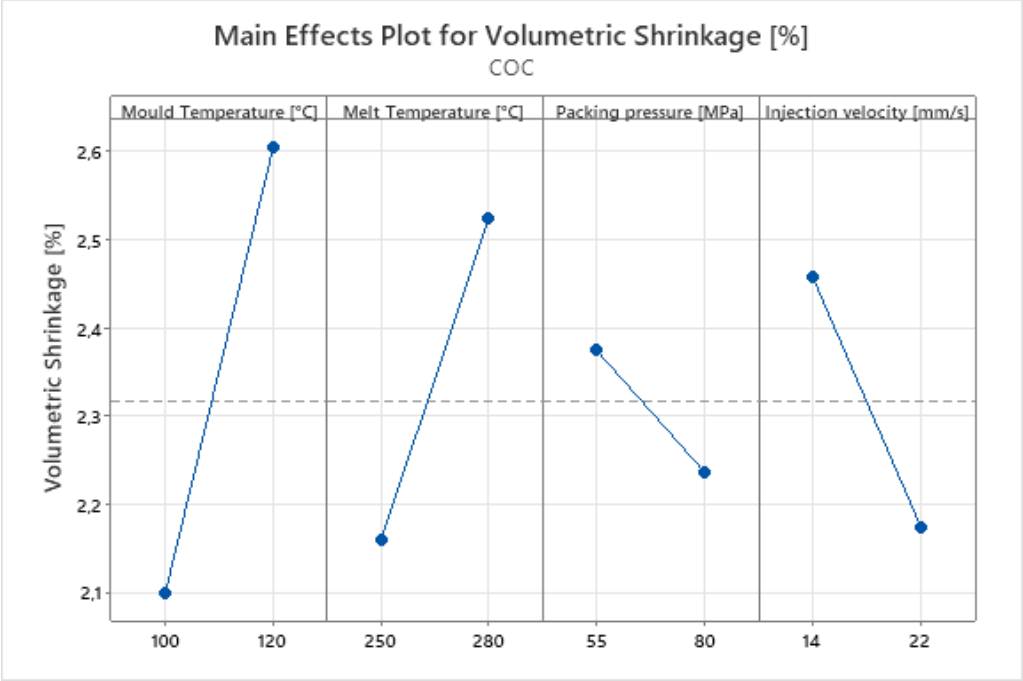

Figure 6.1: Main Effects Plot for Volumetric Shrinkage

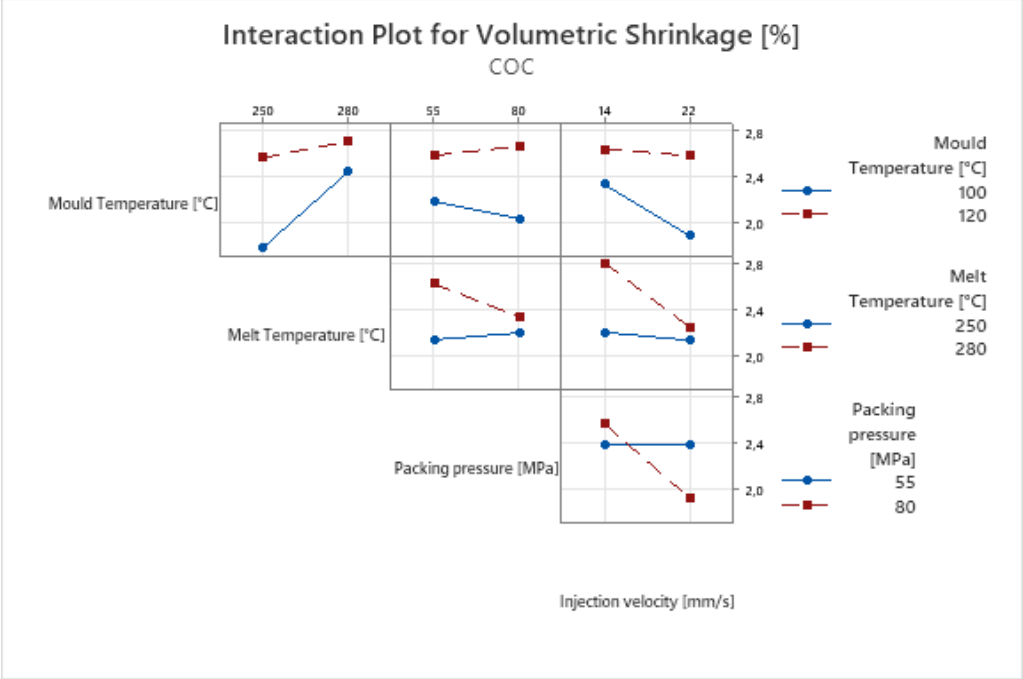

Figure 6.2: Interaction Plot for Shrinkage

6.2 DoE PMMA results

Also in this case, the reader can observe in detail the results in the Appendix in Table A.9.

All the results of the main effects plot and interactions are reported in Figure 6.3 and 6.4. The most significant factors are the melt temperature and the packing pressure. Looking at the Figure A.16 the most interesting interactions are:

- The one that links Melt temperature and injection velocity. As the two factors are directly defining the polymer melt viscosity [20], keeping a low level of injection velocity and Melt temperature, an high amount of shrinkage is observed. We can explain this fact with the theory: a low melt temperature implies high viscosity and therefore higher resistance for the flow to fill the cavity. The pressure gradient at the gate and at the end of the flow will be high. Hence, shrinkage also will be increased.

  On the other hand if the injection speed is too low the melted polymer might freeze before the cavity is completely filled. Therefore, the shrinkage will be higher.

  It is clear that the combinations of these factors might lead to a premature solidification of the plastic before the packing phase.

- The one between mold temperature and packing pressure. When both the levels are kept on high levels the shrinkage is minimized. This combination is the most effective. Behind this result there is once again an explanation: after the melted polymer injected into the cavity, the temperature difference between the melt and the mold will cause the melt to cool and shrink quickly. Therefore, if the mold temperature is high, this process will be slower. Otherwise, more polymer material needs to be filled into the cavity to continuously compensate the shrinkage. With high packing pressure, more material is injected into the cavity minimizing shrinkage.

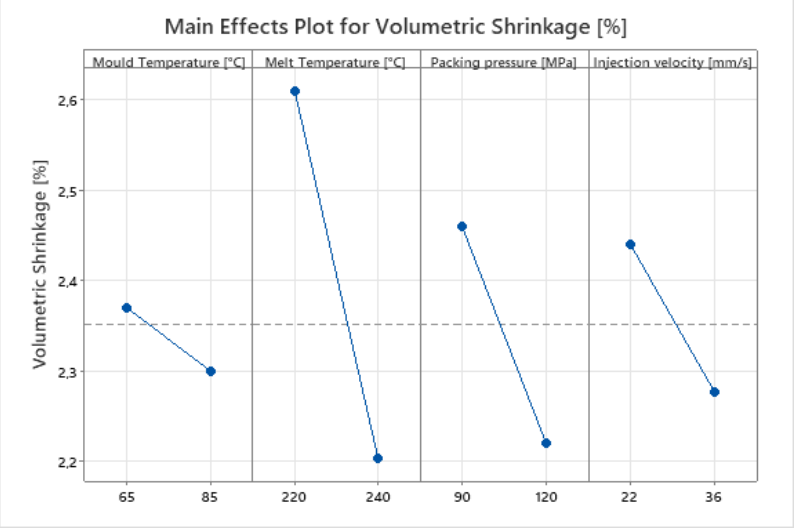

Figure 6.3: Main effects Plot for Volumetric Shrinkage

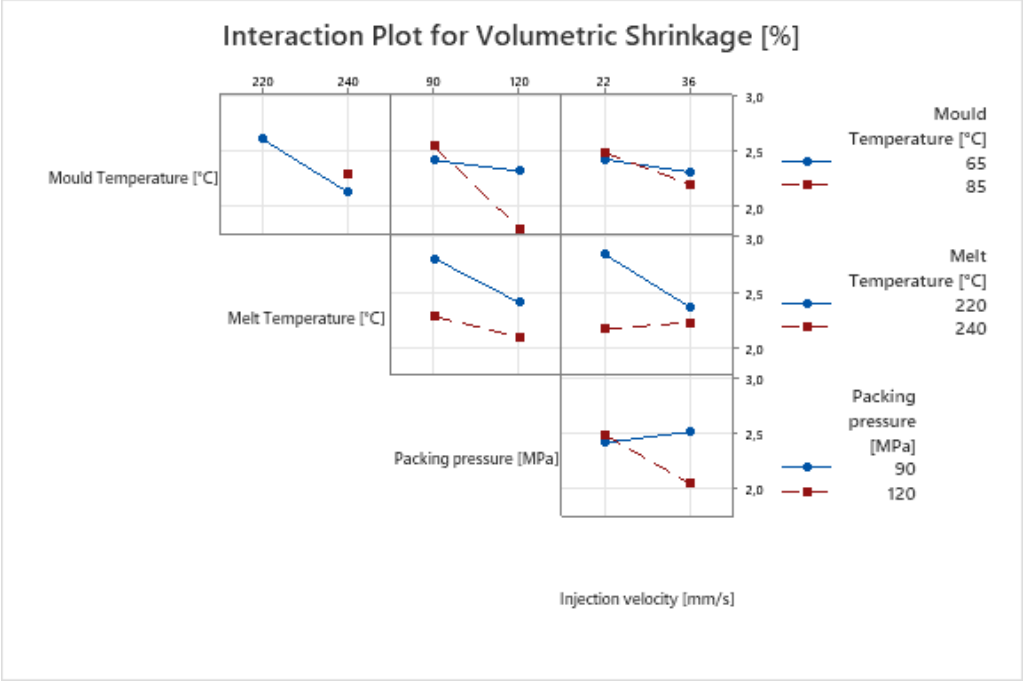

Figure 6.4: Interaction Plot for Volumetric Shrinkage

6.3 Linear shrinkage

For each simulation it was determined the linear shrinkage using the formula 6.1, where D is either the width, depth and length of the micro-channel. The target values are the one from the CAD model (4.6), while the simulated part is the dimension of the deformed model.

Due to the need to be closer to the actual part it was measured along the three directions, as a matter of fact the shrinkage usually occurs differently in XYZ.

Table 6.1 displays the average linear shrinkage of simulations for the two materials for the depth, width and length.

$$L_s = \frac{D_{targetvalue} - D_{simulatedpart}}{D_{targetvalue}} \cdot 100\% \tag{6.1}$$

Table 6.1: Linear shrinkage of simulations

	Average depth [%]	Average width [%]	Average length [%]
COC	0.38	1.40	0.56
PMMA	0.21	1.73	0.43

As well for the simulation, the linear shrinkage for the molded chip, is calculating with the following formula 6.2. In this case the target values are the dimensions measured of the mold (Table 4.6).

$$L_s = \frac{D_{targetvalue} - D_{actualpart}}{D_{targetvalue}} \cdot 100\% \tag{6.2}$$

Table 6.2 displays the average measured linear shrinkage of molded parts for the two materials for the depth, width and length. The mean refers to all the different combinations of parameters.

Table 6.2: Linear shrinkage of produced parts

	Average depth [%]	Average width [%]	Average length [%]
COC	0.54	1.67	0.65
PMMA	0.29	2.44	0.46

The two tables above give us some important results:

- COC and PMMA don't shrink in an isotropic way (i.e. equally in all the directions) but present different values.
- The highest values registered in production and simulation are along the width direction.
- PMMA shrinks more along the width, but less in the other two directions.

The graphs shown in Figure 6.5 and 6.6 have been plotted for the shrinkage values for COC and PMMA respectively. In all cases the simulated shrinkage values appear to be less than the shrinkage of the injection moulded parts.

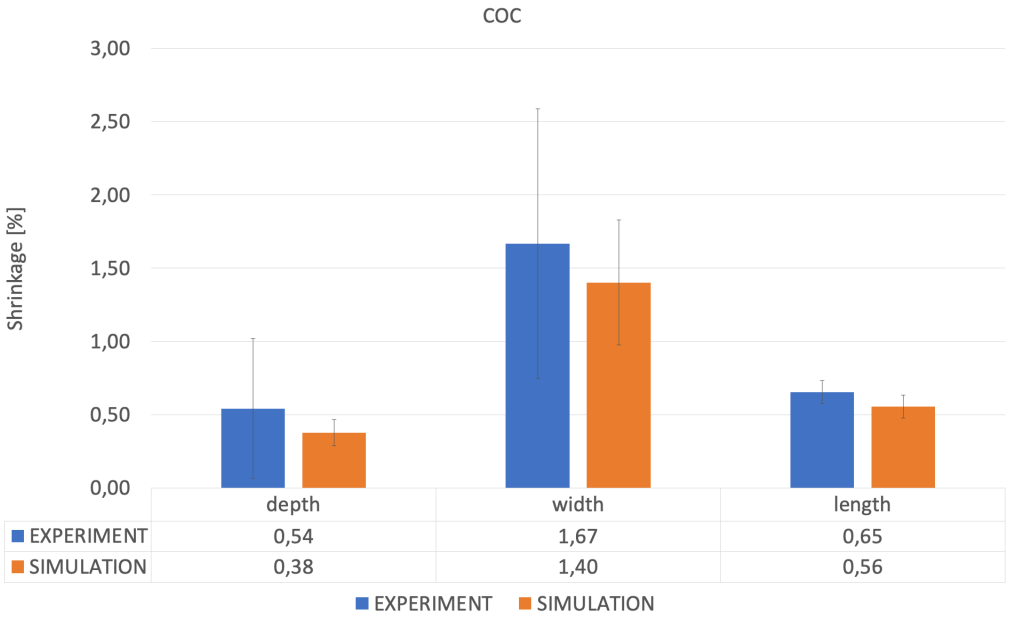

Figure 6.5: Shrinkage comparison for COC along the length, width and depth. The error bars in the plot indicate the standard deviation calculated between the recipes of the DoE.

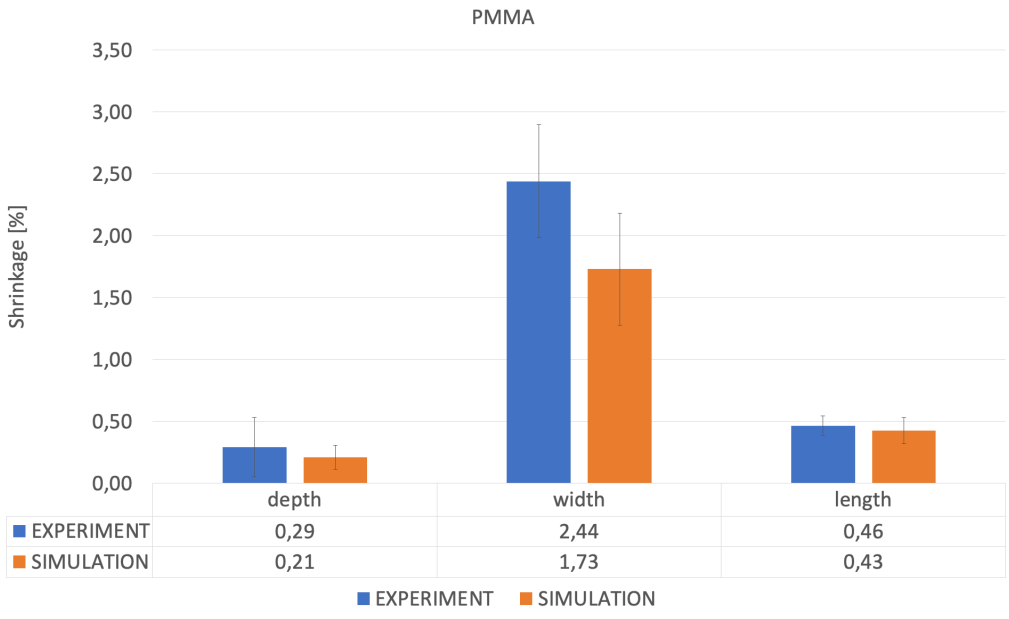

Figure 6.6: Shrinkage comparison for PMMA along the length, width and depth. The error bars in the plot indicate the standard deviation calculated between the recipes of the DoE.

The histograms plotted in Figure A.17 A.18 A.19 show the results for the single recipes.

- For the depth we can note a good agreement between simulation and metrology except for the 2nd recipe and for the ninth, where the injection molded parts show much higher shrinkage.
- For the width there is something weird in the 2nd recipe, where apparently the metrology reveals a negative shrinkage (i.e. expansion of the plastic). Perhaps due to noise in the acquisition that have affected the measure.
- The length result seem to confirm the trend: except of some rare cases the virtual part predict less shrinkage.

From the analysis of the histograms of depth, width and length respectively in Figure A.20 A.21 A.22 the extent of shrinkage is almost higher for the molded parts.

- Looking at the depth only the simulation n°9 overestimates the shrinkage.
- In figure A.21 only the simulation 11, where the simulation is slightly higher.
- The shrinkage of the actual part along the length is higher in all the configurations except the n°6 and n°11

6.4 Volumetric shrinkage

The volumetric shrinkage for the simulations was calculated using the formula 6.3

$$V_s = \frac{V_{nominal} - V_{simulated}}{V_{nominal}} \cdot 100\% \tag{6.3}$$

where $V_{nominal}$ indicates the volume of the micro-channel calculated with the nominal values derived from the CAD and $V_{simulated}$ is calculated once the deformed part was exported from Moldex3D.

the table 6.3 reports the maximum, minimum and average value for each of the material for the simulations.

Table 6.3: Volumetric shrinkage of simulations

	Maximum [%]	Minimum [%]	Average [%]
COC	2.97	1.49	2.32
PMMA	2.92	1.81	2.35

The same approach was used to determine the shrinkage of the actual part:

$$V_s = \frac{V_{nominal} - V_{moldedpart}}{V_{nominal}} \cdot 100\% \tag{6.4}$$

$V_{nominal}$ in this case is the volume of the micro-channel of the mold, $V_{moldedpart}$ is derived from the metrology data.

Table 6.4 below shows the experimental results.

Table 6.4: Volumetric shrinkage of actual part

	Maximum [%]	Minimum [%]	Average [%]
COC	4.61	1.51	2.84
PMMA	4.03	2.46	3.32

The figure 6.7 is very important since allows the reader to look in one graph at the deviation between injection molded part and simulation.

COC in particular shows satisfying results. Observing the mean for injection moulded samples the shrinkage was around 2.8% against the predicted range of 2.3%.

PMMA showed shrinkage values of practical samples in the range 2.9 − 3.8% against the prediction of 1.9 − 2.9 %. Thus it can be observed that the predictions vary by a maximum of 30 %.

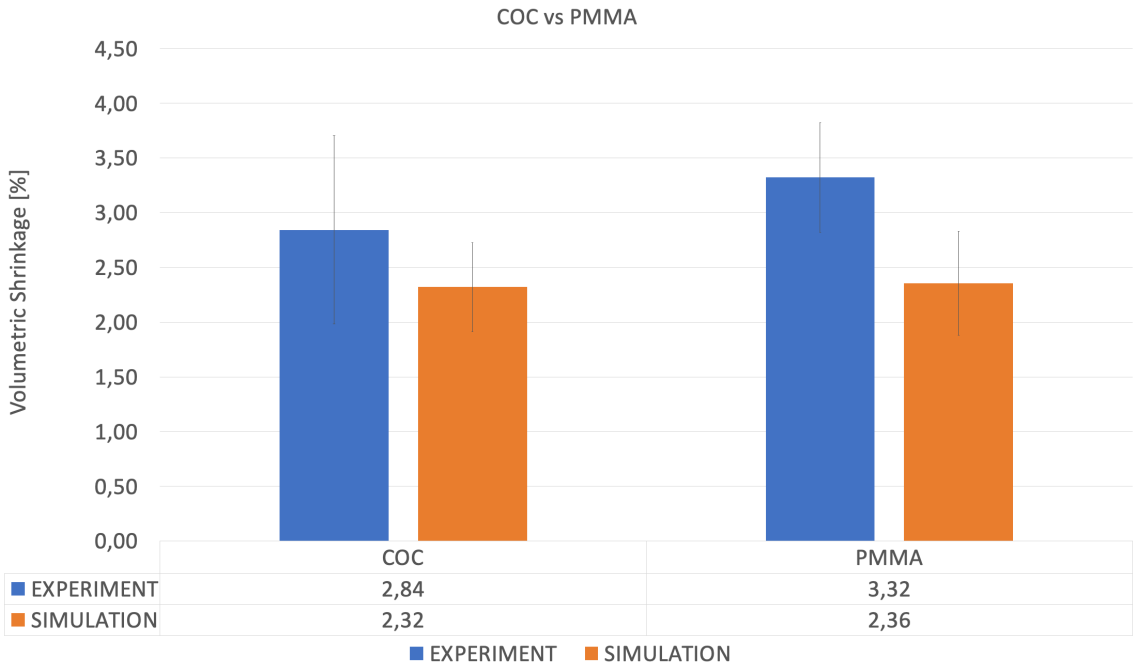

Figure 6.7: Volumetric Shrinkage comparison between PMMA and COC. The error bars in the plot indicate the standard deviation calculated between the recipes of the DoE.

In Appendix are reported the volumetric shrinkage for each recipe of the DoE for both the materials. (Figure A.23a and A.23b)

Hence, summarizing:

- The discrepancy between the experiments and simulations may come from the fact that all the simulations were run with a cooling time a bit shorter (10 s), in the experiments has been set a cooling time of 15 s to make sure to have a cooled part once ejected from the mold.

- The profile temperature of the melt was set by using 5 °C intervals per each heating zone of the reciprocating screw to facilitate a gradual heating of the material throughout the barrel [Figure 4.5]. This differs compared to the simulation in which the temperature is constant. Moreover the temperature near the hopper is lower to avoid the pellets stick in the barrel.
- As mentioned in the second chapter it must not be forgotten that Moldex3D is developed to simulate the behaviour of traditional injection moulding [38], hence the reader should not be surprised to see different results.
- It can be noted a common trend in the charts: all the simulations predict a smaller shrinkage compared to the experiments.
- The previous point brings us to a conclusion: even if the results predicted from the simulations are not completely exact, this comparison may be used for further studies on this project keeping in mind that all the simulations underestimate the volumetric shrinkage of the actual part.

7 Conclusion

The final chapter presents a discussion based on the whole content of the work. It summarizes the conclusion and suggests some inputs for future works.

7.1 Epilogue

Two different materials were tested during this work, with the aim to optimize the production of the chip by minimising the deformation of the micro-channel caused from the cooling process. All the efforts were concentrated on the micro-channel, since the shrinkage is critical in presence of micro-features and the acoustic resonance for blood separation is sensitive to the channel dimensions.

Based on the metrology analysis of produced chips and the simulations, COC showed satisfying results in term of volumetric shrinkage, with the dimensions of the channel closer to the mold value. COC has the least shrinkage values both in practice and simulation. The lowest amount of volumetric shrinkage is 1.49 % (see Table A.8).

PMMA, amorphous polymer like COC, shows higher shrinkage but still acceptable for the functionality of the chip.

It was demonstrated that for both the materials, in order to obtain an acceptable part, the injection speed has to be changed. The values used in the production are considerably lower than the parameters recommended by the resin manufacturer.

Another aim of the thesis was also the validation of the simulations results. To obtain closest possible results the same inputs were used for injection moulding and the simulation, some outputs received from the moulding process were also used for simulations. As a matter of fact, when in production the values of injection velocity were changed, the new values were used as input to run the simulations. Practical and the simulated results were compared to get an estimation of the accuracy of simulations. In particular, an accurate comparison was done with the DoE carried out during the lab sessions. Comparisons were made using linear and volumetric shrinkage. With regard to volumetric shrinkage, main goal of the thesis, the most accurate simulation results showed deviations in the order of 0.2 % for COC. Observing the mean for injection moulded COC samples the shrinkage was around 2.8% against the predicted of 2.3%.

All the simulations for PMMA have larger deviations from the real values; PMMA showed shrinkage values of practical samples in the range $2.9 - 3.8\%$ against the prediction of $1.9 - 2.9$ %. Thus, it can be observed that the predictions vary by a maximum of 30 % (taking the average value for both simulations and experiments, see Figure 6.7)

Even if what predicted from the simulations is not completely exact, the results obtained from this comparison may be used for further studies on this project keeping in mind that all the simulations underestimate the volumetric shrinkage of the actual part. The simulated results show lower values of shrinkage compared to the practical since include some approximations and boundary conditions that are not in the reality. Furthermore, Moldex3D works on a macro scale, not taking into consideration specific aspects such as [38]:

- The melt has an higher risk of slipping in μIM due to the viscoelastic behavior and increased pressure.

- Heat transfer coefficient, ventilation, wall slip, and freeze temperature are crucial in μIM.
- Microcavities have a more difficult filling behavior than more extensive cavities.

Even though not completely accurate, the simulated data can be used in cases of new developments or to understand the effects of design changes, material changes or any other process changes without much wastage of money, time, and material.

7.2 Suggestions for future works

Based on the results of this project, it is worth to point out some considerations for potential future developments.

- First of all, the next user should consider to make a new mold, since the one that it was used so far is quite old and now presents a damaged cavity that affects the quality of the molded part. The reason behind this could be the material. The mould used was made of aluminium since it is not designed for an industrial production. If the mold had been made of steel perhaps the issue would not have occurred. The choice of the material to build a mould is primarily economic; in general, steel moulds are more expansive, but their longer lifespan offsets the higher initial cost.
- Also the CAD model should be modified, currently the chip is not the same as in the real part but includes the cold runner, as it can be seen in Figure 7.1. This could bring more precise results between simulations and experiments.

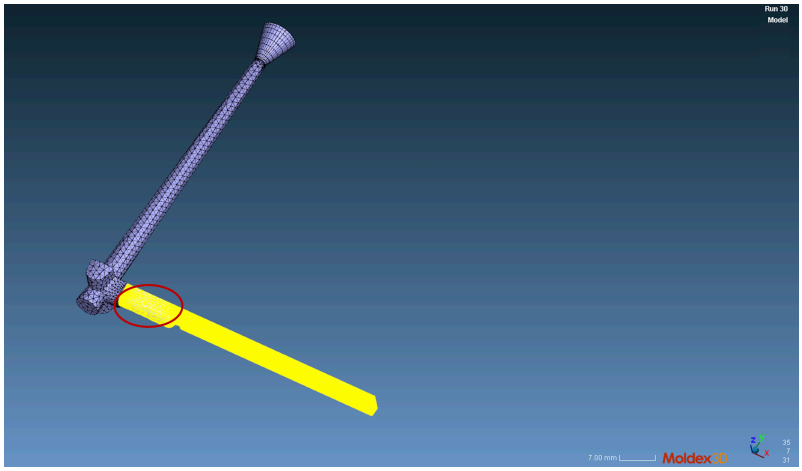

Figure 7.1: CAD defect. Note the part is longer than it supposed to be.

- The issues during the lab session with COC could be due to high values of mold temperature, melt temperature and packing pressure in the same run. In particular the latter, on one hand, contributes to reduce the shrinkage as much as possible thanks to a continuous application of pressure during the packing phase. On the other hand, such high values could risk to damage the mold which is made of aluminium. It was decided to adopt these values for the pressure because of previous productions. It is recommended to reduce slightly the high level of packing pressure for future DoE.

Bibliography

[1] acousort.com. *Acousort tech*. 2021. URL: https://www.acousort.com/technology/%20acoustic-separation..

[2] Gava Alberto. *Modelling of the micro injection molding process*. 2008. URL: http://paduaresearch.cab.unipd.it/1541/2/29_04_Tesi_dottorato_Alberto_Gava.pdf.

[3] Likith Gowda Alberto Santi Julia Fibla. *Micro injection moulding simulation for optimization of polymer lab-on-a-chip platforms 41739*. 2021. URL: https://www.mek.dtu.dk/english.

[4] arburg.com. *allrounder 370a*. 2021. URL: https://www.arburg.com/fileadmin/redaktion/Mediathek/Technische_Daten/ARBURG_ALLROUNDER_370A_TD_526447_en_GB.pdf.

[5] Federico Baruffi, Matteo Calaon, and Guido Tosello. "Effects of micro-injection moulding process parameters on accuracy and precision of thermoplastic elastomer micro rings". In: *Precision Engineering* 51 (Jan. 2018), pp. 353–361. DOI: 10.1016/j.precisioneng.2017.09.006.

[6] Federico Baruffi et al. "Comparison of micro and conventional injection moulding based on process precision and accuracy". In: 75 (Sept. 2018), pp. 149–154. DOI: 10.1016/j.procir.2018.04.046.

[7] E.B. Brousseau, Stefan Dimov, and D. Pham. "Some Recent Advances in Multi-Material Micro- and Nano-Manufacturing". In: *International Journal of Advanced Manufacturing Technology* 47 (Mar. 2010), pp. 161–180. DOI: 10.1007/s00170-009-2214-5.

[8] Matteo Calaon et al. "Functional Analysis Validation of Micro and Conventional Injection Molding Machines Performances Based on Process Precision and Accuracy for Micro Manufacturing". In: *Micromachines* 11 (Dec. 2020), p. 1115. DOI: 10.3390/mi11121115.

[9] Nikolaos Giannekas. "Precision injection moulding of microfeatures using integrate process and product quality assurance". In: Dec. 2018, pp. 1–2. ISBN: 978-1-56990-653-8. DOI: 10.3139/9781569906545.009.

[10] *Global Polymer Microinjection Molding Market*. 2020. URL: https://www.maximizemarketresearch.com/market-report/global-polymer-microinjection-molding-market/30285/.

[11] globenewswire.com. *Global Polymer Microinjection Molding Market*. 2021. URL: https://www.globenewswire.com/fr/news-release/2021/10/26/2320273/0/en/Global-Polymer-Microinjection-Molding-Market-is-Anticipated-to-Reach-USD-6-667-billion-by-2028-Fior-Markets.html.

[12] TOPAS Advanced Polymers GmbH. *Topas coc Cyclic Olefin Copolymer*. 2019. URL: https://topas.com/sites/default/files/PRODUCTS-E-13.06.19.pdf.

[13] Patrick Guerrier, Guido Tosello, and J.H. Hattel. "Flow visualization and simulation of the filling process during injection molding". In: *CIRP Journal of Manufacturing Science and Technology* 16 (Aug. 2016). DOI: 10.1016/j.cirpj.2016.08.002.

[14] Julian Heinisch, Yannik Lockner, and Christian Hopmann. "Comparison of design of experiment methods for modeling injection molding experiments using artificial neural networks". In: *Journal of Manufacturing Processes* 61 (Jan. 2021), pp. 357–368. DOI: 10.1016/j.jmapro.2020.11.011.

[15] *Image Metrology 2020 Scanning Probe Image Processor*. 2020.

[16] *ISO 15530-3: Geometrical Product Specifications (GPS)—Coordinate Measuring Machines (CMM): Technique for Determining the Uncertainty of Measurement; ISO: Geneva, Switzerland*. 2011.

[17] Henrik Bruus Guido Tosello Komeil Saeedabadi Fabian Lickert and Matteo Calaon. *Dimensional characterization of micro-milled polymer channels for acoustic blood plasma separation*. 2021. URL: https://www.euspen.eu/knowledge-base/MN21107.pdf.

[18] lgchem.com. *injection molding guide*. 2017. URL: http://www.lgchem.com/upload/file/chinaplas/Division_Info/LG20MMA.pdf.

[19] Dario Loaldi et al. "Experimental Validation of Injection Molding Simulations of 3D Microparts and Microstructured Components Using Virtual Design of Experiments and Multi-Scale Modeling". In: *Micromachines* 11 (June 2020), p. 614. DOI: 10.3390/mi11060614.

[20] Dario Loaldi et al. "Product Fingerprints for the Evaluation of Tool/Polymer Replication Quality in Injection Molding at the Micro/Nano Scale". In: *Nanomanufacturing and Metrology* 4 (May 2021). DOI: 10.1007/s41871-021-00105-7.

[21] Maximilian Marhöfer et al. "Advancements on the Simulation of the Micro Injection Moulding Process". In: Jan. 2013, pp. 77–81. ISBN: 978-981-07-7248-2. DOI: 10.3850/978-981-07-7247-5-426.

[22] Maximilian Marhöfer et al. "Gate Design in Injection Molding of Microfluidic Components Using Process Simulations". In: *Journal of Micro and Nano-Manufacturing* 4 (Dec. 2015). DOI: 10.1115/1.4032302.

[23] Schut geometrische meettechniek. *3D CNC Coordinate Measuring Machines*. 2021. URL: https://www.schut.com/Products/DeMeet/index.htm.

[24] Image Metrology. *Getting started with the SPIP™ Image Processing Software*. URL: https://www.imagemet.com/media-library/spip-tutorials/.

[25] Minitab.com. *Effects plots for Analyze Factorial Design*. 2019. URL: https://support.minitab.com/en-us/minitab/18/help-and-how-to/modeling-statistics/doe/how-to/factorial/analyze-factorial-design/interpret-the-results/all-statistics-and-graphs/effects-plots/.

[26] Minitab.com. *How to create a boxplot*. 2019. URL: https://support.minitab.com/en-us/minitab-express/1/help-and-how-to/graphs/boxplot/before-you-start/overview/.

[27] moldex3d.com. 2021. URL: http://support.moldex3d.com/r16/en/post-processing_resultinterpretations_warp_volumetricshrinkage.html.

[28] moldex3d.com. 2021. URL: https://www.moldex3d.com/blog/tips-and-tricks/exporting-deformed-model-in-moldex3d/.

[29] moldex3d.com. *Moldex3D*. 2021. URL: http://support.moldex3d.com/r16/en/analysissetup_prepareanalysis_materialwizard_tabsinmaterialdatawindow.html.

[30] Olympus.com. *LEXT OLS 4100*. URL: http://www.techsansystem.co.kr/image/4100/OLS4100_.pdf.

[31] Tim A. Osswald. *Understanding Polymer Processing, Processes and Governing Equations*. 2010.

[32] Tim A. Osswald and Georg Menges. "Materials Science of Polymers for Engineers". In: 2014, pp. 204–205. ISBN: 978-1-56990-653-8. DOI: 10.3139/9781569906545.009.

[33] V. Bellantone R. Surace G. Trotta and I. Fassi. *The Micro Injection Moulding Process for Polymeric Components Manufacturing*. 2020.

[34] Solidworks. 2021. URL: http://help.solidworks.com/2021/english/SolidWorks/sldworks/hidd_measure.htm.

[35] Marco Sorgato, Davide Masato, and Giovanni Lucchetta. “Effect of vacuum venting and mold wettability on the replication of micro-structured surfaces”. In: *Microsystem Technologies* 23 (July 2017). DOI: 10.1007/s00542-016-3038-5.

[36] topas.com. *processing datasheet*. 2019. URL: https://topas.com/sites/default/files/PDS20Topas205013L-10.pdf.

[37] G. Tosello and F. S. Costa. “High precision validation of micro injection molding process simulations”. English. In: *Journal of Manufacturing Processes* 48 (2019), pp. 236–248. ISSN: 1526-6125. DOI: 10.1016/j.jmapro.2019.10.014.

[38] Guido Tosello and David Marhöfer. “Modeling and Simulation of Micro Injection Molding”. In: Aug. 2018, pp. 213–240. ISBN: 978-1-56990-653-8. DOI: 10.3139/9781569906545.009.

[39] Guido Tosello et al. “Study of process parameters effect on the filling phase of micro-injection moulding using weld lines as flow markers”. In: *International Journal of Advanced Manufacturing Technology* 47 (Mar. 2010), pp. 81–97. DOI: 10.1007/s00170-009-2100-1.

[40] Min-Wen Wang, Fatahul Arifin, and Van-Hanh Vu. “"The Study of Optimal Molding of a LED Lens with Grey Relational Analysis and Molding Simulation"”. In: *Periodica Polytechnica, Mechanical Engineering* 64 (Aug. 2019), pp. 278–294. DOI: 10.3311/PPme.13337.

[41] westfall. *micropart*. 2019. URL: https://www.moldhotrunnersolutions.com/micromolding.html.

[42] Lei Xie, Longjiang Shen, and Bingyan Jiang. “Modelling and Simulation for Micro Injection Molding Process”. In: July 2011. ISBN: 978-953-307-169-5. DOI: 10.5772/16283.

A Supplementary Material

PMMA & SMMA

Molding Guide

Pre-drying

PMMA and SMMA resins can be used without pre-drying, but they absorb moisture if they are stored for long time or stored under unfavorable conditions. When moisture absorption rate exceeds 0.1%, the molded product can have silver streak formed on the surface or foams formed on the inside. It is desirable to perform preliminary drying according to the following conditions.

Grade	Temperature	Time
Optical, General PMMA, SMMA	70~80℃	4~6hr
Impact resistant PMMA	60~70℃	

Annealing

When the molded product contacts paint or organic chemical solvents, it is essential for preventing craze or crack caused by internal stress of the molded product. Effective annealing condition is the highest temperature at which the molded product does not show deformation.

Grade	Temperature	Time
HP202, EH910, EG920	Max. 90℃	Over 5hr
IH830, IH830C, IH830A	Max. 80℃	
IF850, IF870S, SMMA (HX238, HX208)	Max. 70℃	
Impact resistant PMMA	Max. 60℃	

Injection Molding Condition

Grade	Melting temperature	Mold temperature
HP202, EH910, EG920, Heat resistant PMMA	230~260℃	60~80℃
IH830, IH830C, IH830A	220~250℃	50~70℃
IF850, IF870S, SMMA (HX238, HX208)	210~240℃	
Impact resistant PMMA		

14

Figure A.1: PMMA LG Data sheet

LG MMA

Handling & Use

Static Electricity

It is important to keep the area clean where the material is stored and the surroundings of injection molders as the material easily absorbs dust due to static electricity.

Cautions in mixing with other grades and resins

Take caution against mixing the material with other grades or resins when molding products.

Moisture Absorption

Do not leave the dry material in the air or neglect open sacks of the material.

Chemical Resistance

Suitable	Requires attention	Unsuitable	
Dilute acid	Hydrochloric acid	Acid	Ketone
Hydrochloric acid (10%)	Alcohol	Sulfuric acid	Acetone
Sulfuric acid (30%)	Methanol	Nitric acid	Methyl ethyl ketone
Nitric acid (30%)	Ethanol	Acetic acid	Methyl Isobutyl ketone
Acetic acid (10%)	Isopropyl alcohol	Formic acid	Ether
Alkali	Butyl alcohol	Aromatic hydrocarbon	Furan
Sodium hydroxide (50%)	Ether	Benzene	Tetrahydrofuran
Aqueous ammonia (10%)	Methyl ether	Toluene	Ester
Aliphatic hydrocarbon	Diethyl ether	Xylene	Methyl methacrylate
n-Hexane	Isopropyl ether	Phenol	Methyl acrylate
n-Heptane	Cyclohexane	Alicyclic hydrocarbon	Methyl acetate
n-Octane	Tetrachloromethane	Chlorobenzene	Ethyl acetate
Paraffin	Cyclohexanon	Alcohol	Propyl acetate
Inorganic salt solution	Benzaldehyde	Benzyl alcohol	
Aqueous salt solution (10%)		Furfuryl alcohol	
Oil and fats		Chlorinated aliphatic	
Turpentine oil		Methylene dichloride	
Kerosene		Ethylene dichloride	
Gasoline		Ethylene drichloride	
Solvent naphtha		Chloroform	
Water		Nitromethane	
Sea water		Nitroethane	
Soapy water (1%)		Nitrobenzene	
Oxygenated water (10%)		Acetaldehyde	
Dibutyl phthalate		Propylene oxide	
Dioctyl phthalate		Dioxane	
Formaline (40%)		Ethyl formate	
Ethylene diamine		Acetonitrile	
Diethylamine		Acrylonitrile	
		Dimethyl formamide	
		Aniline	

15

Figure A.2: PMMA LG Data sheet

PROCESSING DATASHEET

TOPAS Advanced Polymers

TOPAS® 5013L-10

Cyclic Olefin Copolymer

Processing Conditions for Injection Molding

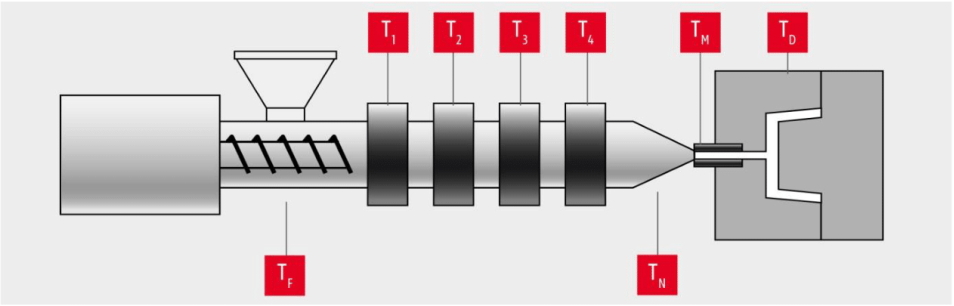

Processing Temperatures

T_F	T_1	T_2	T_3	T_4	T_N	T_M	T_D
< 100 °C	230-260 °C	240-270 °C	250-280 °C	260-290 °C	240-300 °C	240-300 °C	95-125 °C
< 212 °F	446-500 °F	464-518 °F	482-536 °F	500-554 °F	464-572 °F	464-572 °F	203-257 °F

Max. Residence Time	< 15 min; short interruption to cycle: reduce Tx= 170 °C | 338 °F !
Injection Pressure	P_{Sp} = 500 - 1100 bar | 7- 16 kpsi (specific)
Hold on Pressure	P_N = 300 - 600 bar | 4- 9 kpsi (specific)
Back Pressure	P_{St} = 150 bar | 2200 psi max. (specific)
Screw Speed	n_s = 50 - 200 rpm
Injection Speed	moderate to fast (50 mm/sec - 150 mm/sec)
Nozzle Type	free – flow
Pre Drying	100°C (212 °F) / 6hours

Note	Shrinkage is dependent on processing conditions and part design. Typical shrinkage values are 0,4 - 0,7% TOPAS Advanced Polymers recommends only external heated hot runner systems. For molded parts with especially high requirements to the surface quality we recommend to choose the highest possible mold temperature.

TOPAS Advanced Polymers GmbH | Am Prime Parc 9 | 65479 Raunheim | Germany
+49 (0) 1805-1-86727 (EU) | +1 248 479 8928 (USA) | +81 3 6711 8615 (Asia/Pacific) | www.topas.com

Figure A.3: COC Topas 5013L-10 Data sheet

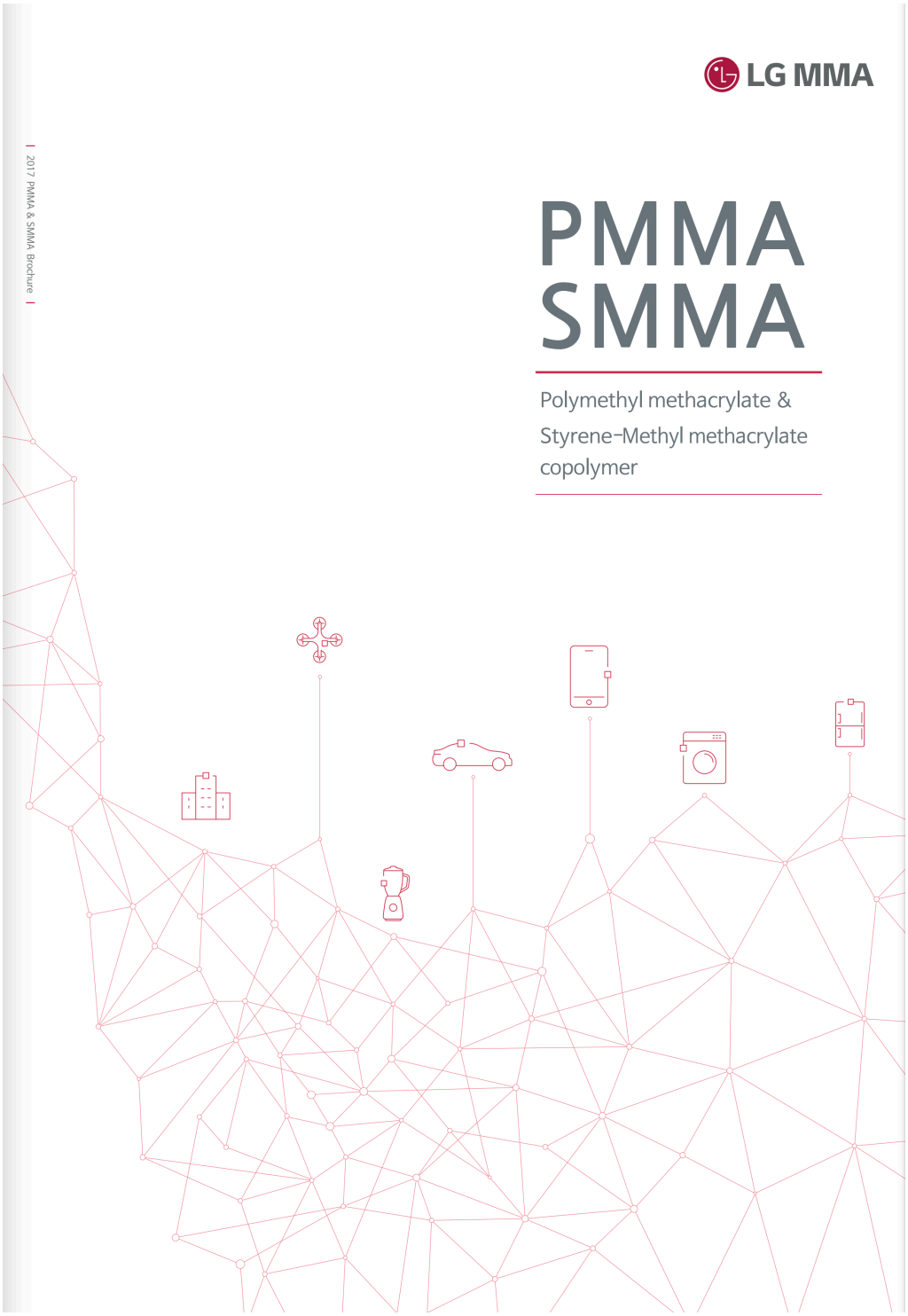

Figure A.4: PMMA LG Brochure

Figure A.5: PMMA LG Brochure

LG MMA

Capacity : 1,000MT/year

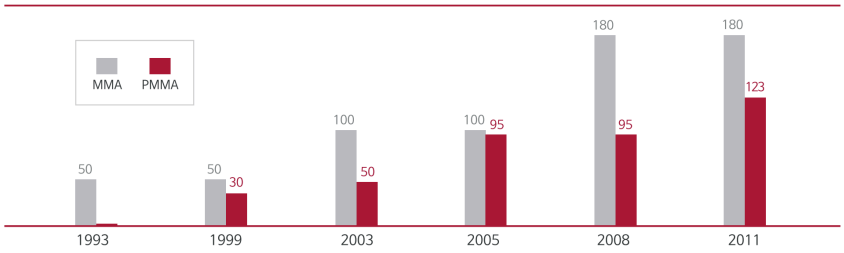

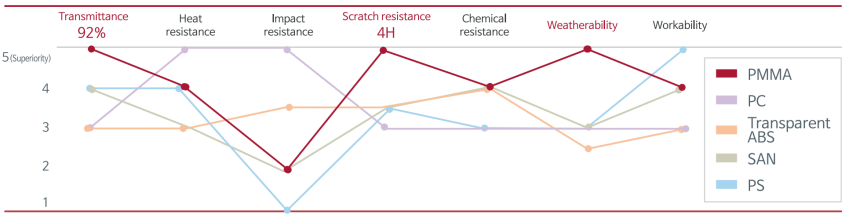

PMMA is synthetic resin mainly composed of MMA monomer. With its excellent transparency, weatherability and colorability this highly polymerized material is widely used for automobile and electronic parts.

High Transparency

The most excellent transparency among all plastics (Transmits more than 92% of the visible ray area)

Excellent Weatherability

The most excellent weatherability among plastics

High Scratch Resistance

Excellent scratch resistance with its high degree of surface hardness among plastics

Item		LG PMMA
Flammability	UL 94 (HB) / CSA (HB)	All Grades
Weatherability	AMECA	IH830, IH830A, IH830C, IH830CA, IH830HR, EG920, EH910, HP202, HI835MS, HI835H
Hazardous Material	RoHS (Directive 2002/95/EC) JHPC / IMDS	All Grades
FDA	US FDA regulation / 21CFR177.1010	IH830, IG840, IF850, IF870S, HI855M, HI855S, HI855H
Management System	ISO14000 (Environment) KGS18000 (Safety) / ISO/TS 16949 (Quality)	All Grades

03

Figure A.6: PMMA LG Brochure

Figure A.7: PMMA LG Brochure

LG MMA

Properties

	Item	Unit	Injection Grade							
			IH830	IH830L	IH830C	IH830HF	IG840	IF850	IF860	IF870S
Optical Properties	Light transmittance	%	92	92	92	92	92	92	92	92
	Haze	%	<0.5	<0.5	<0.5	<0.5	<0.5	<0.5	<0.5	<0.5
Thermal Properties	Melt flow index	g/10min	2.3	2.3	2.0	4.5	5.7	13	16	23
	Heat deflection temperature	℃	101	102	101	103	102	92	91	90
	Vicat softening temperature	℃	109	111	108	112	98	88	87	86
Mechanical Properties	Charpy Impact strength	kJ/m²	1.5	1.5	1.5	1.5	1.5	1.5	1.5	1.5
	Rockwell hardness	-	99	101	100	100	95	92	91	89
	Tensile strength	MPa	71	72	74	64	65	62	60	56
	Tensile elongation	%	5.0	4.5	5.0	3.0	4.0	4.0	3.0	2.8
	Tensile modulusFlexural	GPa	2.8	2.9	2.9	2.9	2.8	2.8	2.8	2.8
	Flexural strength	MPa	111	113	113	116	105	101	96	94
	Flexural modulus	GPa	3.0	3.0	3.0	3.1	3.0	2.9	2.8	2.8

	Item	Unit	Heat Resistant Grade			
			IH830HR	IH830XT	EF120	IH830HT
Optical Properties	Light transmittance	%	92	92	92	92
	Haze	%	<0.5	<0.5	<0.5	<0.5
Thermal Properties	Melt flow index	g/10min	1.7	2.5	1.1	1.7
	Heat deflection temperature	℃	113	114	118	113
	Vicat softening temperature	℃	105	111	109	106
Mechanical Properties	Charpy Impact strength	kJ/m²	1.5	1.5	1.5	1.5
	Rockwell hardness	-	102	101	100	97
	Tensile strength	MPa	75	68	75	67
	Tensile elongation	%	5.0	5.0	5.0	3.0
	Tensile modulusFlexural	GPa	3.2	3.2	3.2	3.3
	Flexural strength	MPa	120	120	120	92
	Flexural modulus	GPa	3.1	3.2	3.1	3.0

	Item	Condition	Unit	Method (ASTM/ISO)	Value (in common)
General Properties	Density	-	g/cm³	ISO 1183	1.19
	Refractive index	nd	-	ISO 489	1.49
	Water absorption	24hr	%	ASTM D570	0.3
	Mold shrinkage	-	%	ASTM D955	0.2-0.6
	Coefficient of linear expansion	-	1/℃	ASTM D696	6×10^{-5}
	Flammability	1.5mm	Class	UL94	HB
Electrical Properties	Volume resistivity	-	Ω · cm	ASTM D257	$>10^{15}$
	Dielectric strength	4kV/s	kV/mm	ASTM D149	20
	Dielectric constant	60Hz	-	ASTM D150	3.1
	Power factor	60Hz	-	ASTM D150	0.05

REMARKS : The listed values should be used for reference purpose only.

07

Figure A.8: PMMA LG Brochure

2. Grades, supply form, colors

Topas® COC resin is currently supplied as an unreinforced water-clear transparent material. Glass-filled, tinted and pigmented formulations are also under development.

Currently available basic grades differ primarily in their heat deflection temperature HDT/B. The heat deflection temperature is determined by the ratio of the comonomers. Topas® COC grades with higher cyclo-olefin content have higher heat resistance. Flow characteristics may be adjusted independently of heat resistance.

The product nomenclature contains a 4 digit number. The first two digits indicate the viscosity number, the last two digits describe the heat deflection temperature HDT/B. The flowability decreases with increasing viscosity number.

The table on the right lists the Topas® COC basic grades. Of these grades, specific sub-grades are avail-able on request, which are particularly well suited for optical, medical and diagnostic applications, for extrusion and injection blow molded applications.

Grade	Description
8007	Clear grade with a heat deflection temperature HDT/B of 75 °C. It is especially suited for packaging of moisture-sensitive products because of its low water absorption and very good barrier properties. Grade 8007 has a lo-wer elastic modulus and higher elongation than other Topas® COC grades.
5013	Clear grade with a heat deflection temper-ature HDT/B of 130 °C. This grade is char-acterized by high flowa-bility and excellent optical properties. Recommended for applications such as optical parts, e. g. lenses, and optical storage media, where low birefringence and high molding accuracy (pit replication) are essential, as well as for medical and diagnostic applications.
6013	Clear grade with a heat deflection temperature HDT/B of 130 °C, a value which cannot be attained by many amor-phous polymers. Its combination of high purity, chemi-cal resistance, high transparency and high HDT/B makes this material useful for prod-ucts such as labware. Parts made from 6013 can be gamma- and steam-sterilized.
6015	Clear grade similar to 6013, with a heat deflection tem-perature HDT/B of 150 °C, a value which cannot be at-tained by many amorphous polymers.
6017	Clear grade with a heat deflection temper-ature HDT/B of 170 °C. For parts requiring resistance to short-term, high-temperature exposure.

Figure A.9: COC Brochure

Table A.1: Specification of the injection moulding machine Arburg 370A Allrounder used to produce the chip[4].

Arburg 370A Allrounder	
Clamping force max [kN]	600
Opening stroke max [mm]	300
Mould height min-max [mm]	200-400
Mould mounting platens(WxH) [mm]	510x510
Ejector force max [kN]	25
Ejector stroke max [mm]	100
Screw diameter [mm]	18
Injection pressure max [Bar]	2500

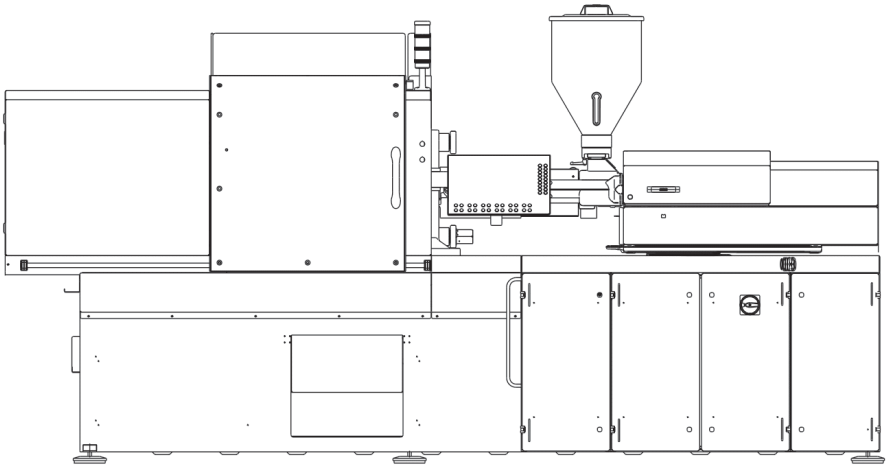

ALLROUNDER 370 A

Distance between tie bars: 370 x 370 mm
Clamping force: 600 kN
Injection unit (acc. to EUROMAP): 100, 170, 290

ARBURG

TECHNICAL DATA | 370 A

Clamping unit				370 A
with clamping force		max.	kN	600
Opening force | stroke		max.	kN | mm	--- | 300
Mould height, fixed | variable		min.-max.	mm	--- | 200-400
Platen daylight fixed | variable		max.	mm	--- | 500-700
Distance between tie bars (w x h)			mm	370 x 370
Mould mounting platens (w x h)		max.	mm	510 x 510
Weight of movable mould half		max.	kg	360
Ejector force | stroke		max.	kN | mm	25 | 100
Dry cycle time EUROMAP	Comfort	min.	s - mm	1,2 - 259
	Ultimate	min.	s - mm	0,8 - 259

Injection unit				100			170			290		
with screw diameter			mm	20	25	30	25	30	35	30	35	40
Effective screw length			L/D	25	20	16,7	24	20	17	23,3	20	17,5
Screw stroke		max.	mm		100			120			150	
Calculated stroke volume		max.	cm³	31	49	71	59	85	115	106	144	188
Shot weight		max.	g PS	29	45	65	54	77	105	97	132	172
Material throughput		max.	kg/h PS	5,5	8	9,5	10	13,5	16	17	20,5	24,5
		max.	kg/h PA6.6	2,8	4	4,9	5	7	8	8,5	10,5	12,5
Injection pressure		max.	bar	2500	2000	1390	2500	2000	1470	2500	2000	1530
Holding pressure time		max.	s - bar	300-2500	300-1600	300-1110	300-2310	300-1600	300-1170	300-2180	300-1600	300-1220
Injection flow ²	Comfort [+]	max.	cm³/s	64 [83]	100 [130]	144 [187]	79 [104]	114 [150]	155 [203]	105 [140]	144 [191]	188 [250]
	Ultimate [+]	max.	cm³/s	94 [125]	148 [197]	214 [285]	148 [197]	214 [285]	290 [387]	212 [283]	288 [384]	376 [501]
Injection speed ⁵	Comfort [+]	max.	mm/s		280 [350]			215 [280]			215 [280]	
	Ultimate [+]	max.	mm/s		350 [400]			350 [400]			360 [400]	
Screw circumferential speed		max.	m/min	40	50	60	50	60	70	51	60	69
Screw torque		max.	Nm	120	150	180	210	250	290	320	380	430
Nozzle contact force | retraction stroke		max.	kN | mm		50 | 230			50 | 300			50 | 300	
Heating capacity | zones			kW		4,9 | 5			9,4 | 5			6,4 | 5	
Feed hopper			l		50			50			50	

Drive and connection			Comfort			Ultimate			
with injection unit			100	170	290	100	170	290	
Net weight of machine		kg	3740	3740	3800	3740	3740	3800	
Sound press. level | Insecurity ⁴		dB(A)		66 | 3			66 | 3		
Electrical connection ³		kW	13	19	20	18	24	25	
	Total	A	50	63	63	63	80	80	
	Machine	A		---			---		
	Heating	A		---			---		
Cooling water connection		max. °C		30			30		
		min. Δp bar		1,5 | DN 25			1,5 | DN 25		

Machine type
with EUROMAP size designation ¹
370 A 600-100 | 170 | 290

Upon request: other machine types and mould installation heights, screws, drive powers etc.
All specifications relate to the basic machine version. Deviations are possible depending on variants, process settings and material type. Depending on the drive, certain combinations, e.g. max. injection pressure and max. injection flow may be mutually exclusive.

1) Clamping force (kN) - size of injection unit = max. stroke volume (cm³) x max. injection pressure (kbar)
2) Specification of maximum injection flow at maximum injection pressure.
3) Specifications relate to 400 V/50 Hz.
4) Emission sound pressure level at the workplace. Detailed information in the operating instructions.
5) Forward speed of plasticising screw at 1000 bar injection pressure.
[ ] Specifications apply to alternative equipment.

MACHINE DIMENSIONS | 370 A

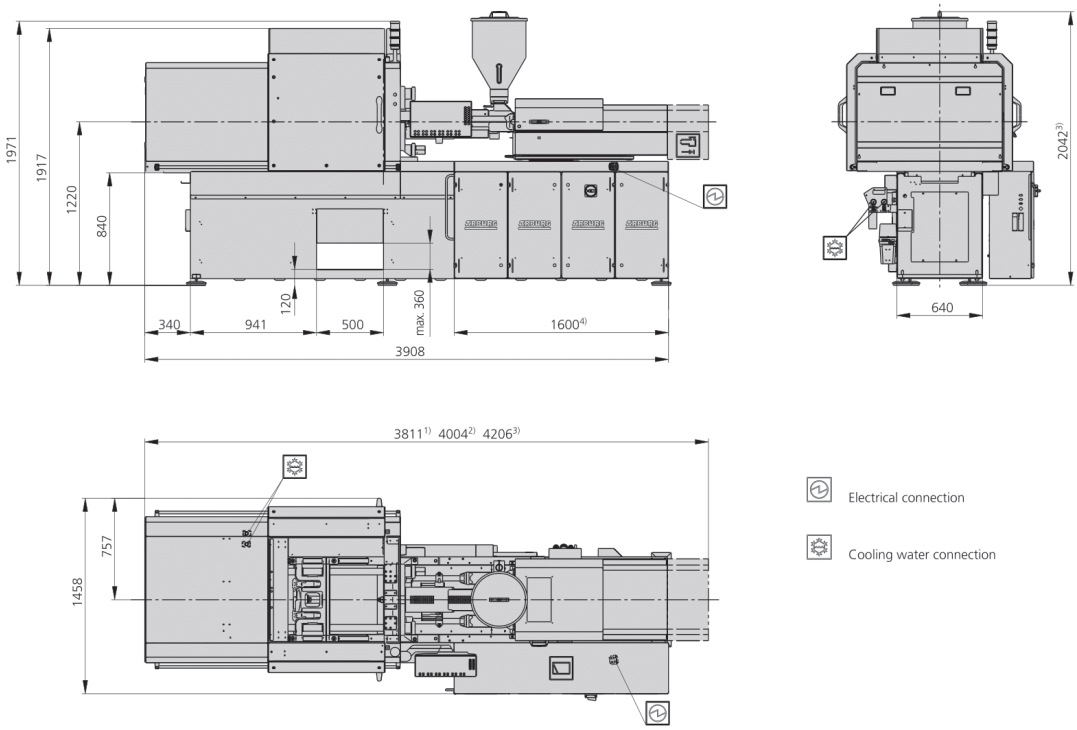

1) Injection unit 100
2) injection unit 170
3) Injection unit 290
4) Depending on the power and size of the injection unit

2

MOULD INSTALLATION DIMENSIONS | 370 A

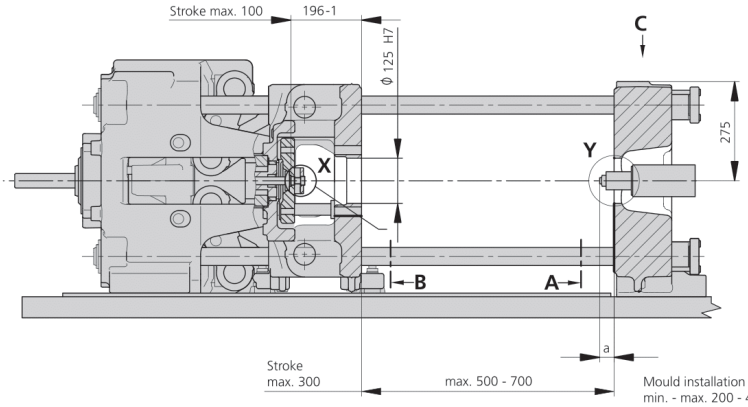

a max.	Injection unit 100 / 170 / 290
Standard	40
Thermoset	20

Ejector bolt | X

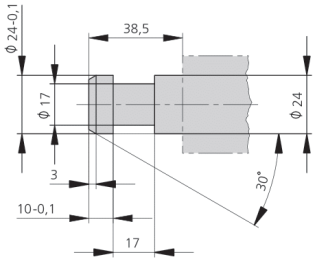

Bore in mould (if required) | Y

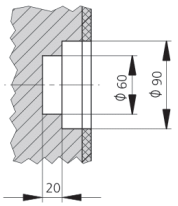

Closing force for spring moulds / during injection compression moulding*

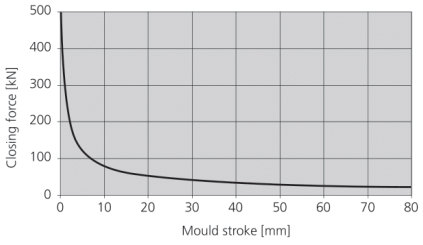

* automatic locking force adjustment up to 20 kN

Robotic system mounting | C

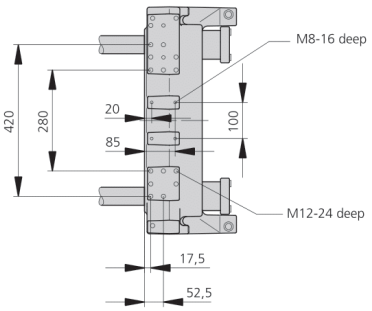

4

MOULD INSTALLATION DIMENSIONS | 370 A

Fixed mould mounting platen | A

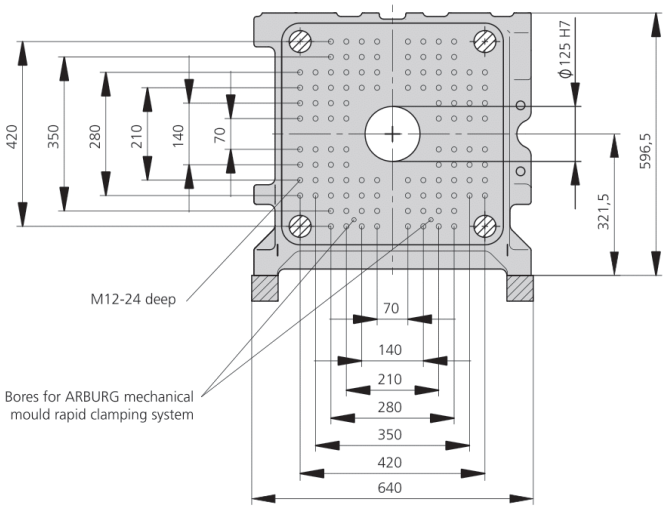

Moving mould mounting platen | B

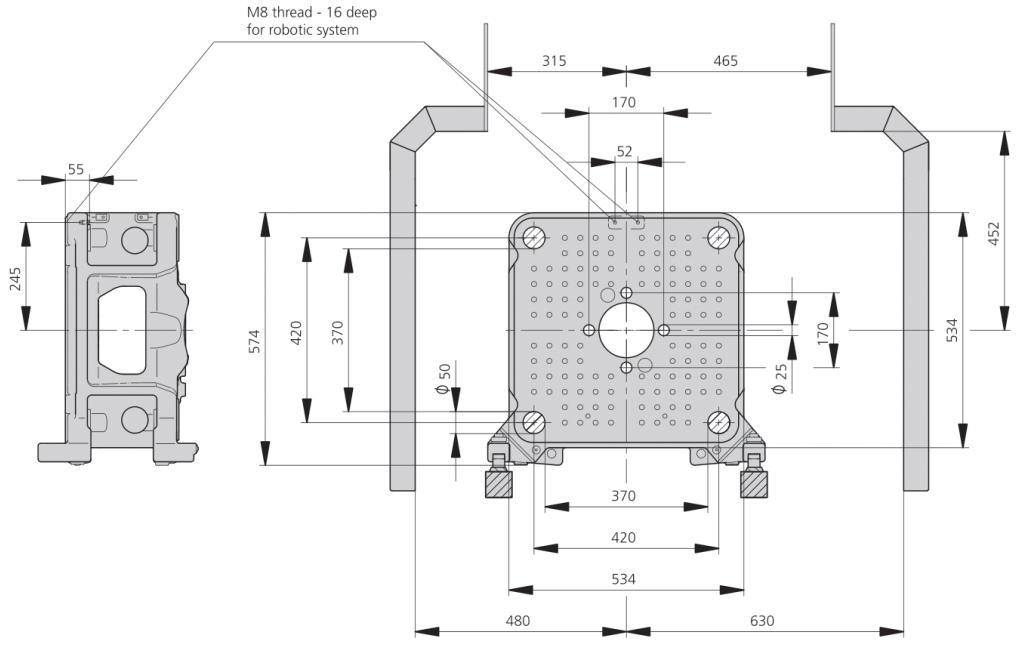

5

SHOT WEIGHTS | 370 A

Theoretical shot weights for the most important injection moulding materials

Injection units according to EUROMAP		100			170			290		
Screw diameter	mm	20	25	30	25	30	35	30	35	40
Polystyrene	max. g PS	29	45	65	54	77	105	97	132	172
Styrene heteropolymerizates	max. g SB	28	44	63	53	76	103	95	129	168
	max. g SAN, ABS[1]	27	43	62	52	74	101	93	126	165
Cellulose acetate	max. g CA[1]	32	50	73	61	87	119	109	148	194
Celluloseacetobutyrate	max. g CAB[1]	30	47	68	56	81	110	101	138	180
Polymethyl methacrylate	max. g PMMA	30	46	67	56	80	109	100	136	178
Polyphenylene ether, mod.	max. g PPE	27	42	60	50	72	98	90	122	160
Polycarbonate	max. g PC	30	47	68	57	81	111	102	139	181
Polysulphone	max. g PSU	31	49	70	58	84	115	105	143	187
Polyamides	max. g PA 6.6 | PA 6[1]	28	44	64	53	77	104	96	131	171
	max. g PA 6.10 | PA 11[1]	26	41	60	50	72	98	90	122	160
Polyoximethylene (Polyacetal)	max. g POM	35	55	80	66	96	130	120	163	213
Polyethylene terephthalate	max. g PET	34	53	77	64	92	126	115	157	205
Polyethylene	max. g PE-LD	22	34	49	41	59	80	73	100	130
	max. g PE-HD	22	35	50	42	60	82	76	103	134
Polypropylene	max. g PP	23	36	51	43	62	84	77	105	137
Fluorpolymerides	max. g FEP, PFA, PCTFE[1]	46	72	103	86	124	169	155	211	276
	max. g ETFE	40	63	91	76	109	148	136	185	242
Polyvinyl chloride	max. g PVC-U	35	54	78	65	94	127	117	159	208
	max. g PVC-P[1]	32	50	72	60	87	118	108	147	192

1) average value

ARBURG GmbH + Co KG
Arthur-Hehl-Strasse
72290 Lossburg
Tel.: +49 7446 33-0
www.arburg.com
contact@arburg.com

526447_EN_GB_092021 · Subject to alterations

Parameters	Values
Injection pressure [Bar]	800
Switch-over by volume[%] filled	98
Filling time [s]	0.4
Screw speed [rpm]	125
Back pressure [Bar]	150
Packing pressure [Bar]	550-550-275
s	1-5-0.5
Cooling time [s]	15

Table A.2: Experimental Parameters for COC. Note the pressure unit is in *Bar* since the Arburg machine doesn't work in *Pa*.

Parameters	Values
Injection pressure [Bar]	1300
Switch-over by volume[%]filled	98
Filling time [s]	0.38
Screw speed [rpm]	125
Back pressure [Bar]	150
Packing pressure [Bar]	1200-900-450
s	0.5-8-2
Cooling time [s]	15

Table A.3: Experimental Parameters for PMMA. The pressure unit is in *Bar* since the Arburg machine doesn't work in *Pa*.

Measurement settings	
Objective	20x
Brightness	49.2
Image size	2564x2568 µm
Laser light	

Table A.4: LEXT measurements settings for mold

Measurement settings	
Lens	5x
Light	37.5

Table A.5: DeMeet measurements settings for mold

Measurement settings	
Objective	20x
Brightness	50
Image size	2564x2568 µm
Laser light	

Table A.6: LEXT measurements settings for molded parts

Measurement settings	
Lens	5x
Light	37.5

Table A.7: DeMeet measurements settings for molded parts

Figure A.10: Bottom section of the channel. The difference of height might affect the measurement of this section

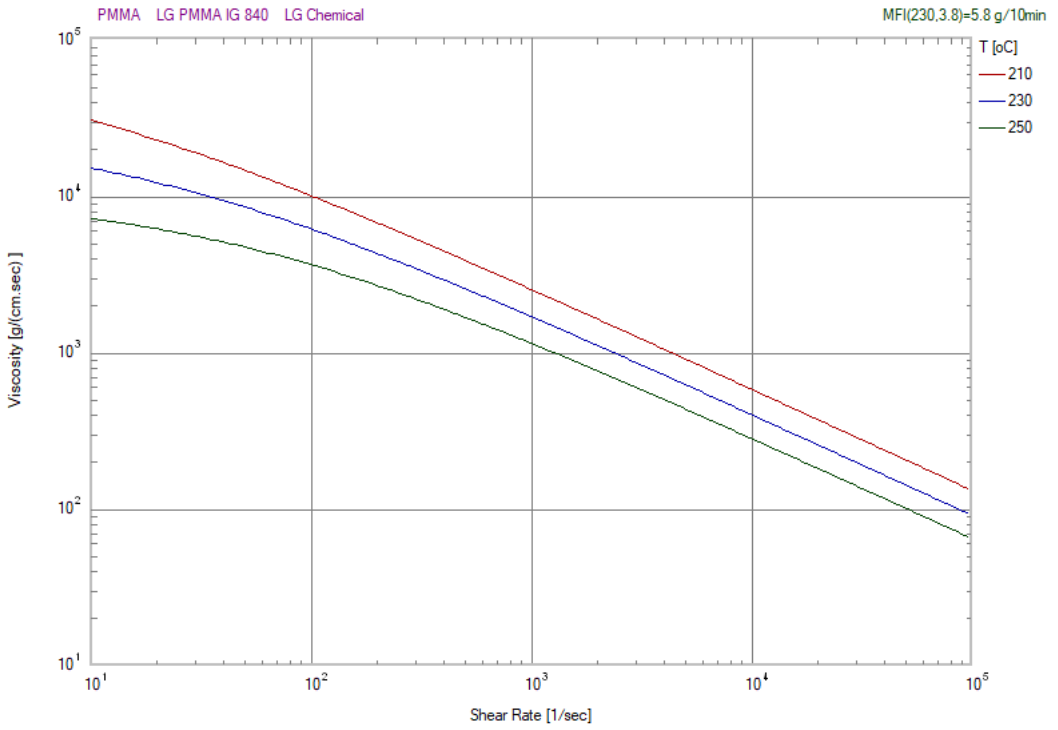

Figure A.11: PMMA viscosity

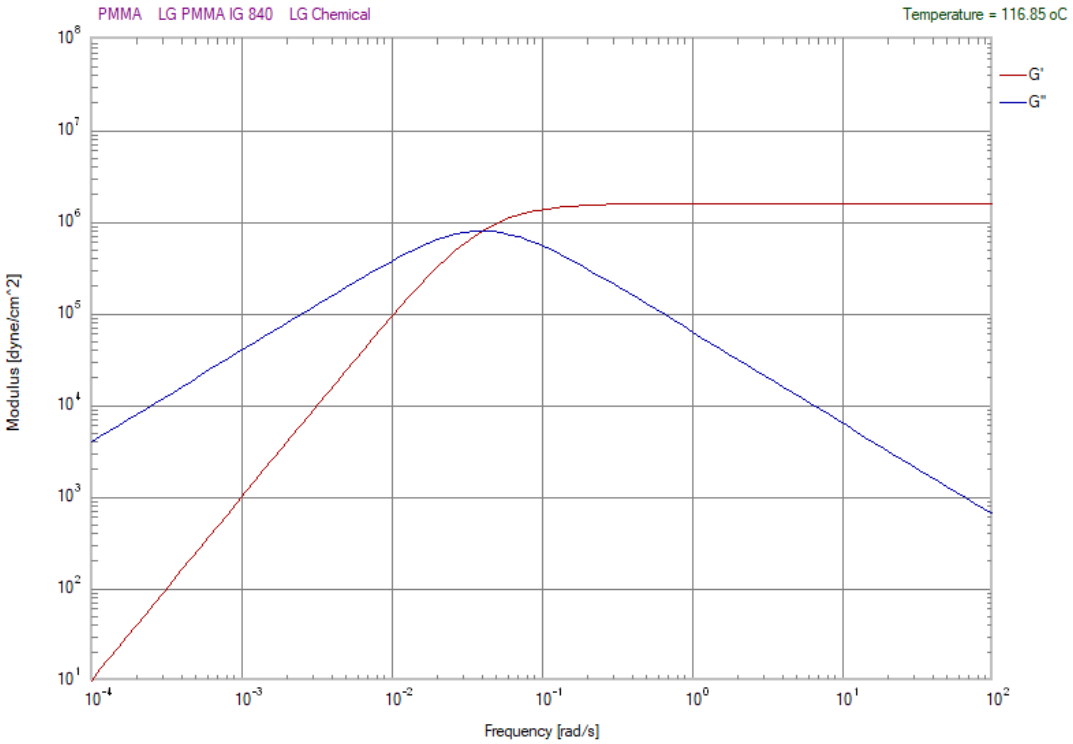

Figure A.12: PMMA viscoelasticity

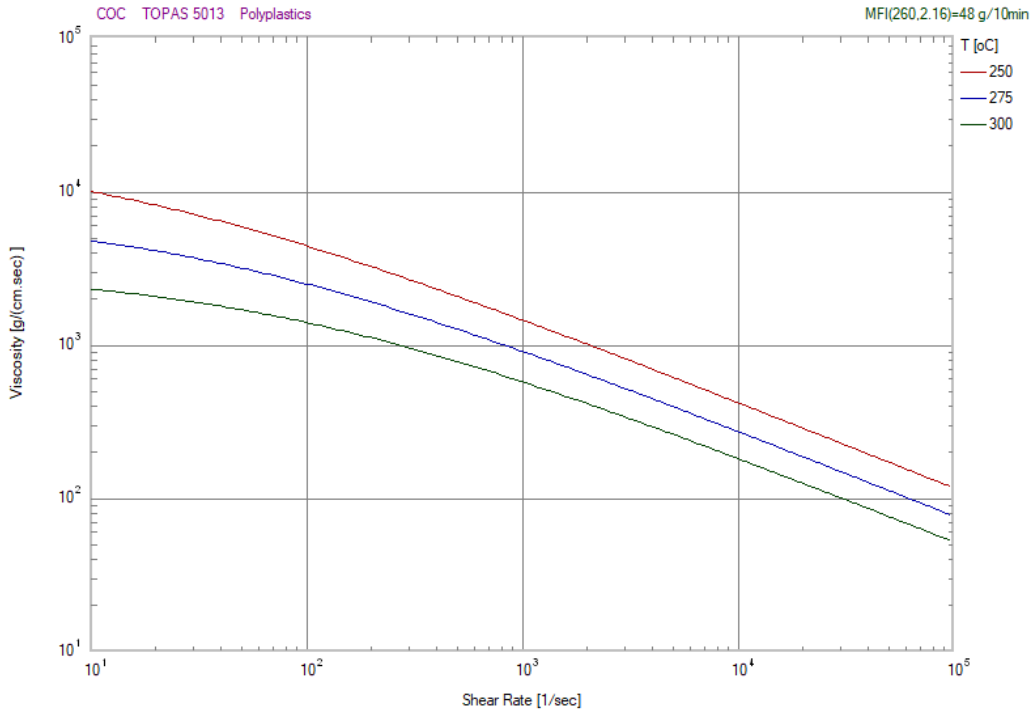

Figure A.13: COC viscosity

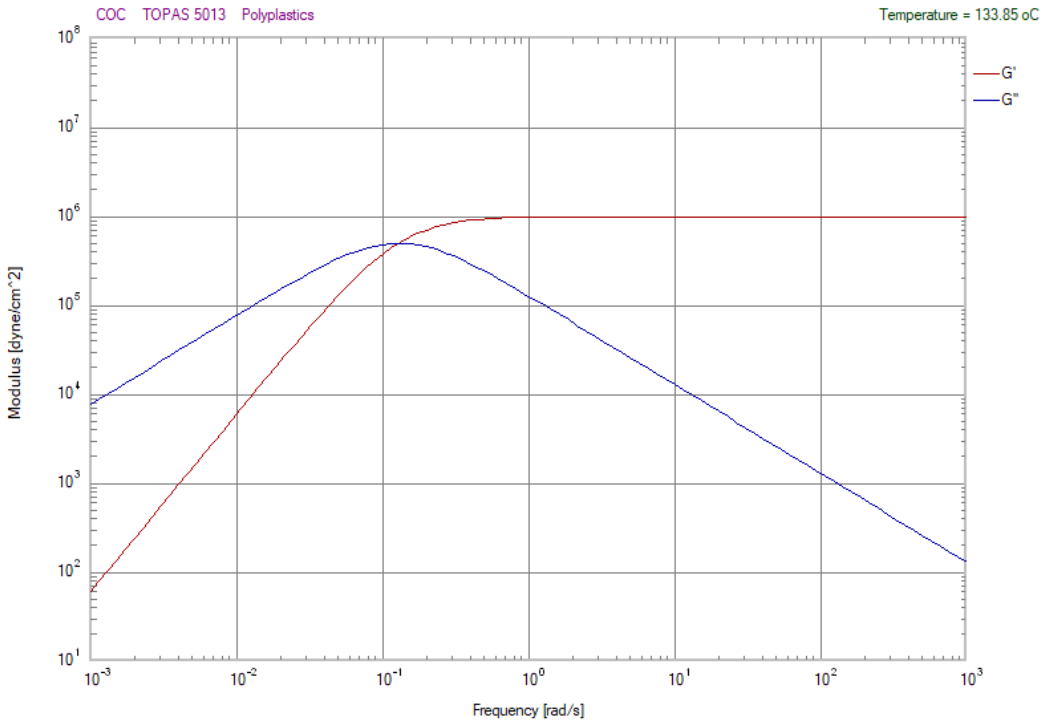

Figure A.14: COC viscoelasticity

Mould Temperature [°C]	Melt Temperature [°C]	Packing pressure [MPa]	Injection velocity [mm/s]	Volumetric Shrinkage [%]
100	280	55	14	2.63
100	250	80	14	1.95
100	250	55	14	1.75
120	250	55	14	2.31
120	280	80	14	
120	280	80	22	
120	250	55	22	2.60
100	250	80	22	1.49
100	280	80	14	2.97
120	250	80	14	2.77
120	280	55	14	2.82
120	250	80	22	2.55
100	250	55	22	1.86
100	280	80	22	1.69
120	280	55	22	2.58
100	280	55	22	2.45

Table A.8: Full factorial design for COC. Note that the recipes 5-6 are both with high levels of Melt Temperature, Mould Temperature and Packing pressure.

Mould Temperature [°C]	Melt Temperature [°C]	Packing pressure [MPa]	Injection velocity [mm/s]	Volumetric Shrinkage [%]
85	220	90	22	
85	240	120	22	
65	240	120	36	2.42
65	220	120	22	2.92
65	220	90	36	2.84
85	240	90	22	2.49
65	220	120	36	1.90
65	220	90	22	2.78
65	240	120	22	2.05
85	220	120	36	
85	220	120	22	
85	220	90	36	
65	240	90	36	2.09
85	240	120	36	1.81
85	240	90	36	2.60
65	240	90	22	1.96

Table A.9: Incomplete DoE for PMMA. Only 11 recipes were molded.

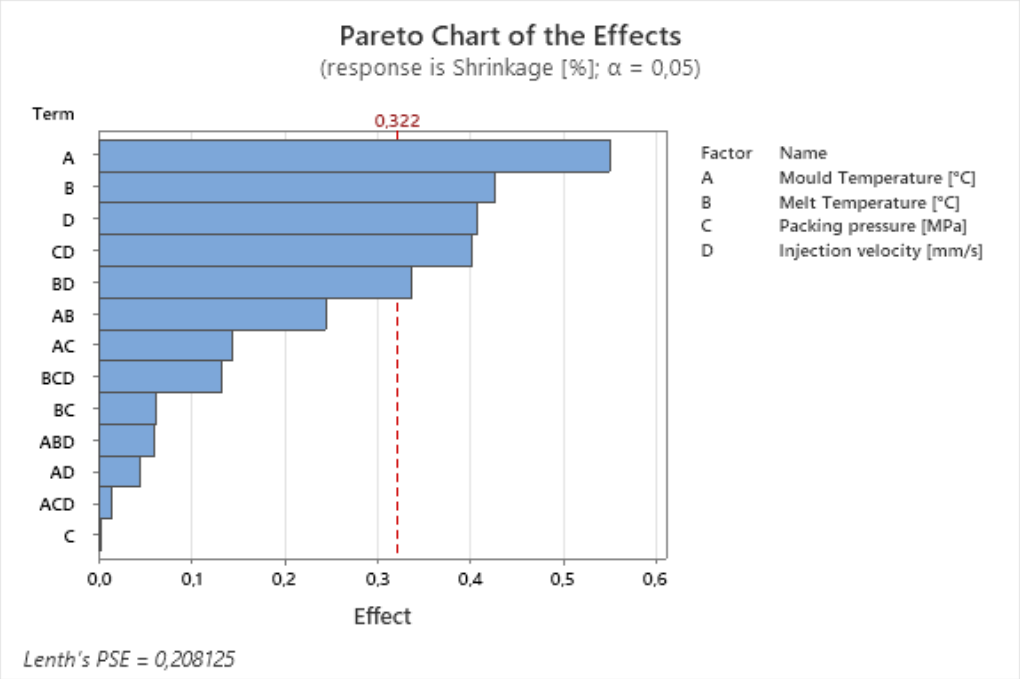

Figure A.15: Pareto chart for COC. Mould Temperature (A), Melt Temperature (B), Injection velocity (D), Packing pressure*Injection velocity (CD), Melt Temperature*Injection velocity (BD) are significant for the output [25]

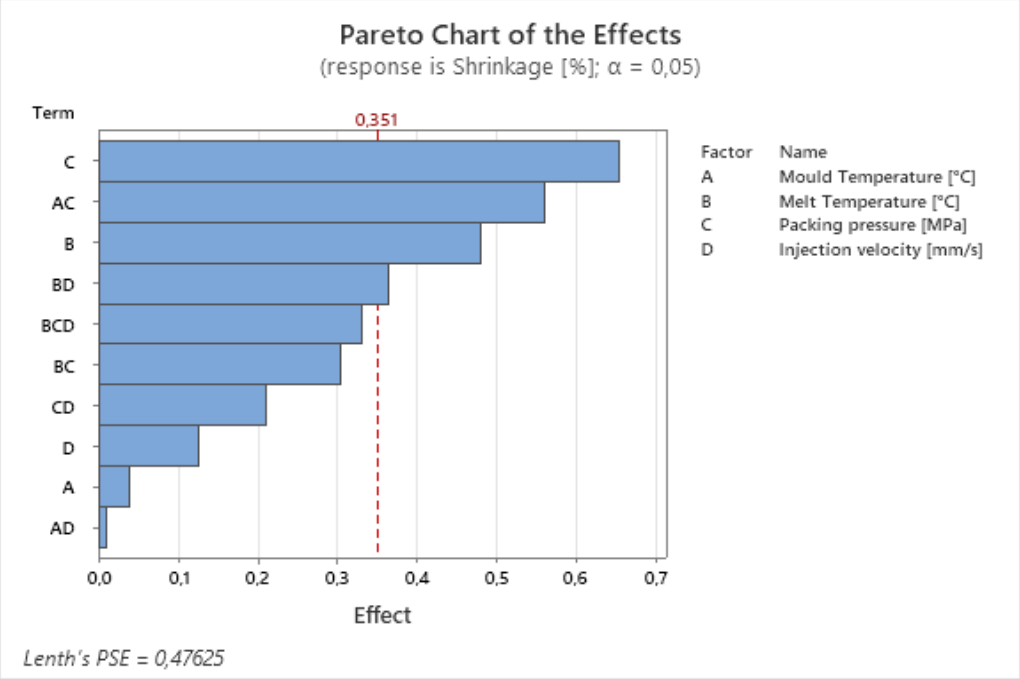

Figure A.16: Pareto chart for PMMA. Any effects that extend beyond the reference line are significant. Packing pressure(C), Melt temperature (C), Mould Temperature*Packing pressure(AC), Melt Temperature*injection velocity(BD) are all significant.

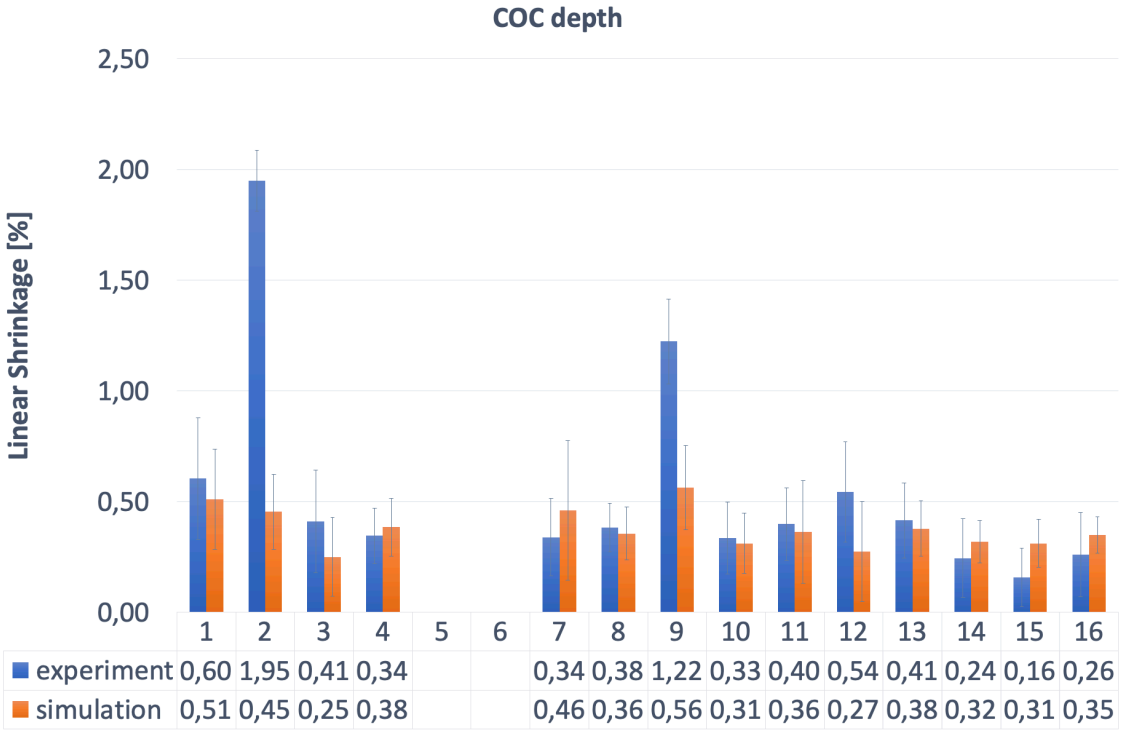

	1	2	3	4	5	6	7	8	9	10	11	12	13	14	15	16
experiment	0,60	1,95	0,41	0,34			0,34	0,38	1,22	0,33	0,40	0,54	0,41	0,24	0,16	0,26
simulation	0,51	0,45	0,25	0,38			0,46	0,36	0,56	0,31	0,36	0,27	0,38	0,32	0,31	0,35

Figure A.17: COC Shrinkage along the depth of the channel. Comparison experiment vs simulation results. The error bars in the plot indicate the standard deviation calculated from the three different samples of each recipe.

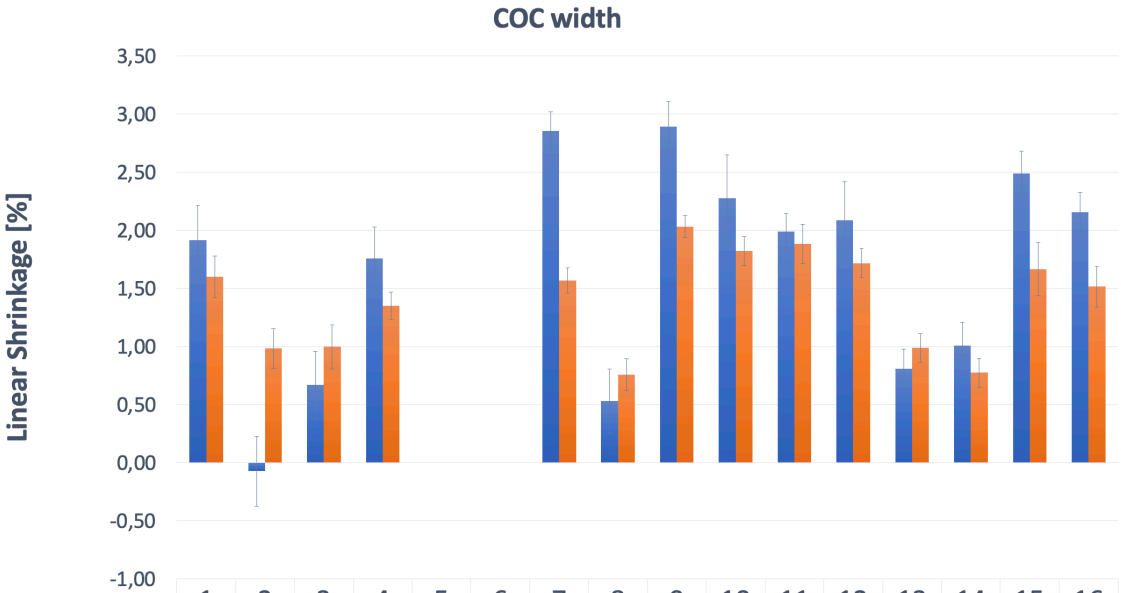

	1	2	3	4	5	6	7	8	9	10	11	12	13	14	15	16
experiment	1,91	-0,0	0,67	1,76			2,85	0,53	2,89	2,28	1,99	2,09	0,81	1,00	2,49	2,15
simulation	1,60	0,98	1,00	1,35			1,57	0,76	2,03	1,82	1,88	1,72	0,99	0,77	1,67	1,51

Figure A.18: COC Shrinkage along the width. Comparison experiment vs simulation results. The error bars in the plot indicate the standard deviation calculated from the three different samples of each recipe.

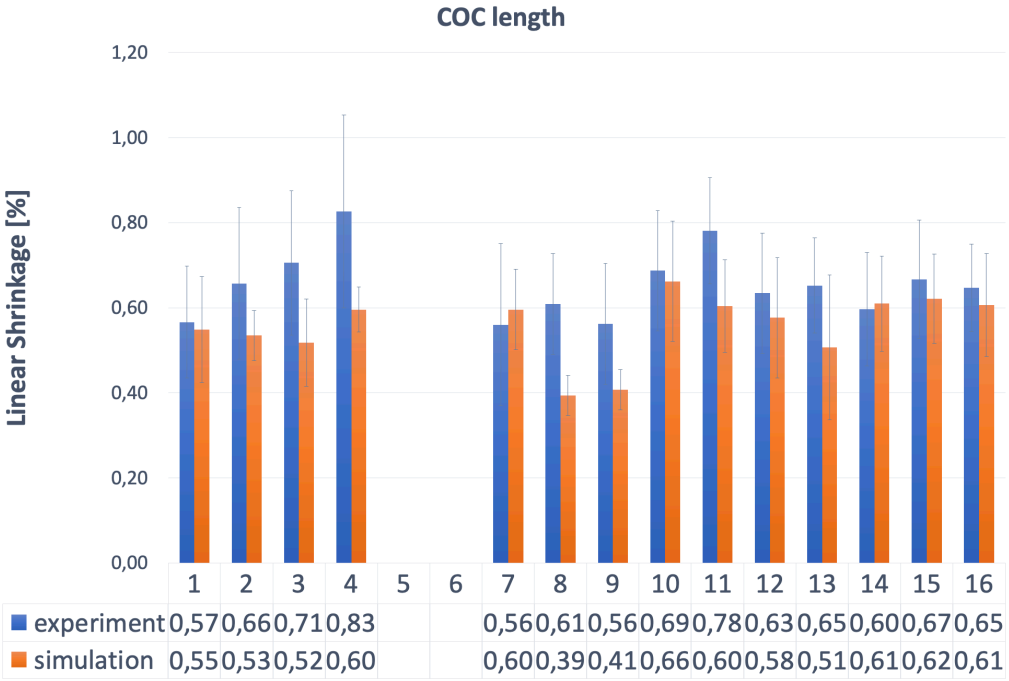

Figure A.19: COC Shrinkage along the length. Comparison experiment vs simulation results. The error bars in the plot indicate the standard deviation calculated from the three different samples of each recipe.

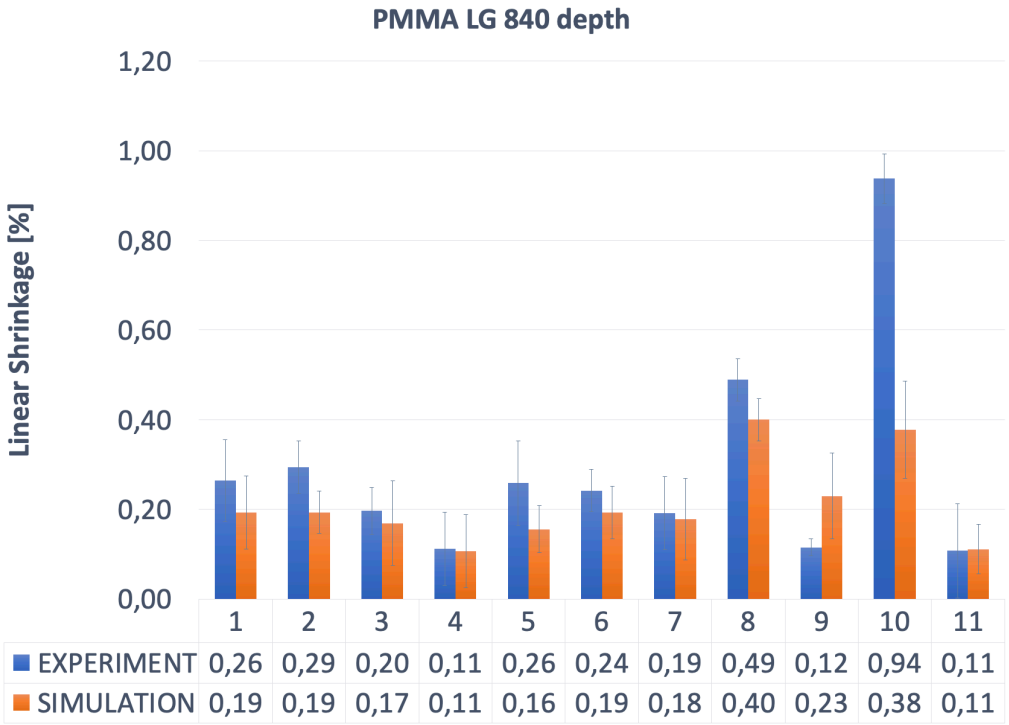

Figure A.20: PMMA Shrinkage along the depth. Comparison experiment vs simulation results. The error bars in the plot indicate the standard deviation calculated from the three different samples of each recipe.

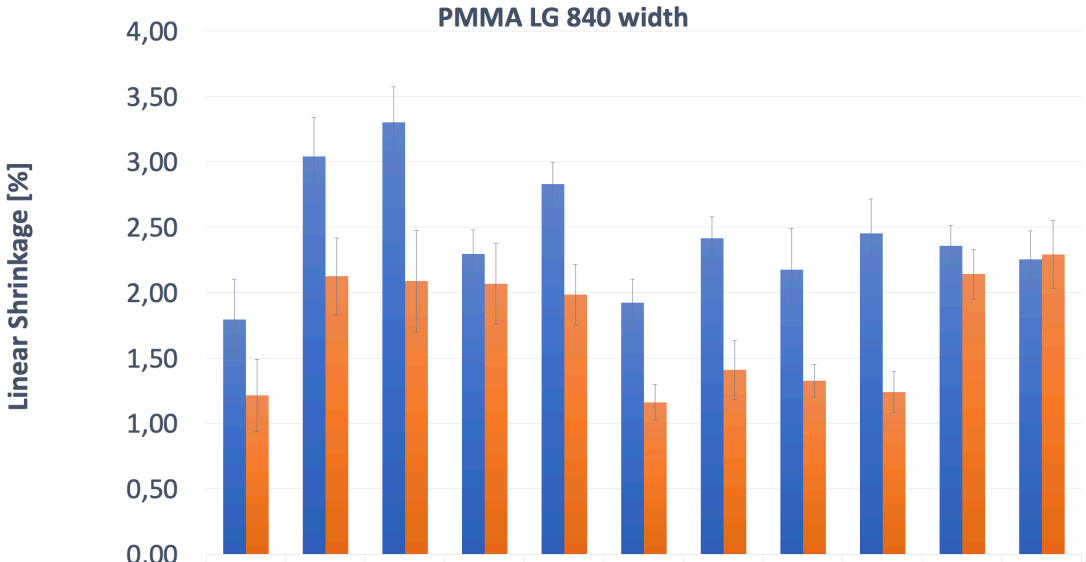

	1	2	3	4	5	6	7	8	9	10	11
EXPERIMENT	1,80	3,04	3,30	2,29	2,83	1,92	2,41	2,18	2,45	2,36	2,25
SIMULATION	1,21	2,12	2,09	2,07	1,98	1,16	1,41	1,32	1,24	2,14	2,29

Figure A.21: PMMA Shrinkage along the width. Comparison experiment vs simulation results. The error bars in the plot indicate the standard deviation calculated from the three different samples of each recipe.

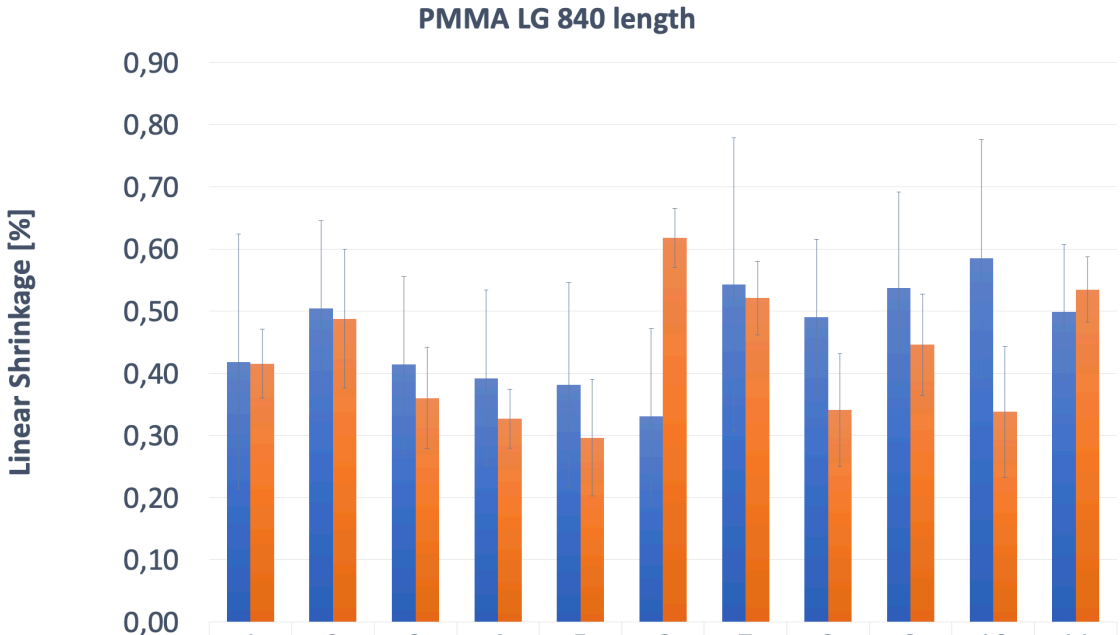

	1	2	3	4	5	6	7	8	9	10	11
EXPERIMENT	0,42	0,50	0,41	0,39	0,38	0,33	0,54	0,49	0,54	0,59	0,50
SIMULATION	0,42	0,49	0,36	0,33	0,30	0,62	0,52	0,34	0,45	0,34	0,53

Figure A.22: PMMA Shrinkage along the length. Comparison experiment vs simulation results. The error bars in the plot indicate the standard deviation calculated from the three different samples of each recipe.

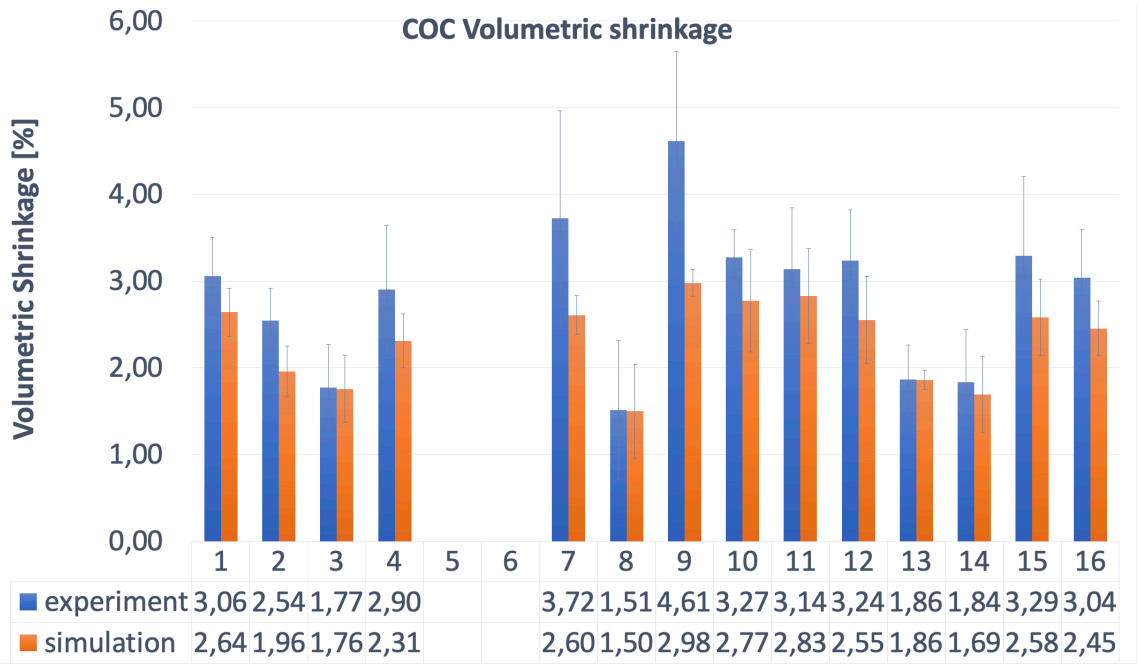

	1	2	3	4	5	6	7	8	9	10	11	12	13	14	15	16
experiment	3,06	2,54	1,77	2,90			3,72	1,51	4,61	3,27	3,14	3,24	1,86	1,84	3,29	3,04
simulation	2,64	1,96	1,76	2,31			2,60	1,50	2,98	2,77	2,83	2,55	1,86	1,69	2,58	2,45

(a) COC results.

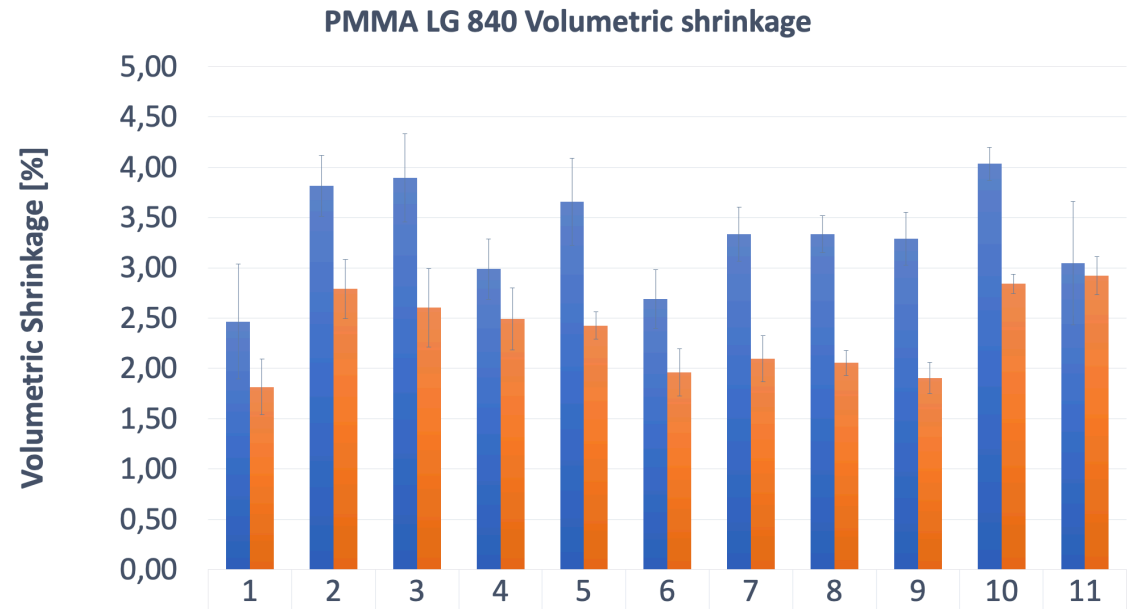

	1	2	3	4	5	6	7	8	9	10	11
experiment	2,46	3,81	3,89	2,99	3,65	2,69	3,33	3,33	3,29	4,03	3,05
simulation	1,81	2,79	2,60	2,49	2,43	1,96	2,10	2,05	1,90	2,84	2,92

(b) PMMA results

Figure A.23: Volumetric shrinkage for both the materials experiment vs simulation. The error bars in the plot indicate the standard deviation calculated from the three batches measured.